NASA TECHNICAL NOTE

NASA TN D-4076

STATIC STABILITY CHARACTERISTICS AT MACH NUMBERS FROM 1.90 TO 4.63 OF A 76° SWEPT ARROW WING MODEL WITH VARIATIONS IN HORIZONTAL-TAIL HEIGHT, WING HEIGHT, AND DIHEDRAL

by Dennis E. Fuller

Langley Research Center
Langley Station, Hampton, Va.

NATIONAL AERONAUTICS AND SPACE ADMINISTRATION • WASHINGTON, D. C. • AUGUST 1967

STATIC STABILITY CHARACTERISTICS AT MACH NUMBERS FROM 1.90 TO 4.63 OF A 76° SWEPT ARROW WING MODEL WITH VARIATIONS IN HORIZONTAL-TAIL HEIGHT, WING HEIGHT, AND DIHEDRAL

By Dennis E. Fuller

Langley Research Center
Langley Station, Hampton, Va.

NATIONAL AERONAUTICS AND SPACE ADMINISTRATION

For sale by the Clearinghouse for Federal Scientific and Technical Information
Springfield, Virginia 22151 – CFSTI price $3.00

STATIC STABILITY CHARACTERISTICS AT MACH NUMBERS FROM 1.90 TO 4.63 OF A 76° SWEPT ARROW WING MODEL WITH VARIATIONS IN HORIZONTAL-TAIL HEIGHT, WING HEIGHT, AND DIHEDRAL

By Dennis E. Fuller
Langley Research Center

SUMMARY

An investigation has been made to determine the effects of horizontal-tail height, wing height, and dihedral on the longitudinal and lateral stability characteristics of a 76° swept arrow wing aircraft model. The horizontal-tail height was varied from a position below the fuselage to a position near the top of the vertical tail, in combination with a high wing having 5°, 0°, and -5° dihedral, and with a low wing having 5° and 0° dihedral. Tests were performed at Mach numbers from 1.90 to 4.63, at angles of attack from about -4° to 20°, and at angles of sideslip from about -4° to 8°.

Results of the investigation indicate that generally, for the angle-of-attack and Mach number range presented herein, the horizontal tail mounted above the fuselage passes through an adverse flow region and results in pitching-moment nonlinearities. The horizontal tail mounted below the fuselage resulted in noticeably higher directional stability in the low angle-of-attack range than did the horizontal tail in the other locations. However, the decrease in directional stability with increasing angle of attack generally was least with the high tail. The low-wing configurations provided higher directional stability than did the high-wing configurations at all test Mach numbers and angles of attack. Positive increments in effective dihedral were produced by the high wing and by positive geometric dihedral, the opposite effect being produced by the low wing or by negative geometric dihedral. A positive increment in effective dihedral was also produced by the high horizontal tail at the lower Mach numbers.

INTRODUCTION

A continuing study is being directed by the National Aeronautics and Space Administration to provide means of improving stability and control characteristics for aircraft configurations at supersonic speeds. One such study is aimed at determining the most favorable location for an aft horizontal tail on an airplane, and references 1 to 3 represent

some of the available data on variations in horizontal-tail location, primarily for low supersonic Mach numbers. Some of the problems concerning aft tail position include wing wake effects on the stability contribution of the tail and the tail effectiveness in the higher supersonic Mach number range.

Accordingly, an investigation was undertaken to determine the effects of horizontal-tail height on a configuration having variations in wing height and dihedral. Tests were made for horizontal-tail heights from a location beneath the fuselage to a near T-tail arrangement in combination with a high and a low 76° swept arrow wing (previously reported in ref. 4) having $\pm 5^{\circ}$ dihedral variations.

The tests were performed in the Langley Unitary Plan wind tunnel at Mach numbers from 1.90 to 4.63 for angles of attack from about -4° to 20° and angles of sideslip from about -4° to 8°.

SYMBOLS

The lateral force and moment data are referred to the body axis system and the longitudinal force and moment data are referred to the stability axis system. The reference center of moments was located at station 29.27 inches (74.35 cm).

b wing span, 20.00 in. (50.08 cm)

$\bar{c}$ mean geometric chord, 13.97 in. (35.50 cm)

C_D drag coefficient, $\frac{\text{Drag}}{qS}$

$C_{D,c}$ chamber drag coefficient, $\frac{\text{Chamber drag}}{qS}$

C_L lift coefficient, $\frac{\text{Lift}}{qS}$

C_l rolling-moment coefficient, $\frac{\text{Rolling moment}}{qSb}$

$C_{l_\beta} = \frac{\Delta C_l}{\Delta \beta}$, per degree

C_m pitching-moment coefficient, $\frac{\text{Pitching moment}}{qS\bar{c}}$

C_n yawing-moment coefficient, $\frac{\text{Yawing moment}}{qSb}$

$C_{n_\beta} = \frac{\Delta C_n}{\Delta \beta}$, per degree

C_Y side-force coefficient, $\frac{\text{Side force}}{qS}$

$C_{Y_\beta} = \frac{\Delta C_Y}{\Delta \beta}$, per degree

L/D lift-drag ratio

S reference wing area, 1.6200 sq ft $(0.146\ m^2)$

M free-stream Mach number

q free-stream dynamic pressure

r radius

x,y coordinates along X- and Y-axes, respectively

α angle of attack, deg

β angle of sideslip, deg

Γ dihedral angle, deg

ϵ adverse downwash angle at horizontal tail

$\frac{\delta C_m}{\delta_h}$ rate of change of pitching-moment coefficient with horizontal-tail deflection for constant angle of attack

δ_h horizontal-tail deflection with respect to fuselage center line, positive when leading edge is up, deg

ΔC_m increment between horizontal-tail-on and tail-off pitching-moment curve for constant angle of attack

APPARATUS AND TESTS

Model

Dimensional details of the model are presented in figure 1. The wing had a 76° sweepback of the leading edge and circular-arc $2\frac{1}{2}$-percent-thick, airfoil sections in the streamwise directions. Five wing configurations were tested; high with 5°, 0°, and -5° dihedral; and low with 0° and 5° dihedral. The vertical tail had 45° leading-edge sweep and consisted of a flat-plate section with beveled leading and trailing edges. The horizontal tail had a symmetrical airfoil section with 52° leading-edge sweep. Five horizontal-tail positions varying from below the fuselage (position 1) to near the top of the vertical tail (position 5) were utilized. The horizontal tail in position 2 (on the fuselage center line) had less exposed area than the horizontal tail in the other positions.

Tunnel

Tests were conducted in both the low and high Mach number test section of the Langley Unitary Plan wind tunnel, which is a variable-pressure continuous-flow tunnel. The test sections are approximately 4 feet (1.24 m) square and 7 feet (2.13 m) long. The nozzles leading to the test sections are of the asymmetric sliding-block type which permits continuous variations in Mach number from about 1.5 to 2.9 in the low Mach number test section, and from about 2.3 to 4.7 in the high Mach number test section.

Test Conditions

The test conditions for the investigation were as follows:

Mach number	Stagnation temperature		Stagnation pressure				Reynolds number			
			Longitudinal data		Lateral data		Longitudinal data		Lateral data	
	°F	°K	lb/sq in.	N/m^2	lb/sq in.	N/m^2	per foot	per meter	per foot	per meter
1.90	150	339	13.21	91 079.74	8.81	60 742.81	3.0×10^6	9.144×10^6	2.0×10^6	6.096×10^6
2.30	150	339	15.92	109 764.53	10.61	73 153.37	3.0	9.144	2.0	6.096
2.96	150	339	22.79	157 131.51	15.17	104 593.46	3.0	9.144	2.0	6.096
3.96	175	352	40.13	276 686.60	40.13	276 686.60	3.0	9.144	3.0	9.144
4.63	175	352	54.75	377 487.96	54.75	377.487.96	3.0	9.144	3.0	9.144

The configurations were tested through an angle-of-attack range from about -4° to 20° and through an angle-of-sideslip range from about -4° to 8°. Sideslip derivatives were obtained from angle-of-attack polars at $\beta = 0°$ and 4°. The stagnation dewpoint was maintained below -30° F in order to avoid condensation effects. Strips of carborundum grains 1/16 inch (0.159 cm) wide were affixed around the body 1 inch (2.54 cm) from the nose and on the wings 1/2 inch (1.27 cm) from the leading edge in a streamwise direction. Number 60 carborundum grit (0.0108 in. (0.0274 cm) nominal diameter) was used for the

nose and number 80 carborundum grit (0.0076 in. (0.0193 cm) nominal diameter) was used for the wings and tail surfaces.

Measurements

Aerodynamic forces and moments were measured by means of a six-component electrical strain-gage balance housed within the model. The balance, in turn, was rigidly fastened to a sting support and thence to the tunnel support system. The balance-chamber pressure was measured for each model and test condition.

Accuracy

The accuracy of the individual measured quantities, based on calibrations, is estimated to be within the following limits:

C_D	±0.0004
C_L	±0.005
C_l	±0.0002
C_m	±0.0005
C_n	±0.0003
C_Y	±0.003
α, deg	±0.10
β, deg	±0.10
Mach number:	
1.90 to 2.96	±0.015
3.96 and 4.63	±0.050

Corrections

Angles of attack were corrected for tunnel flow angularity and angles of attack and sideslip were corrected for deflection of the balance and sting support due to aerodynamic loads. The results were adjusted to free-stream static pressure at the model base and typical chamber drag coefficients are shown in figure 2.

PRESENTATION OF RESULTS

The results of the investigation are presented in the following figures:

DISCUSSION

Longitudinal Characteristics

Longitudinal aerodynamic characteristics of the model with variations in horizontal-tail height, wing height, and wing geometric dihedral are presented in figures 3 to 7. Figures 8 and 9 present a composite of the effects of wing height and geometric dihedral for the horizontal tail in positions 2 and 5, respectively. Geometric dihedral generally leads to small losses in stability at the higher lift coefficients.

The results presented in figure 8 show the low-wing configurations to have a lower level of stability at moderate-to-high lift coefficients than the high-wing configurations through the test Mach number range. In figure 9, the effects of wing height tend to be masked by pitching-moment-curve nonlinearities associated with the high horizontal tail (position 5).

The data indicate a reduction in longitudinal stability for both the high- and low-wing configurations at moderate lift coefficients and at the lower test Mach numbers (fig. 8(a)). For the higher test Mach numbers (for example, fig. 8(e)), the stability loss is still well defined for the low-wing configurations but is not in evidence for the high-wing configurations. The improved stability characteristics of the high-wing configurations are a result of the high dynamic pressure field created beneath the wing at the higher Mach numbers acting on the aft section of the fuselage at the higher angles of attack. For the low-wing configurations, the high dynamic pressure field has little effect on the aft fuselage.

It should be noted that the horizontal tail in position 2 has less exposed area than the horizontal tail at the other test positions. Nevertheless, the contribution for the horizontal tail in position 2 is generally as good as or better than that for the horizontal tail in position 1, except at the higher angles of attack for the low-wing configuration. With the horizontal tail mounted above the fuselage (positions 3, 4, 5), there are significant losses of tail contribution with increasing angle of attack, particularly at the lower test Mach numbers. These losses in contribution lead to rather severe nonlinearities in the model pitching-moment curves (figs. 3 to 7).

The adverse stability effects incurred with the horizontal tails located above the fuselage occur as the horizontal tail enters an unfavorable flow field in the wing wake region. In an attempt to define better the adverse local flow field incurred by the high horizontal tails, the parameter $\frac{\delta C_m/\delta_h}{(\delta C_m/\delta_h)_{\alpha=0^o}}$ is presented in figure 10 to provide an indication of the horizontal-tail effectiveness at some angle of attack with respect to the tail effectiveness at $\alpha = 0^o$.

The values of ϵ, adverse downwash at the tail, were obtained from the data of figures 11 and 12 by using the relation $\epsilon = \alpha + \delta_h - \alpha_t$ where α_t (horizontal-tail angle of attack) is assumed to be zero for those angles of attack at which the tail-on C_m curve intersects the tail-off C_m curve. At other angles of attack, the relation $\alpha_t = \frac{\Delta C_m}{\delta C_m / \delta_h}$ was used.

For $M = 1.90$ the loss in contribution for the high horizontal tail with increasing α may be deduced to be a result of adverse downwash with little change in tail effectiveness. At $M = 4.63$, however, variations in tail effectiveness and downwash are both in evidence. Generally, any loss in tail contribution for the high horizontal tail is realized earlier for the high-wing configurations than for the low-wing configurations. The low horizontal tail generally exhibits linear pitching-moment contributions through the test angle-of-attack range and at the higher Mach number generally produces more pitching-moment contribution than the high tail.

The effects of horizontal-tail deflection on the pitch characteristics of the high- and low-wing configurations are shown in figures 11 and 12. It should again be noted that the exposed area for the low tail is less than that for the high tail. Therefore, a horizontal-tail deflection of -10° generally resulted in greater absolute tail effectiveness for the high tail than for the low tail. However, at the higher angles of attack at the higher Mach numbers, the effectiveness of the low tail, due to the more favorable local flow field, exceeds that for the high tail in some cases. (See figs. 11(d) and 11(e), for example.)

Lateral-Directional Characteristics

The effects of horizontal-tail height on static directional and lateral stability are presented in figures 13 to 17, the effects of wing height and dihedral being summarized in figures 18 and 19. The horizontal tail in position 1 results in the highest level of directional stability at the lower angles of attack of all the test configurations. The directional stability decreases with increasing angle of attack for each configuration but the decrease is somewhat less for the high tail (position 5). (All configurations become directionally unstable at the higher test angles of attack.)

The low-wing tail-on configurations are generally more stable directionally than the high-wing configurations at all Mach numbers and angles of attack (figs. 18 and 19) for each horizontal-tail position. This stability is inherent for a low-wing configuration because of a favorable induced sidewash on the vertical tail. (See ref. 1.)

For the low-wing model, positive geometric dihedral generally leads to slight losses in C_{n_β} throughout the angle-of-attack range. For the high-wing model, positive geometric dihedral generally leads to a slight loss in C_{n_β} at low angles of attack but

produces generally higher values of C_{n_β} at the higher angles of attack. An opposite effect is noted for the negative geometric dihedral with the high-wing model.

The effective dihedral in the low angle-of-attack range is the least with the low-wing models and the greatest with the high-wing models throughout the Mach number range. This result is typical of that which also occurs at subsonic speeds and is due to the differential angle of attack induced near the wing root by the body cross-flow component. The use of geometric dihedral in producing C_{l_β} is also effective throughout the Mach number range and produces results similar to those that occur at subsonic speeds, that is, an increase in $-C_{l_\beta}$ with positive geometric dihedral and a decrease in $-C_{l_\beta}$ with negative geometric dihedral. The effects of wing height and geometric dihedral are additive such that the most negative values of C_{l_β} generally occur for the configuration with the high wing and 5° of geometric dihedral; or the increase in dihedral effect caused by a high wing can be offset to some extent through the use of negative geometric dihedral.

At the lower Mach numbers, slightly more negative values of C_{l_β} were obtained with the high horizontal tail (fig. 19) than with the center-line tail (fig. 19). This condition is a result of the increase in side force on the vertical tail induced by the endplating effect of the high horizontal tail. This effect disappears at the higher Mach numbers.

CONCLUSIONS

Results of wind-tunnel tests to determine the effects of horizontal-tail height, wing height, and dihedral on the longitudinal and lateral-directional stability characteristics of a 76° swept arrow-wing airplane model at Mach numbers from 1.90 to 4.63 indicate the following conclusions:

1. Generally, for the angle-of-attack and Mach number range presented herein, the horizontal tail mounted above the fuselage will pass through an adverse flow region and result in pitching-moment nonlinearities.

2. The horizontal tail mounted below the fuselage resulted in noticeably higher directional stability in the low angle-of-attack range than did the horizontal tail in the other locations. The decrease in directional stability with increasing angle of attack, however, generally was least with the high tail.

3. The low-wing configurations provided higher directional stability than did the high-wing configurations at all test Mach numbers and angles of attack.

4. Positive increments in effective dihedral were produced by the high wing and by positive geometric dihedral, the opposite effect being produced by the low wing or by

negative geometric dihedral. A positive increment in effective dihedral was also produced by the high horizontal tail at the lower Mach numbers.

Langley Research Center,
National Aeronautics and Space Administration,
Langley Station, Hampton, Va., February 23, 1967,
126-13-02-04-23.

REFERENCES

1. Spearman, M. Leroy; and Robinson, Ross B.: Investigation of the Aerodynamic Characteristics in Pitch and Sideslip of a 45° Swept-Wing Airplane Configuration With Various Vertical Locations of the Wing and Horizontal Tail – Static Lateral and Directional Stability; Mach Numbers of 1.41 and 2.01. NACA RM L57J25a, 1957.

2. Robinson, Ross B.: Effects of Vertical Location of the Wing and Horizontal Tail on the Static Lateral and Directional Stability of a Trapezoidal-Wing Airplane Model at Mach Numbers of 1.41 and 2.01. NACA RM L58C18, 1958.

3. Fuller, Dennis E.; and Morris, Odell A.: Effect of Horizontal-Tail Height on Aerodynamic Characteristics of a Transport Model With a Variable-Sweep Warped Wing. NASA TM X-1062, 1965.

4. Fuller, Dennis E.; and Feryn, Maurice: Effect of Wing Height and Dihedral on Stability Characteristics of a 76° Swept Wing Body at Mach Numbers From 1.60 to 4.63. NASA TM X-1023, 1964.

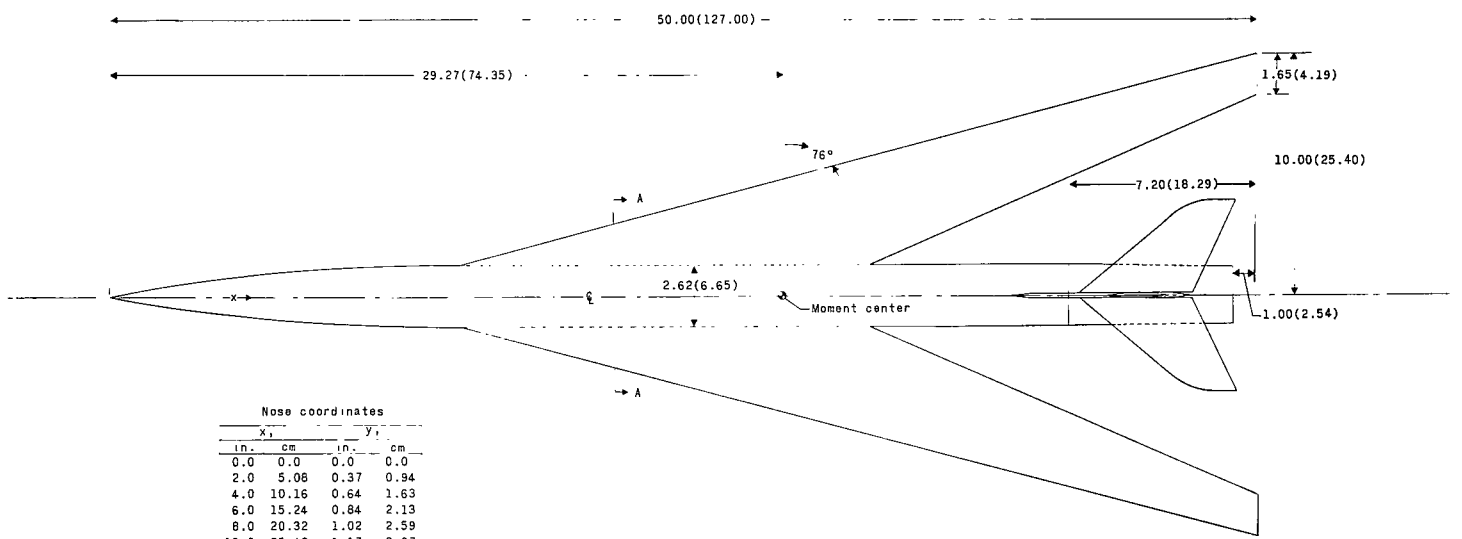

Nose coordinates

x,		y,	
in.	cm	in.	cm
0.0	0.0	0.0	0.0
2.0	5.08	0.37	0.94
4.0	10.16	0.64	1.63
6.0	15.24	0.84	2.13
8.0	20.32	1.02	2.59
10.0	25.40	1.17	2.97
12.0	30.48	1.26	3.20
14.0	35.56	1.31	3.33

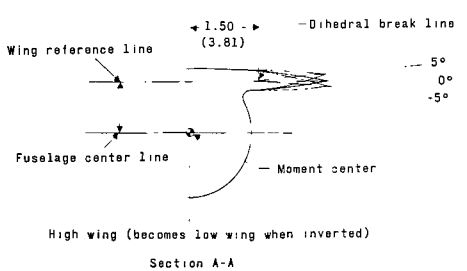

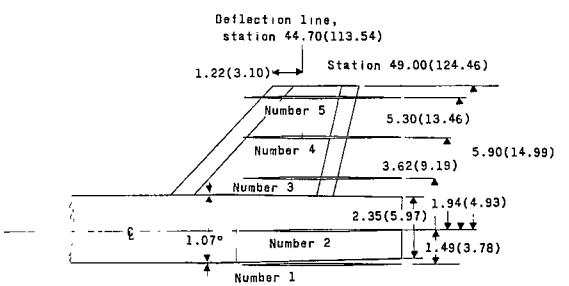

(a) Complete model.

Figure 1.- Model details. (All dimensions are given in inches with centimeters in parentheses, unless otherwise noted.)

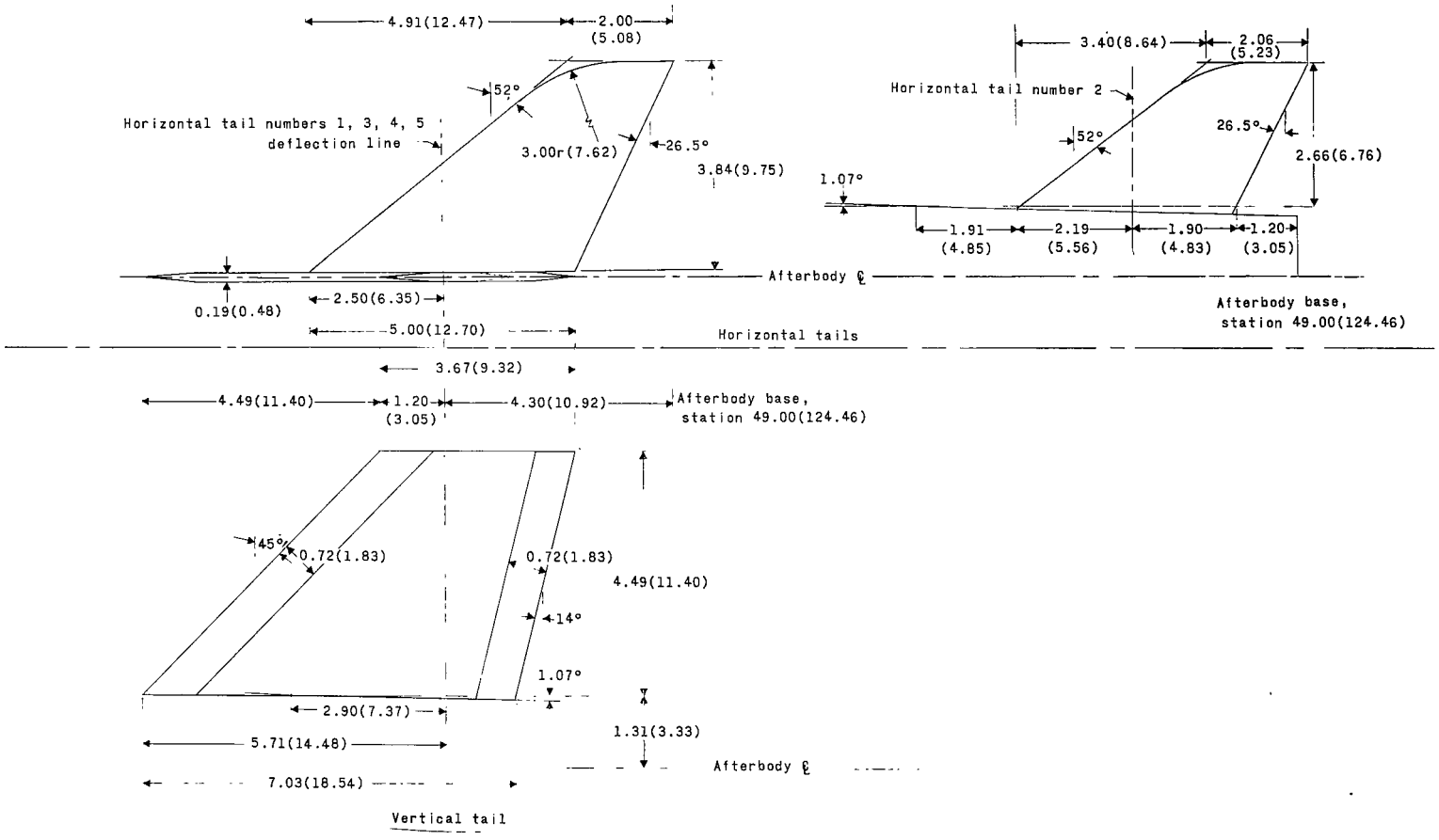

(b) Vertical and horizontal tail.

Figure 1.- Concluded.

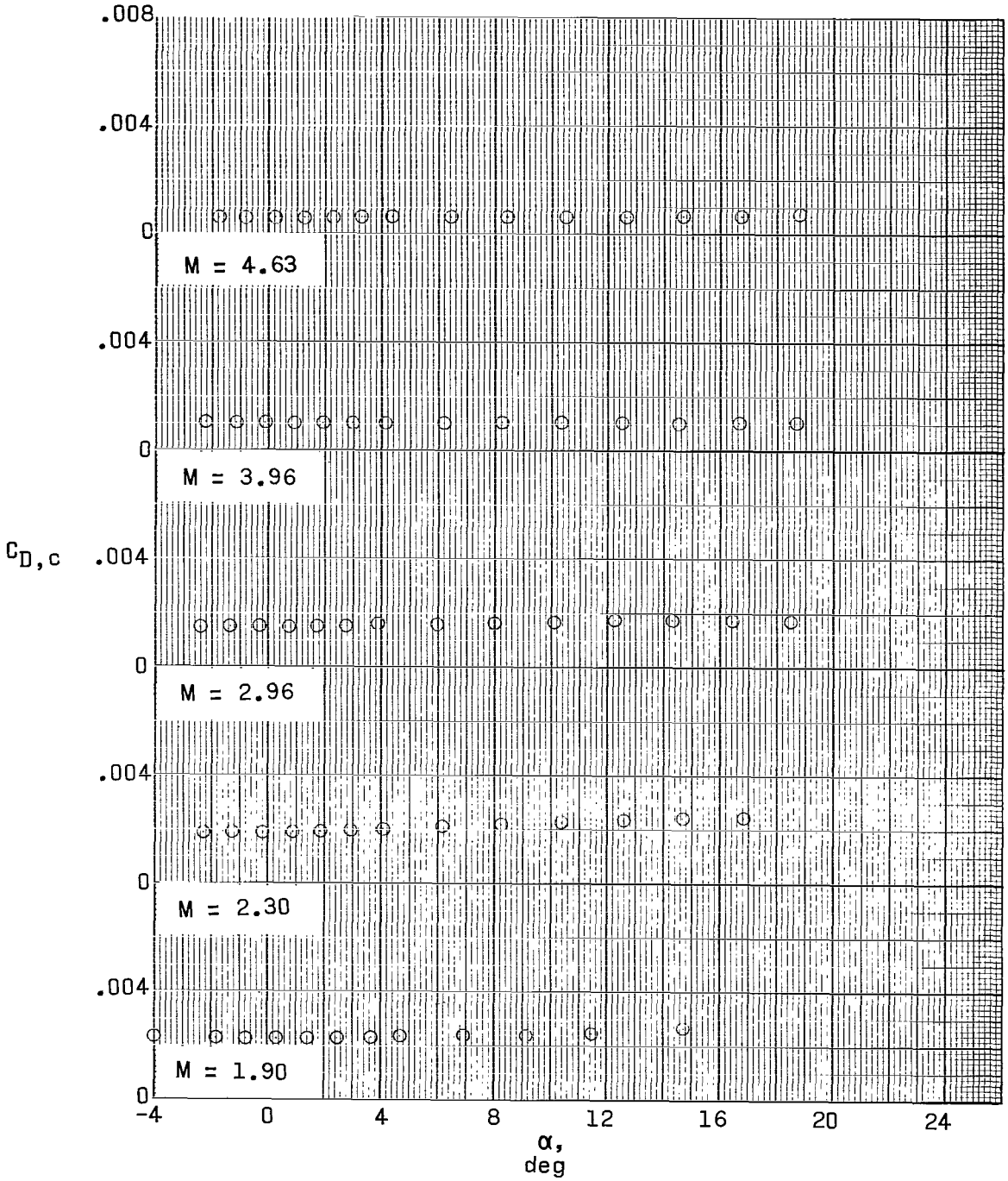

Figure 2.- Typical chamber drag values used for corrections.

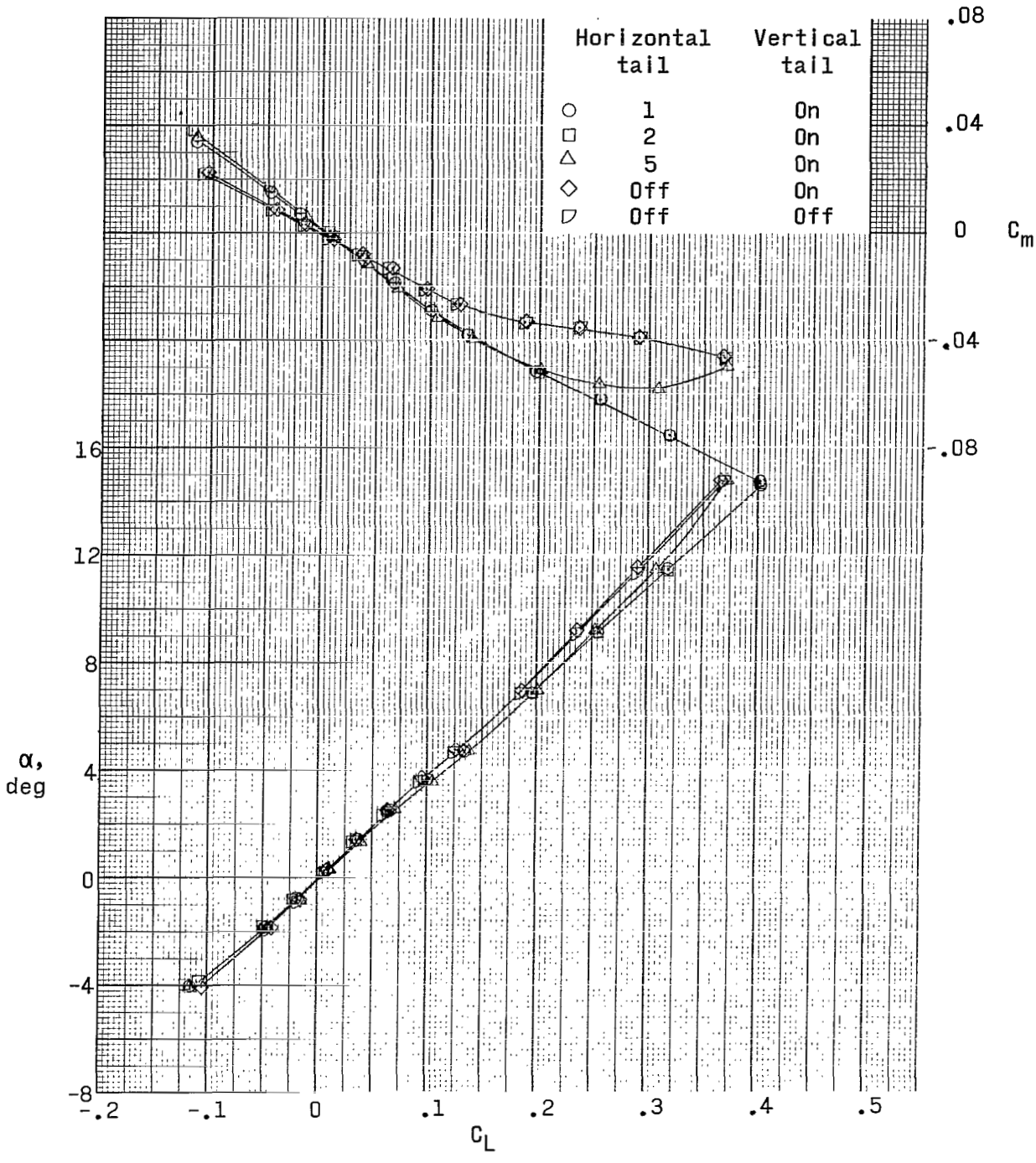

(a) M = 1.90.

Figure 3.- Effect of horizontal-tail height on aerodynamic characteristics in pitch. High wing; 0^o dihedral.

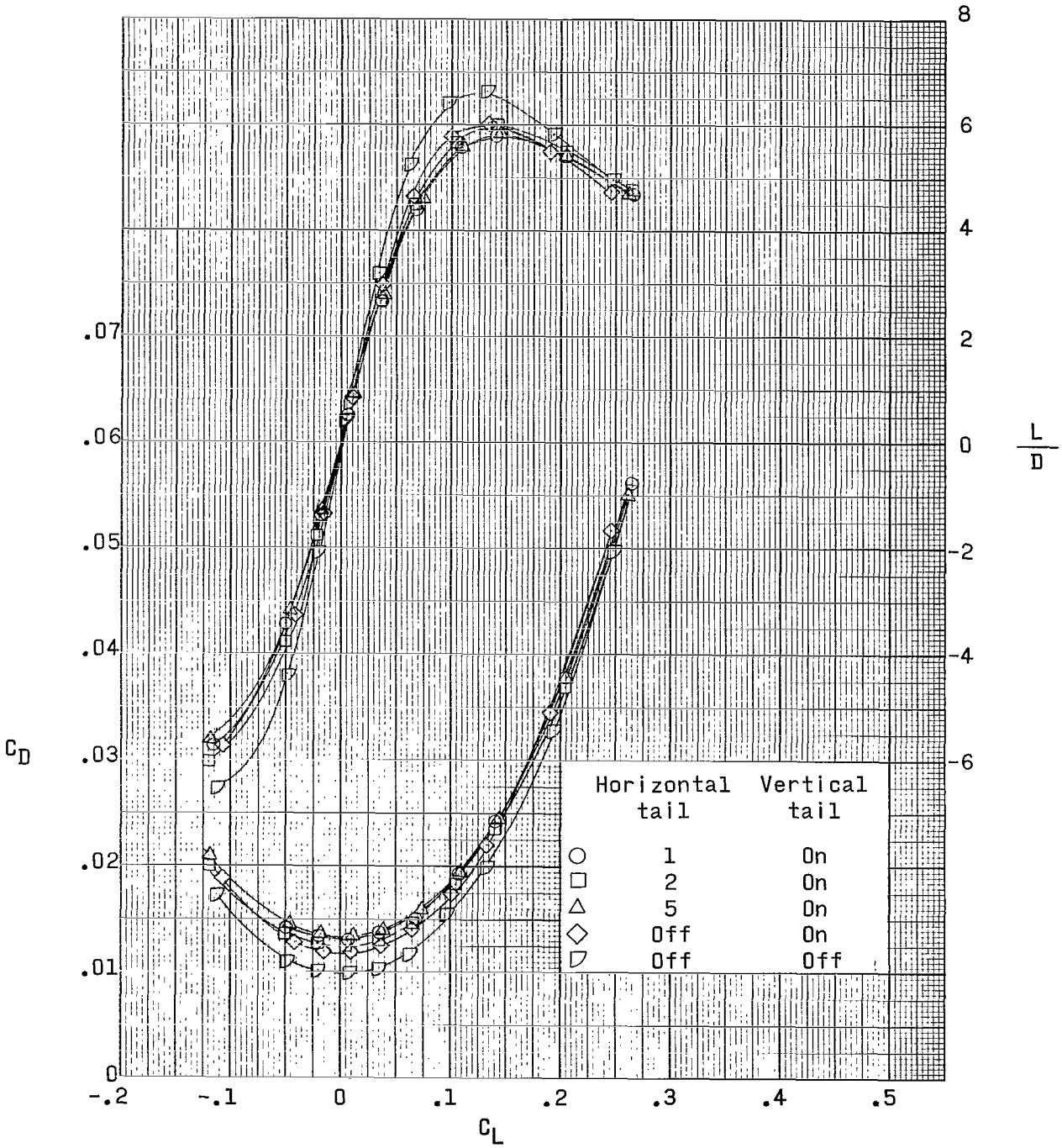

(a) Concluded.

Figure 3.- Continued.

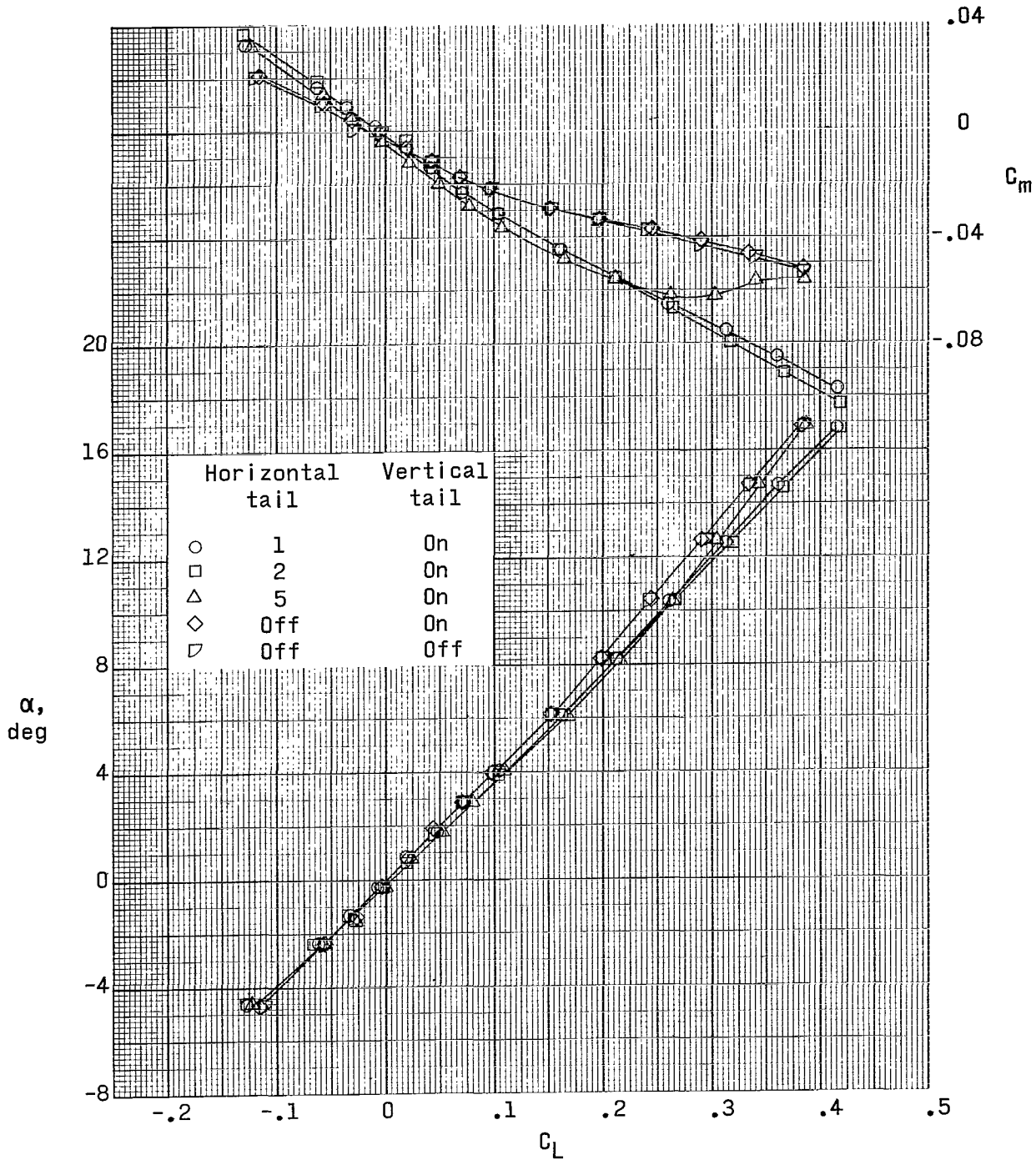

(b) M = 2.30.

Figure 3.- Continued.

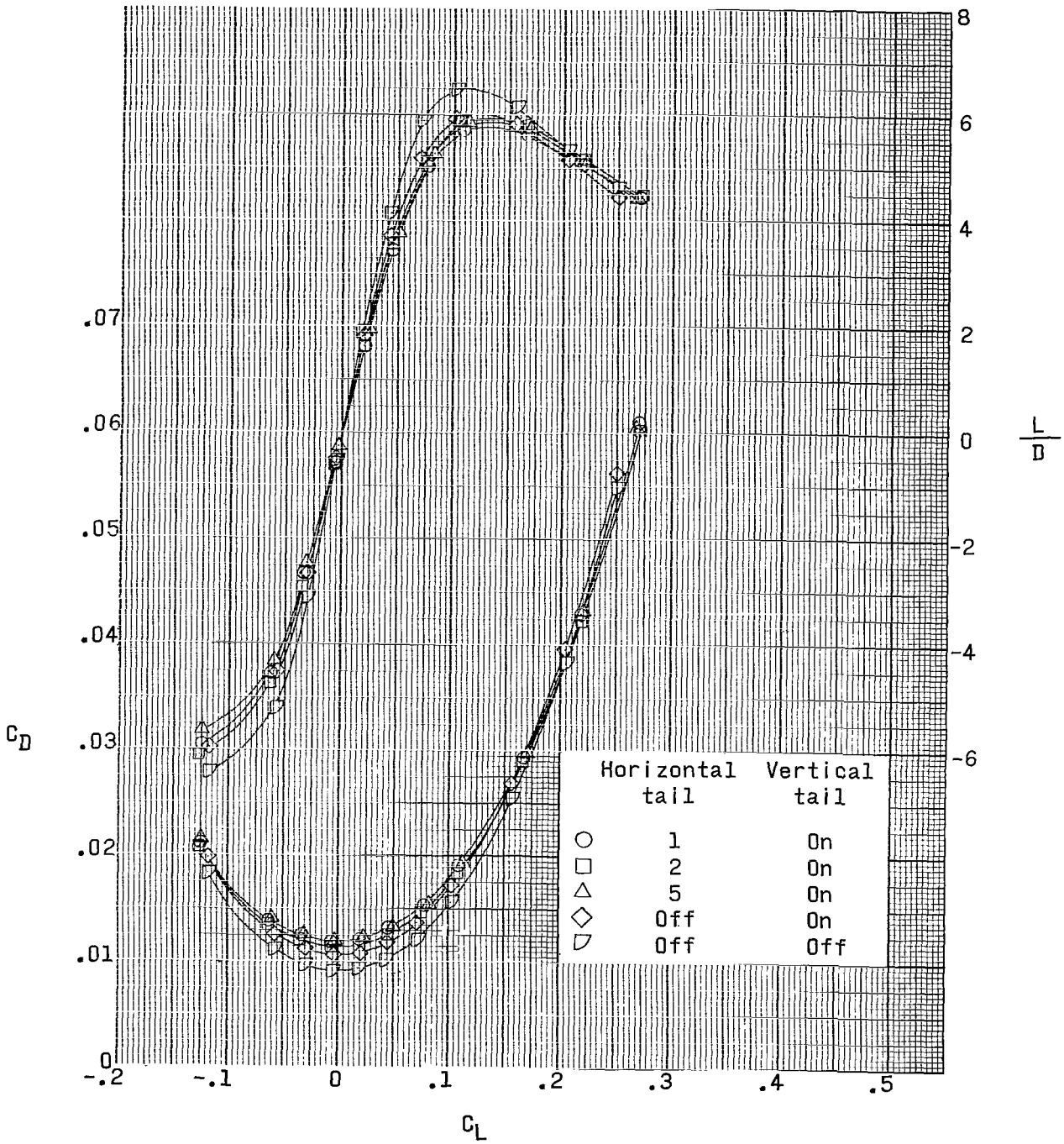

(b) Concluded.

Figure 3.- Continued.

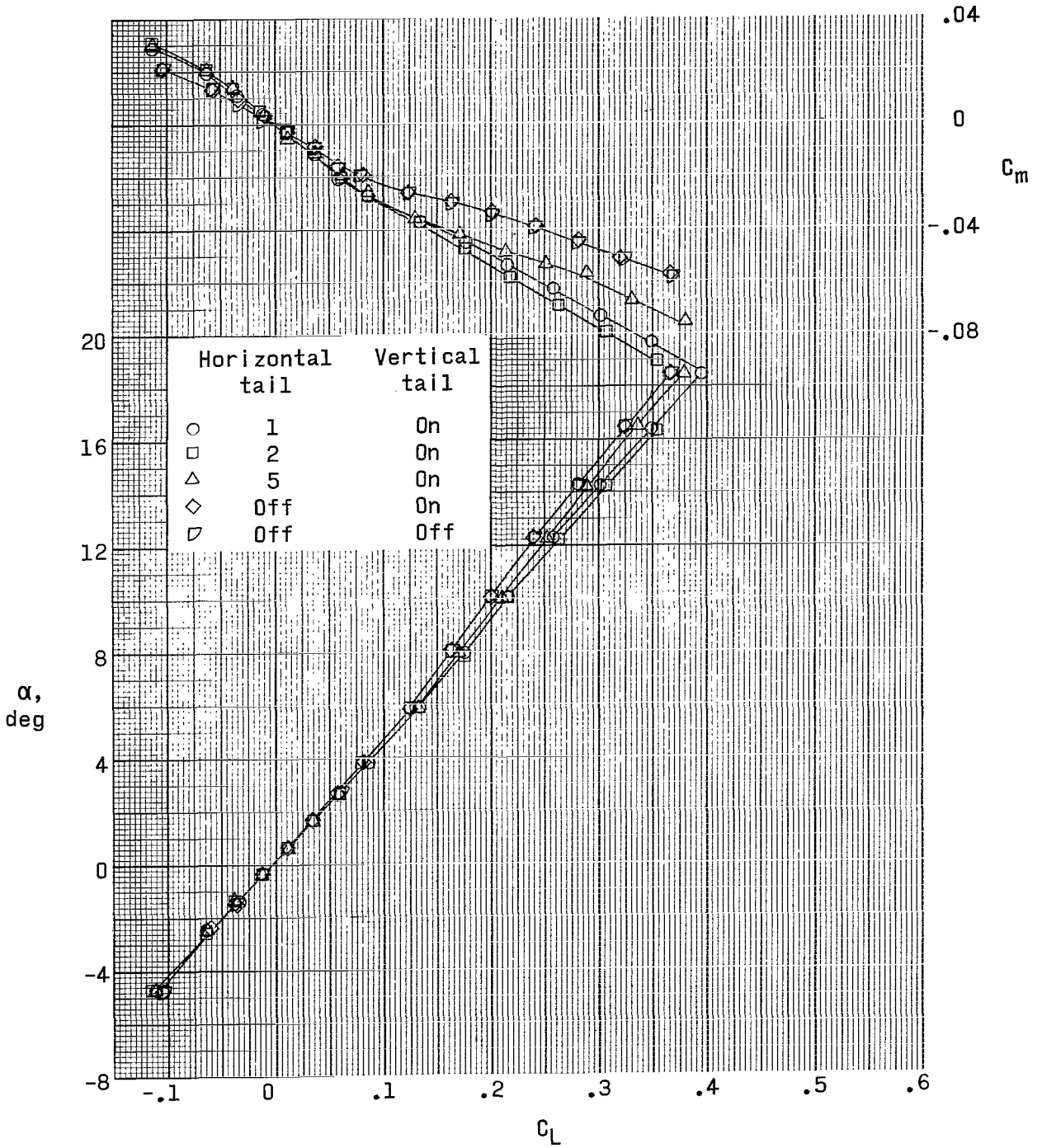

(c) M = 2.96.

Figure 3.- Continued.

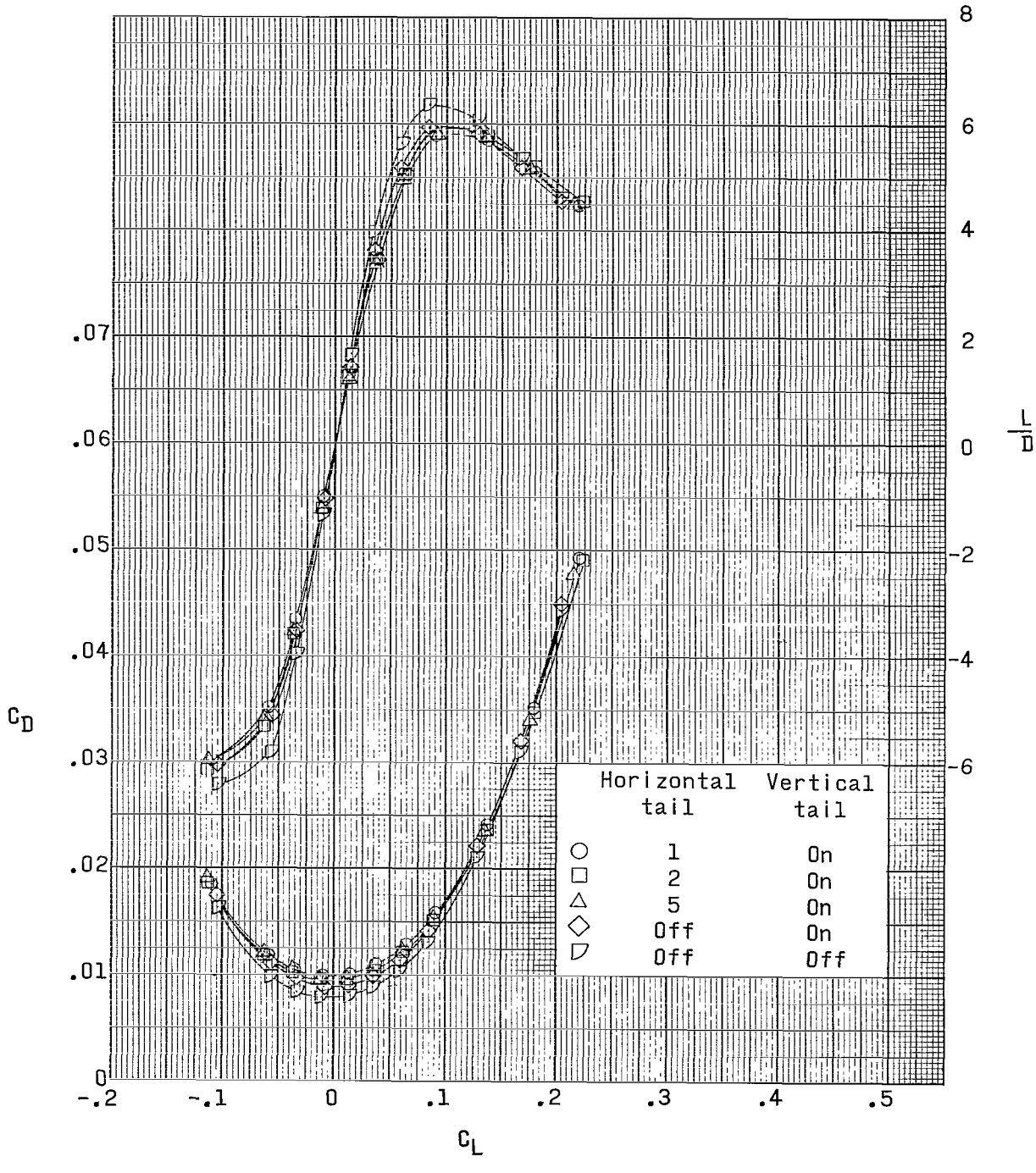

(c) Concluded.

Figure 3.- Continued.

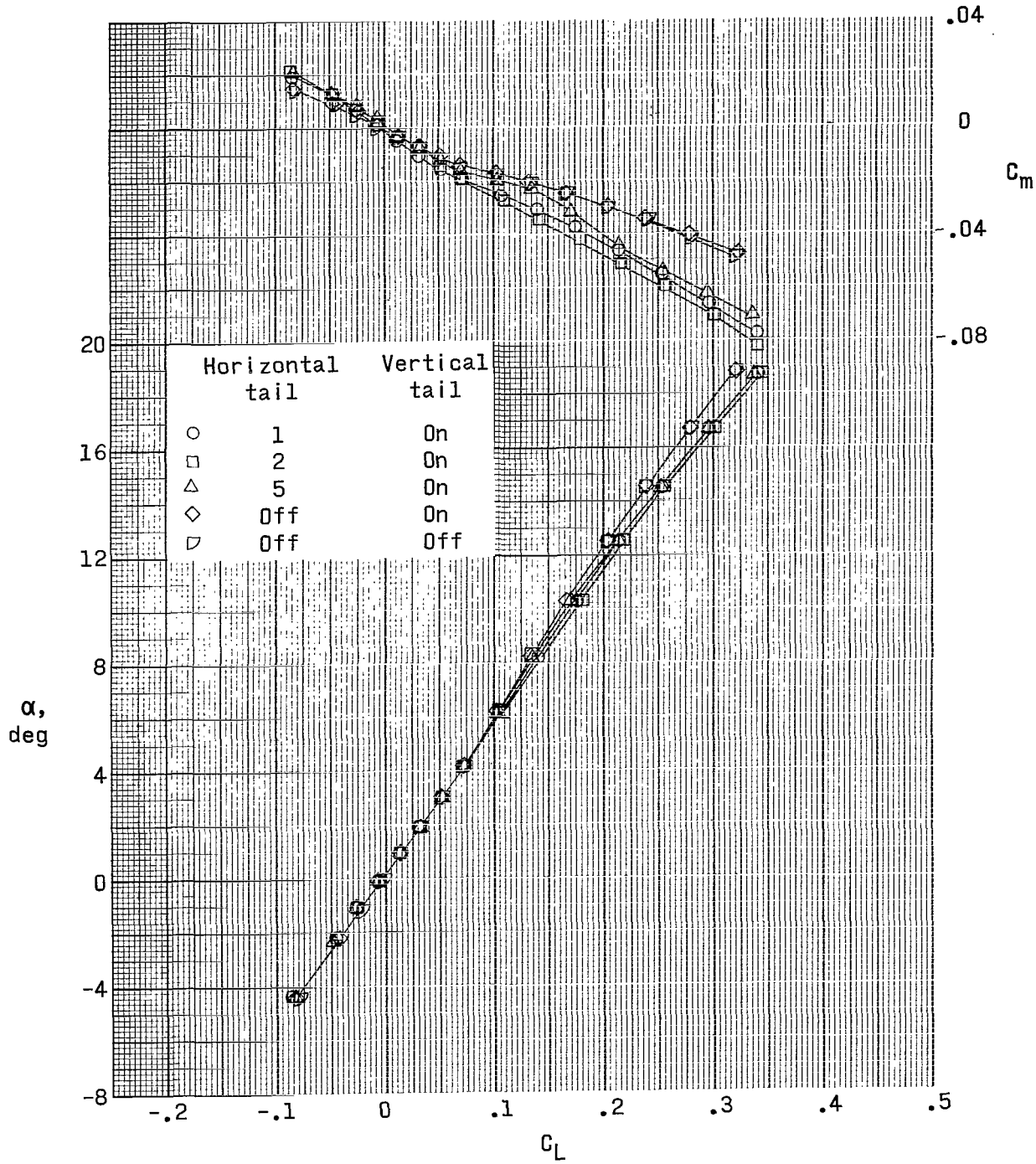

(d) M = 3.95.

Figure 3.- Continued.

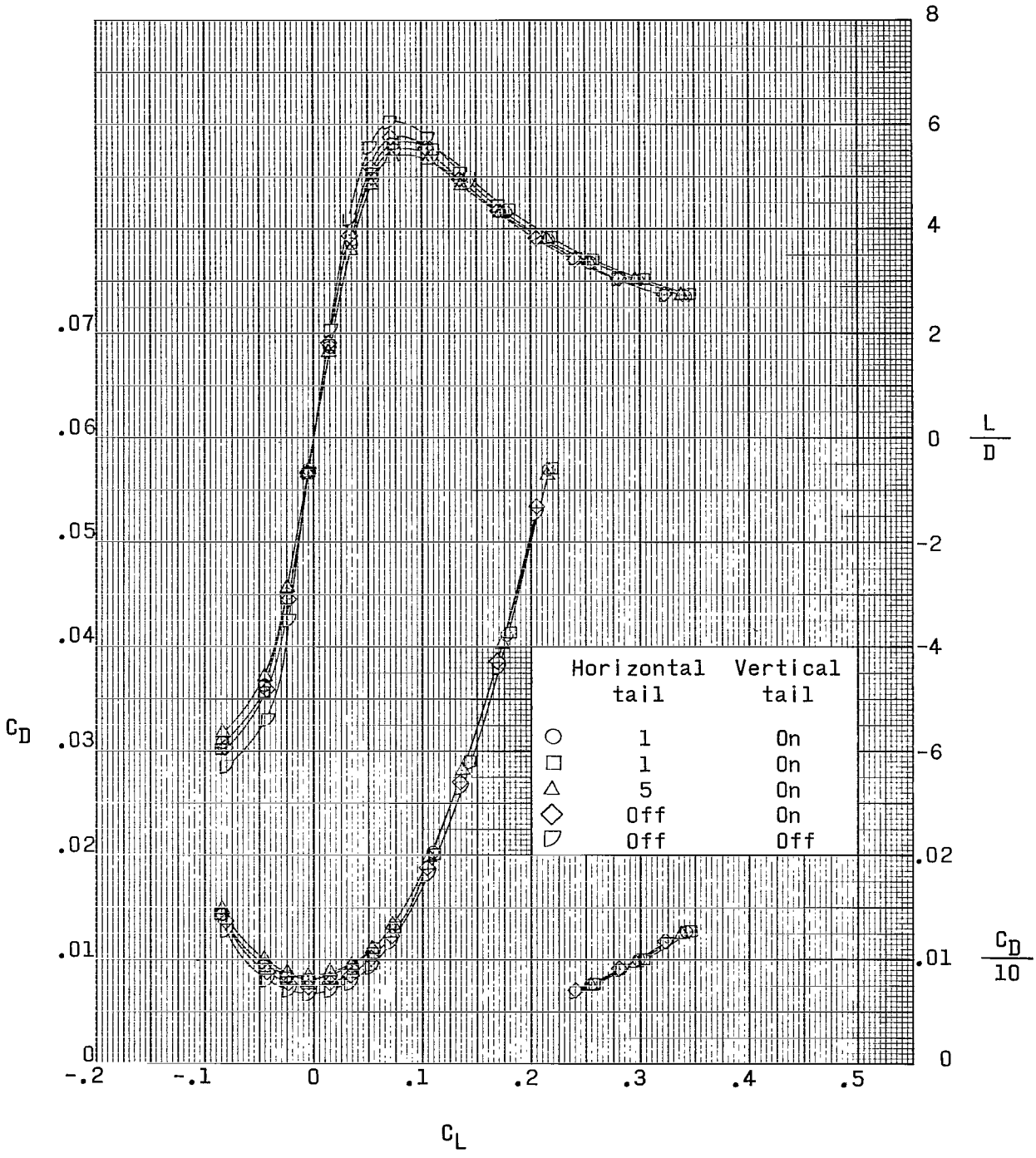

(d) Concluded.

Figure 3.- Continued.

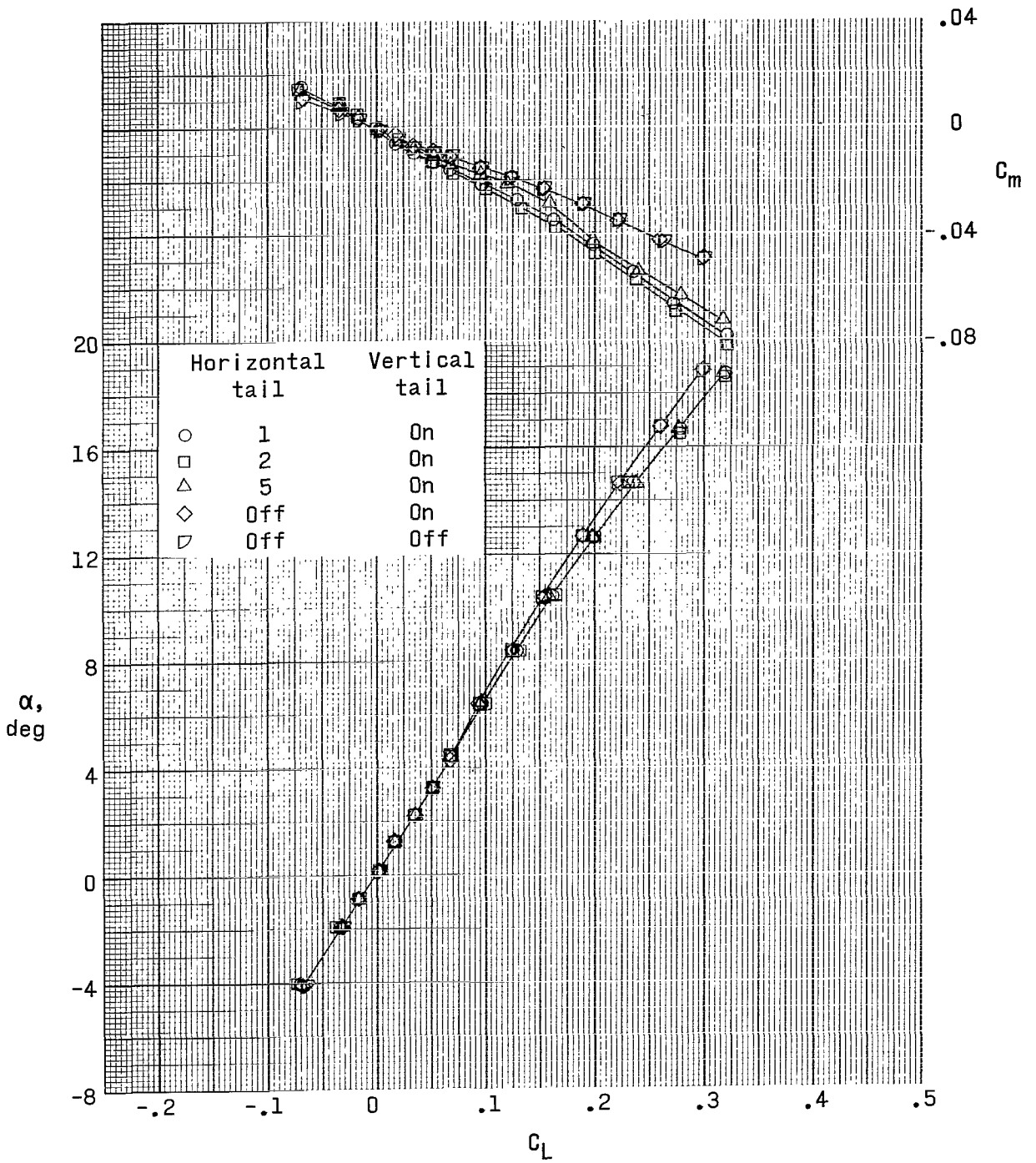

(e) M = 4.63.

Figure 3.- Continued.

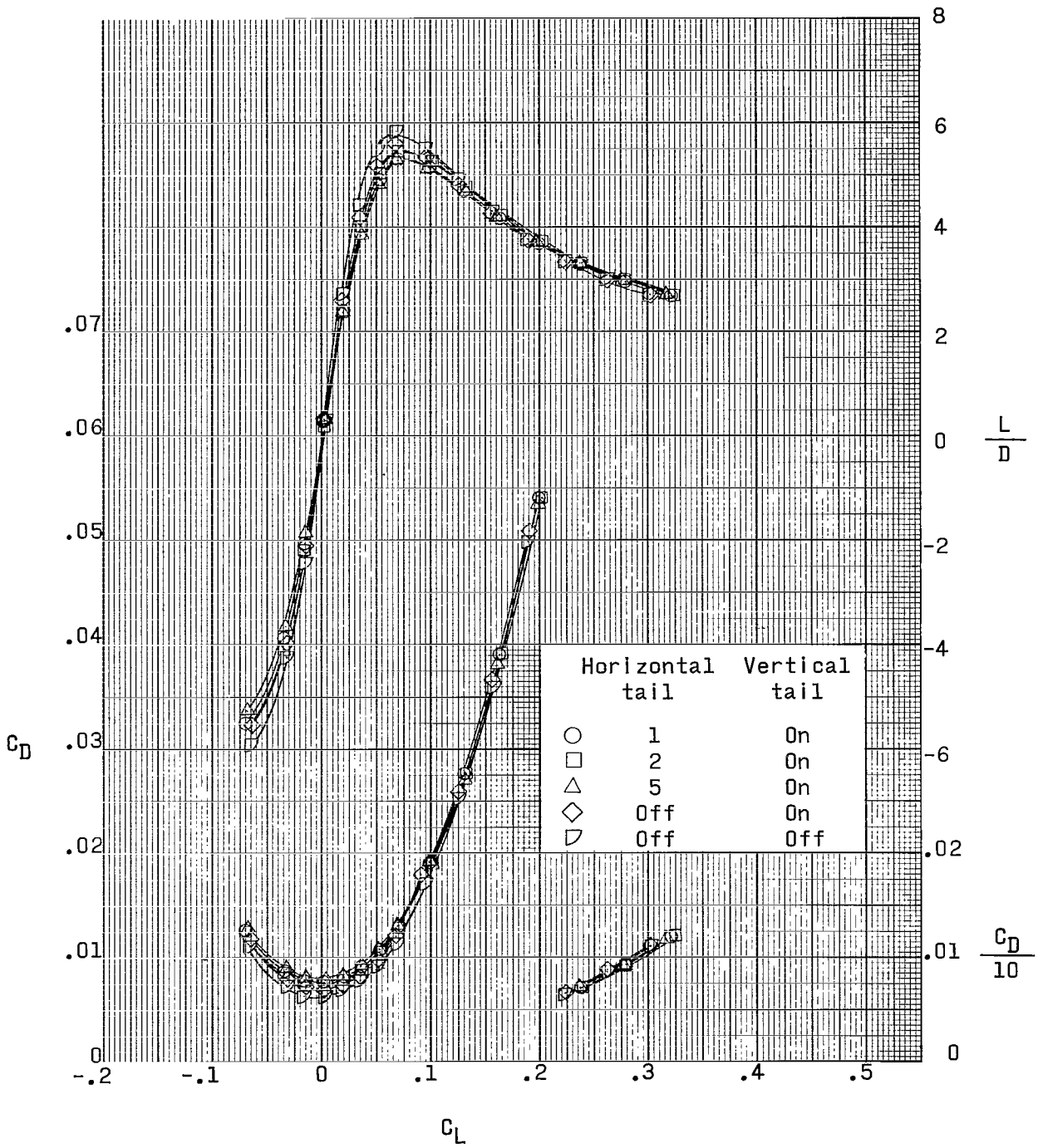

(e) Concluded.

Figure 3.- Concluded.

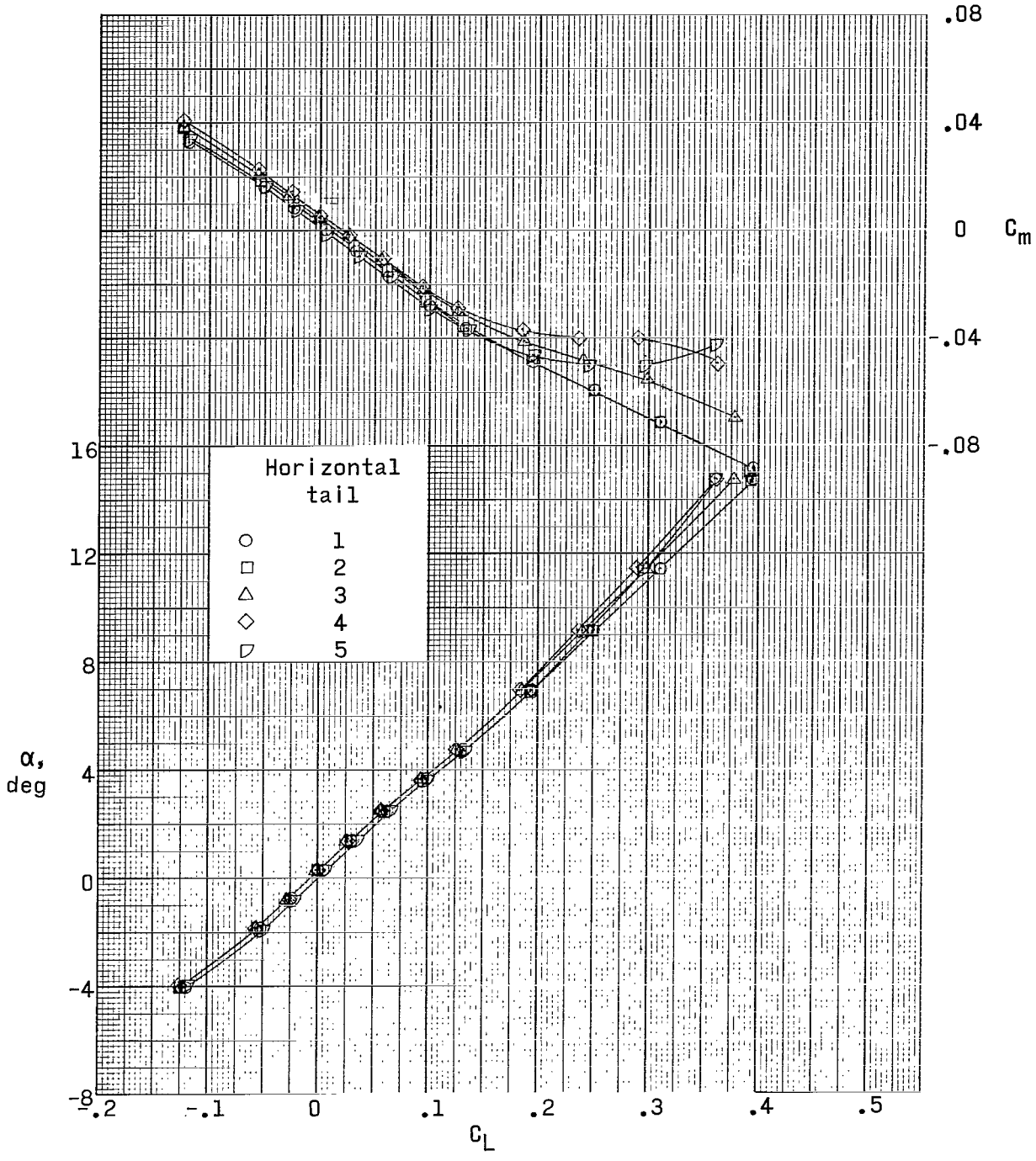

(a) M = 1.90.

Figure 4.- Effect of horizontal-tail height on aerodynamic characteristics in pitch. High wing; 5° dihedral.

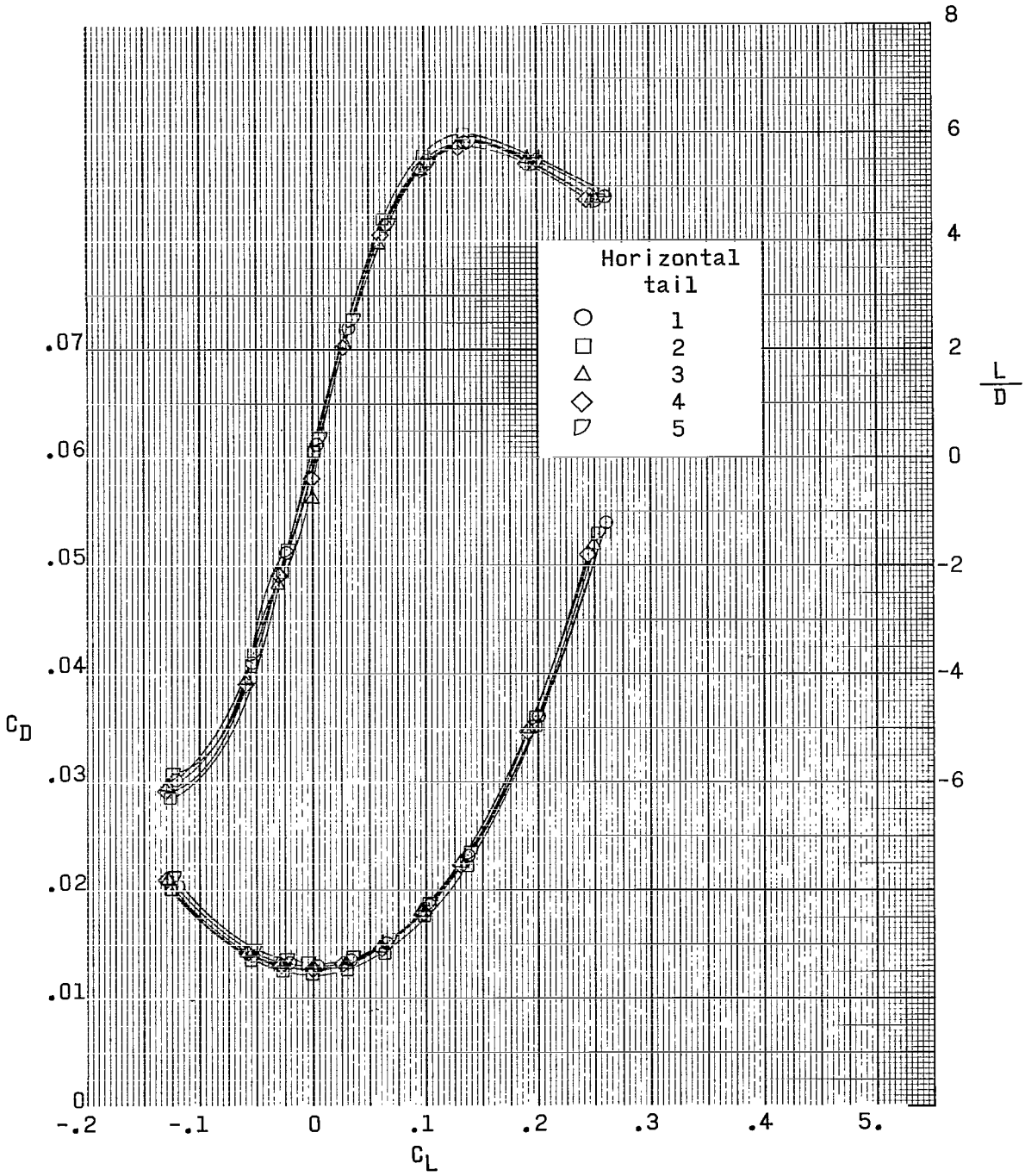

(a) Concluded.

Figure 4.- Continued.

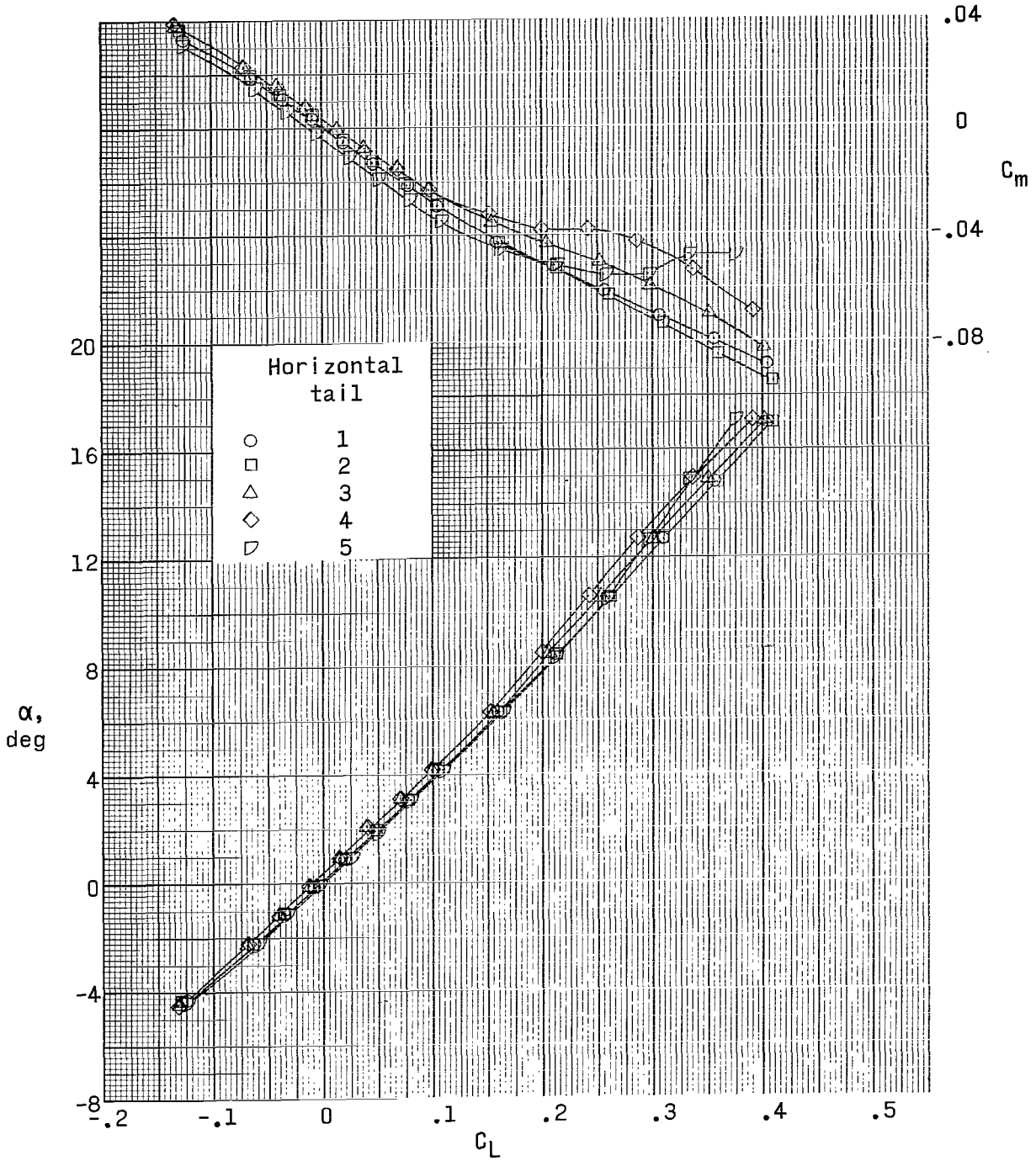

(b) M = 2.30.

Figure 4.- Continued.

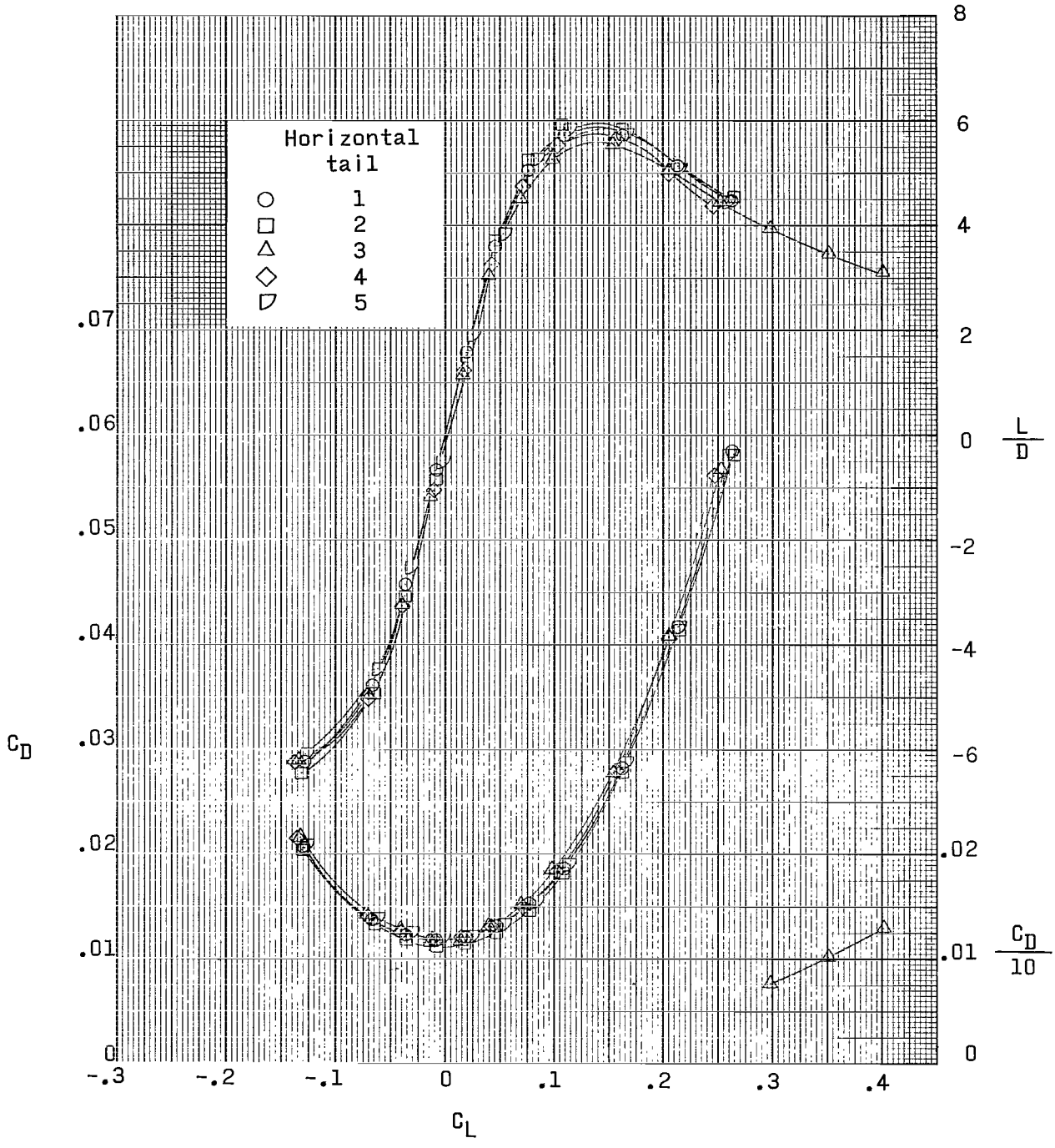

(b) Concluded.

Figure 4.- Continued.

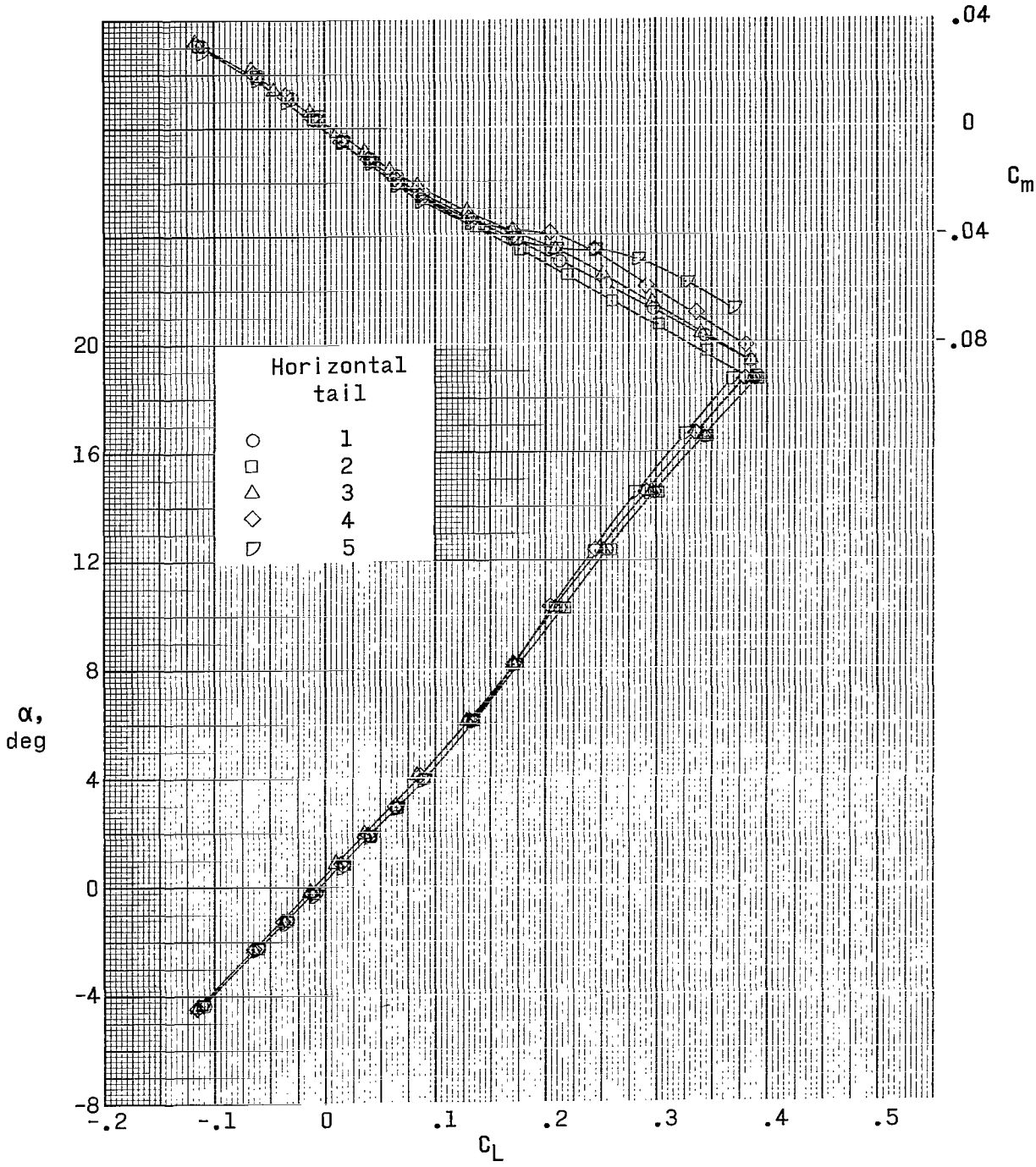

(c) M = 2.96.

Figure 4.- Continued.

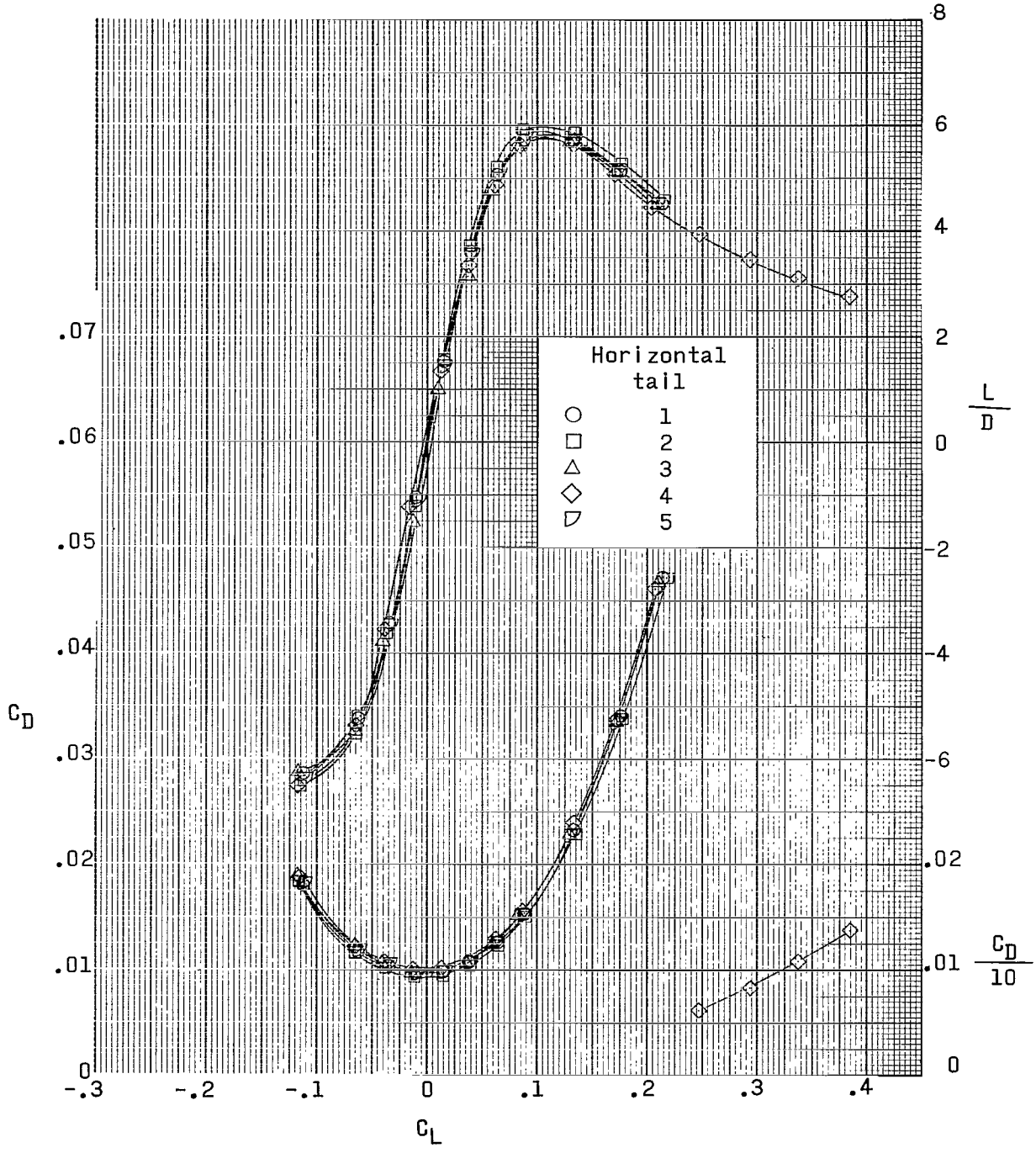

(c) Concluded.

Figure 4.- Continued.

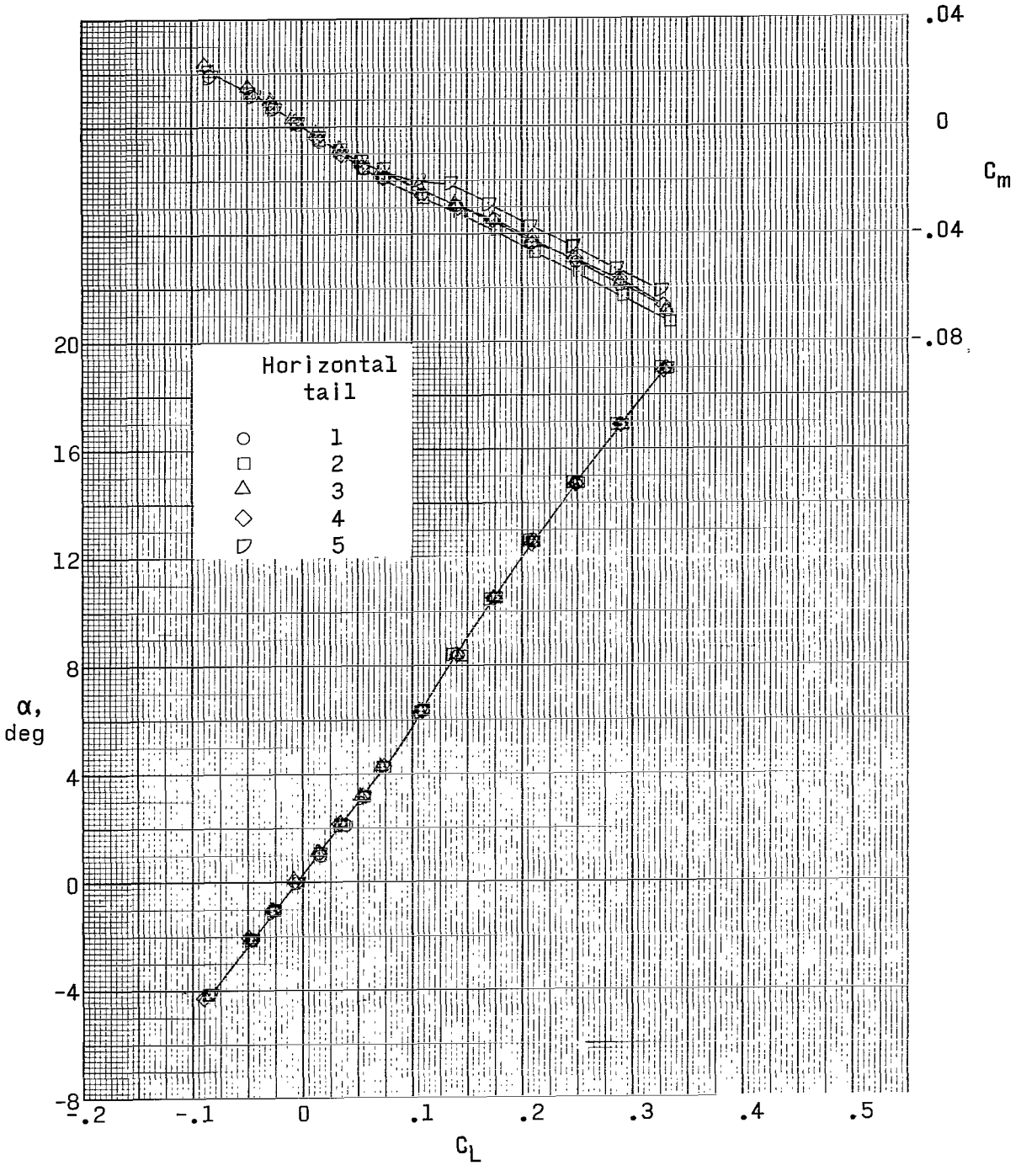

(d) M = 3.95.

Figure 4.- Continued.

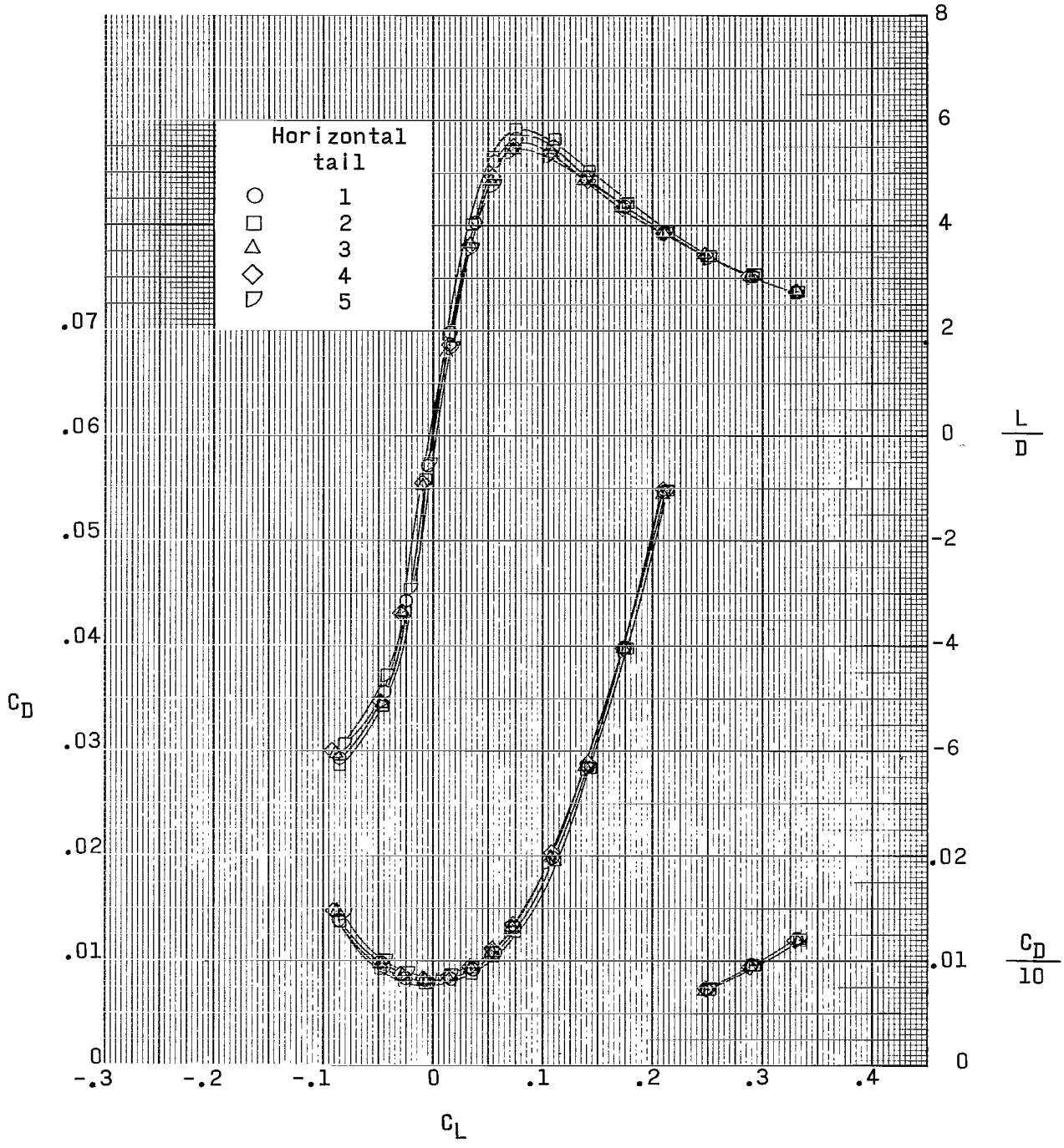

(d) Concluded.

Figure 4.- Continued.

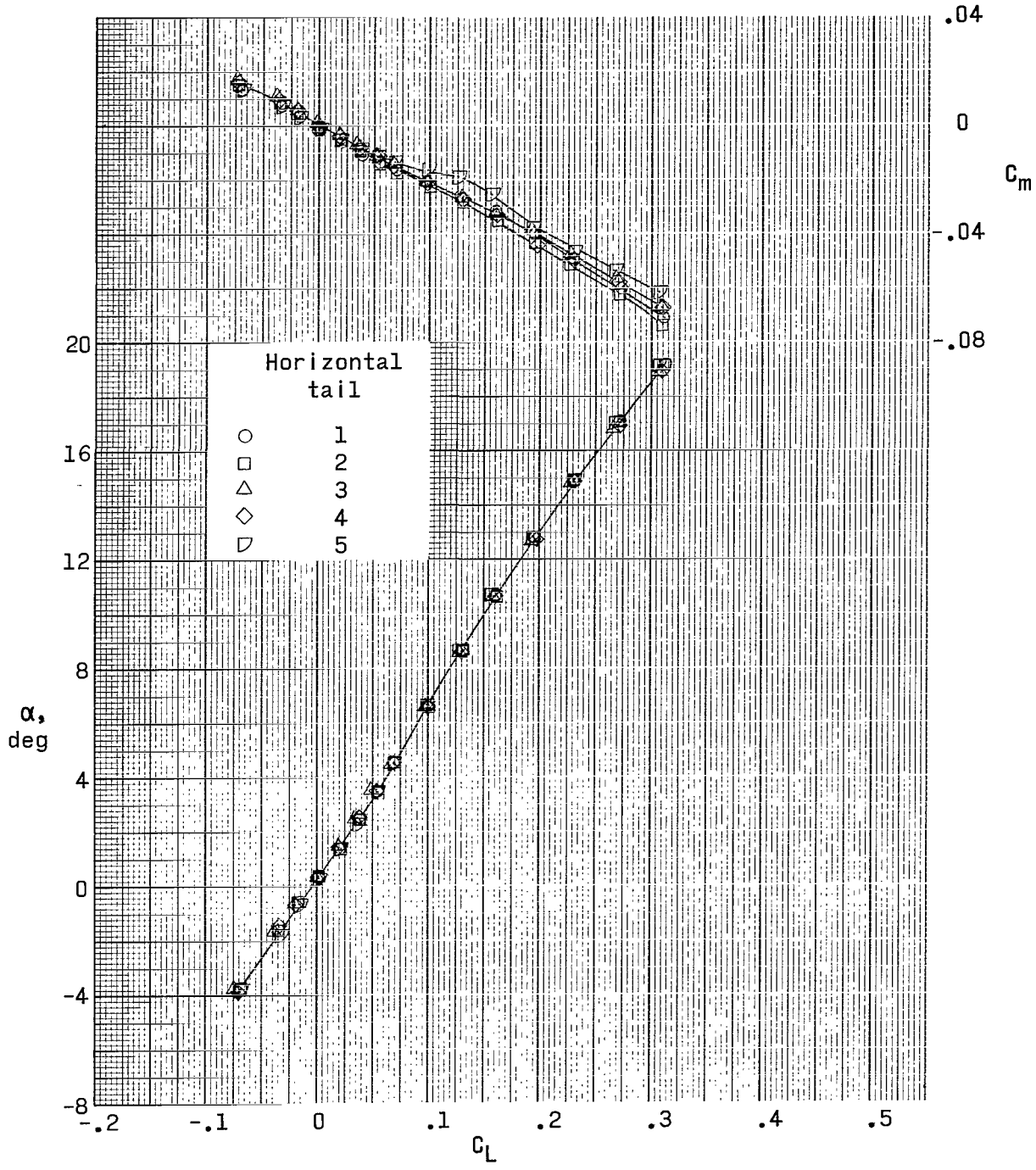

(e) M = 4.63.

Figure 4.- Continued.

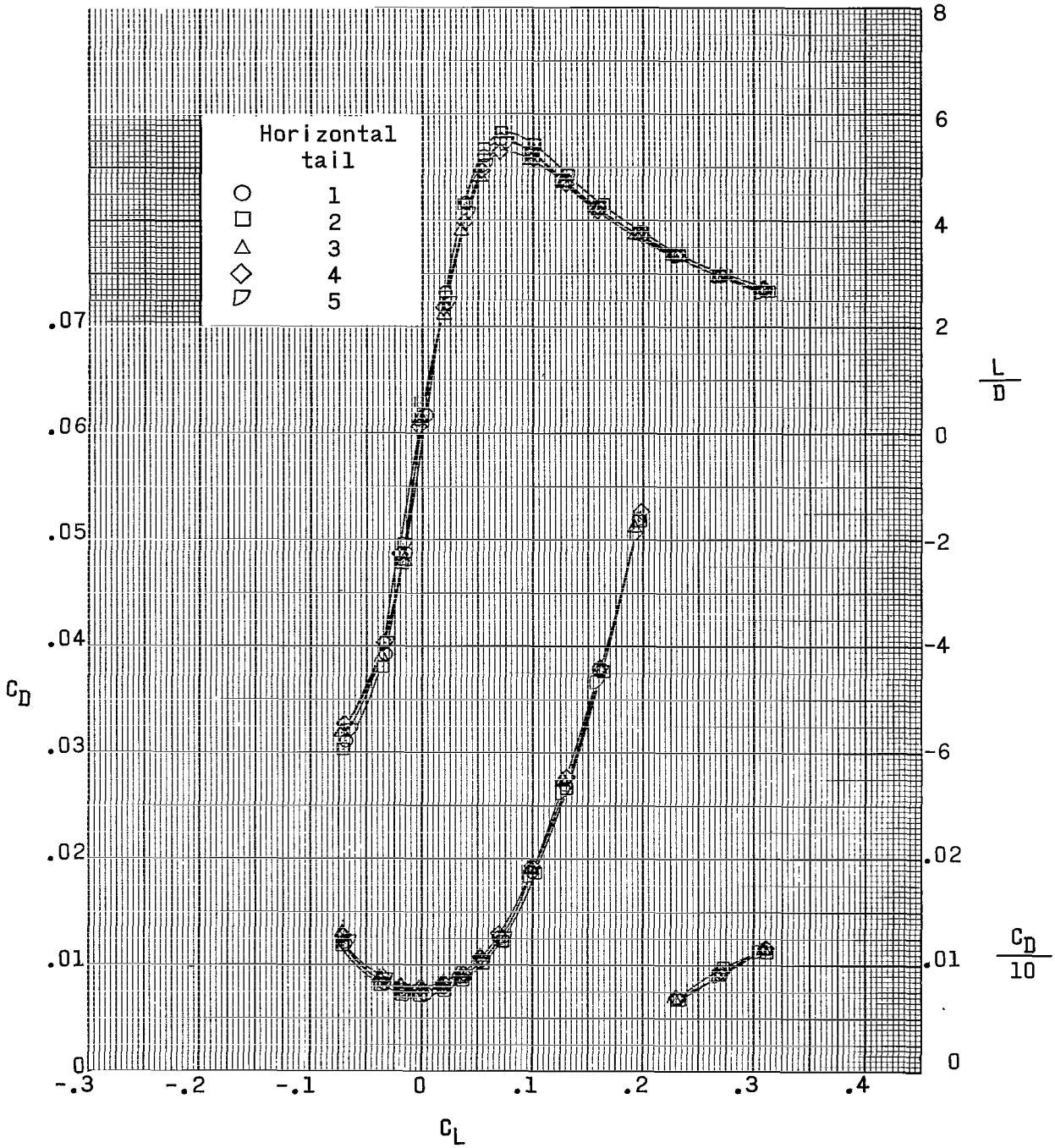

(e) Concluded.

Figure 4.- Concluded.

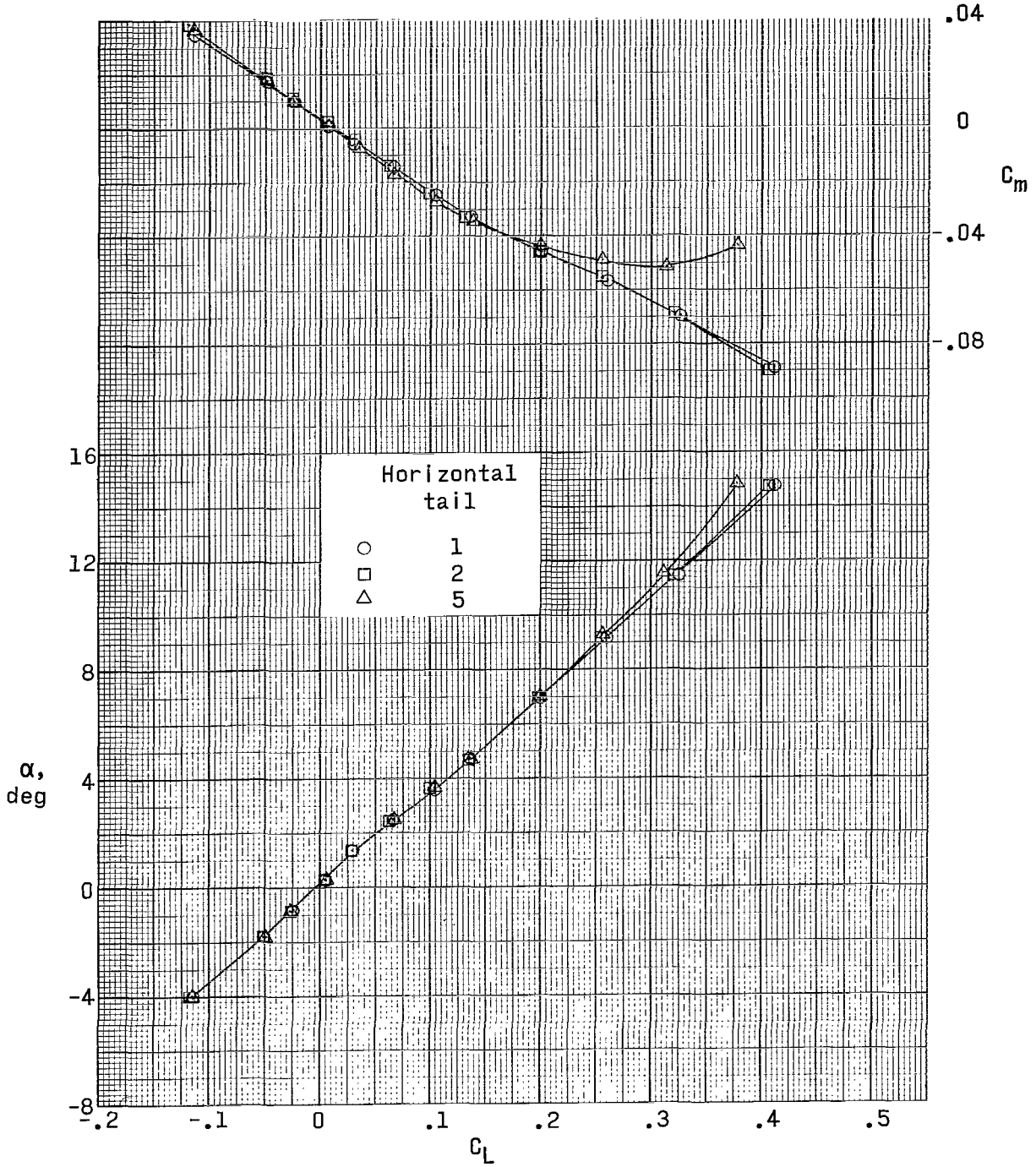

(a) M = 1.90.

Figure 5.- Effect of horizontal-tail height on aerodynamic characteristics in pitch. High wings; -5° dihedral.

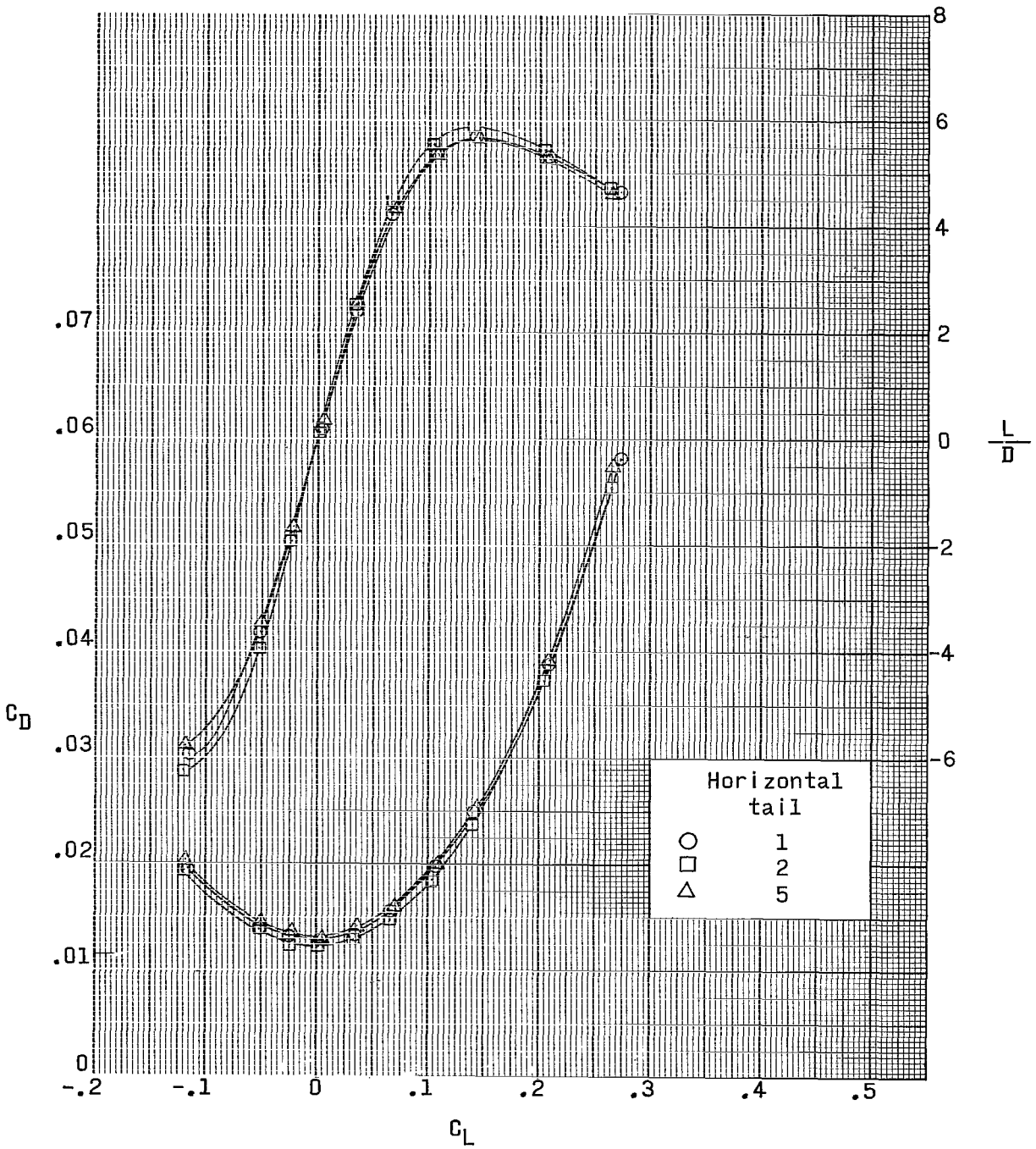

(a) Concluded.

Figure 5.- Continued.

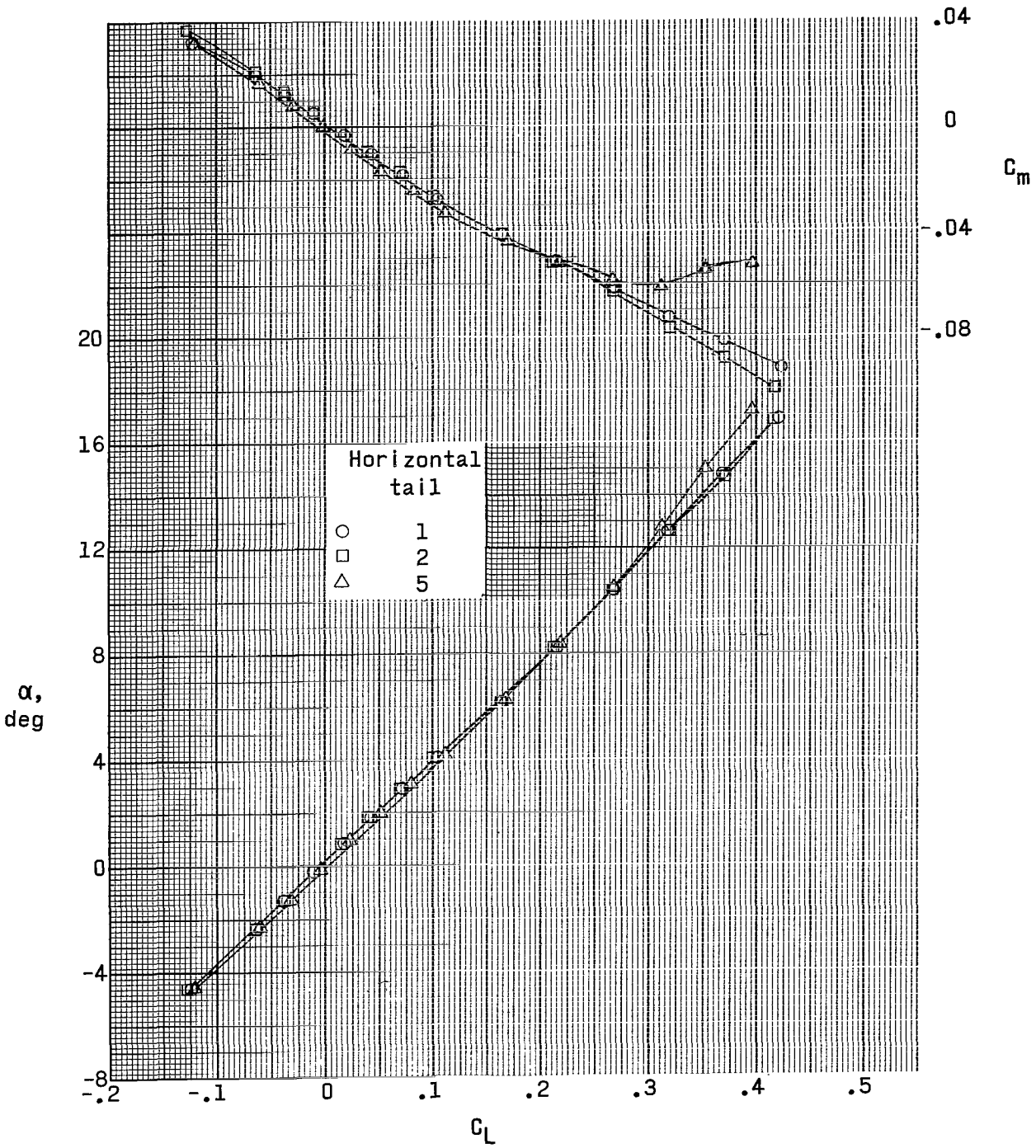

(b) M = 2.30.

Figure 5.- Continued.

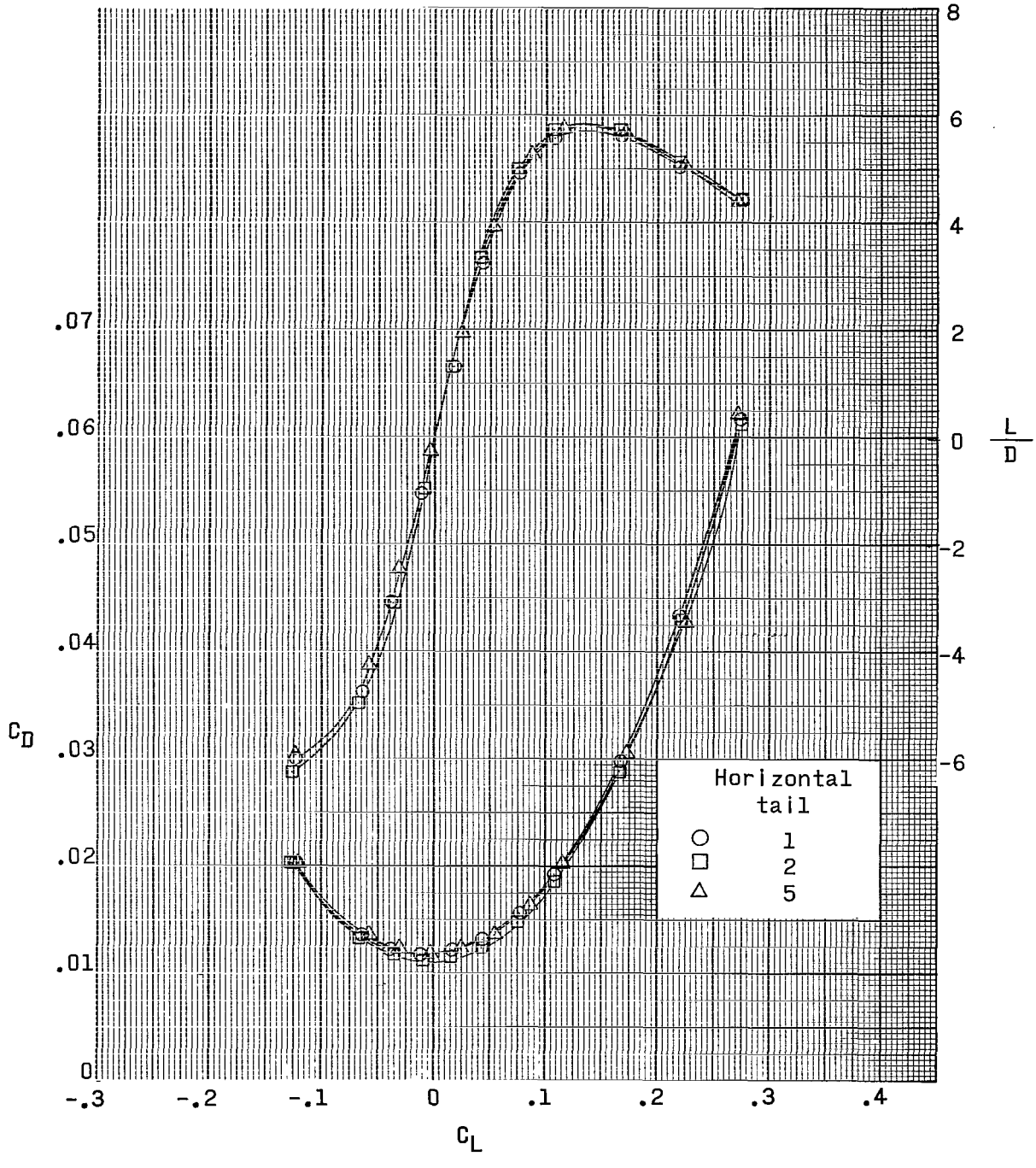

(b) Concluded.

Figure 5.- Continued.

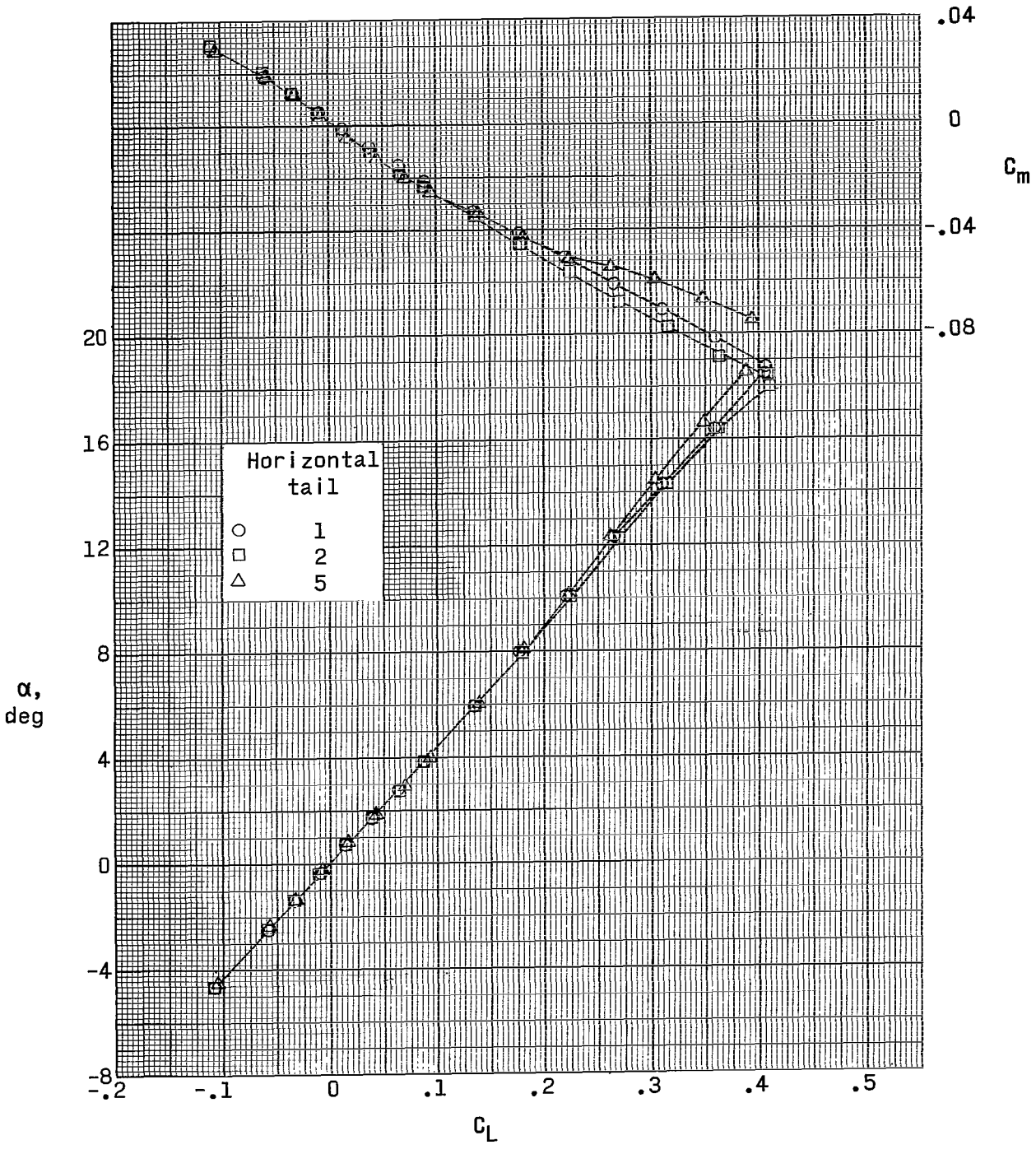

(c) M = 2.96.

Figure 5.- Continued.

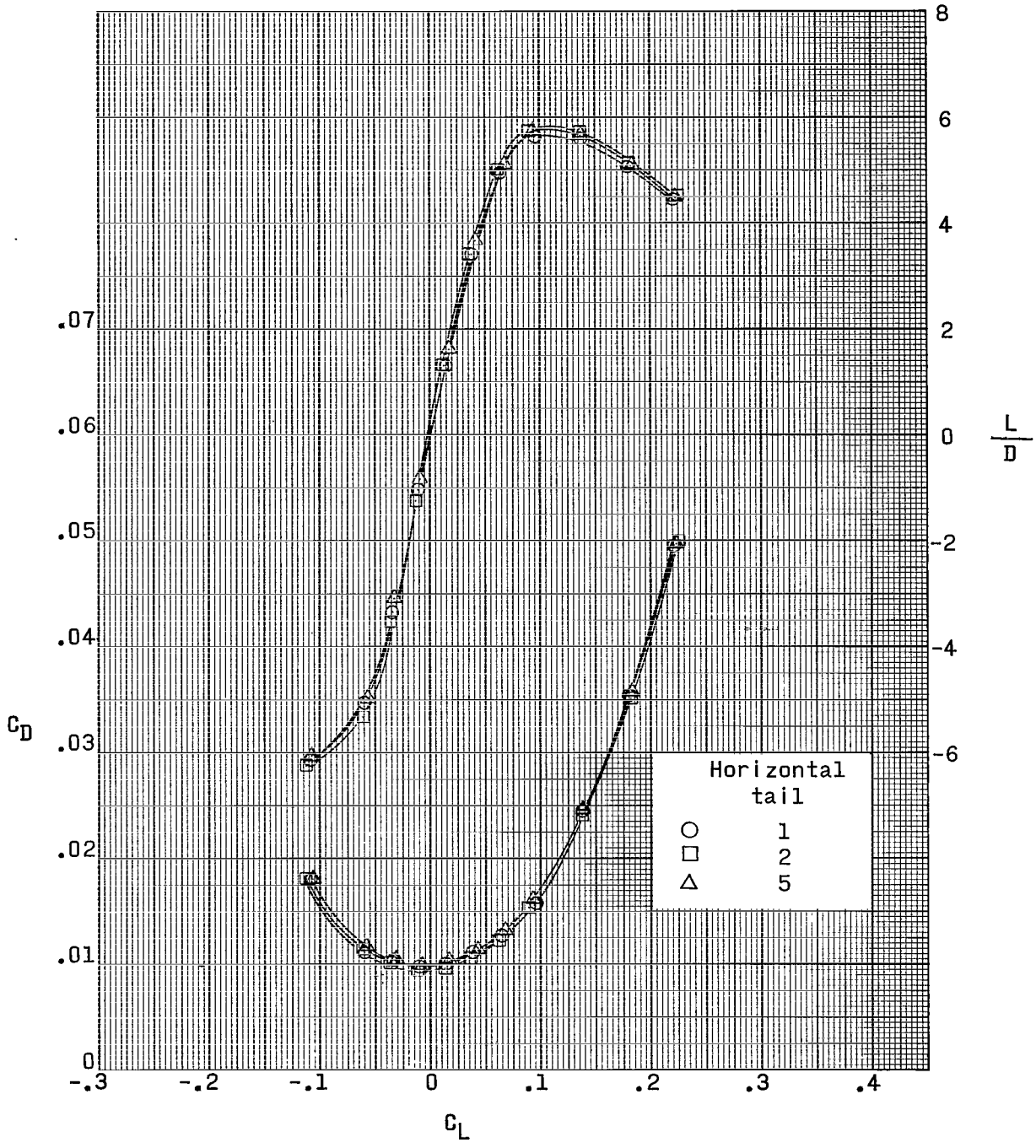

(c) Concluded.

Figure 5.- Continued.

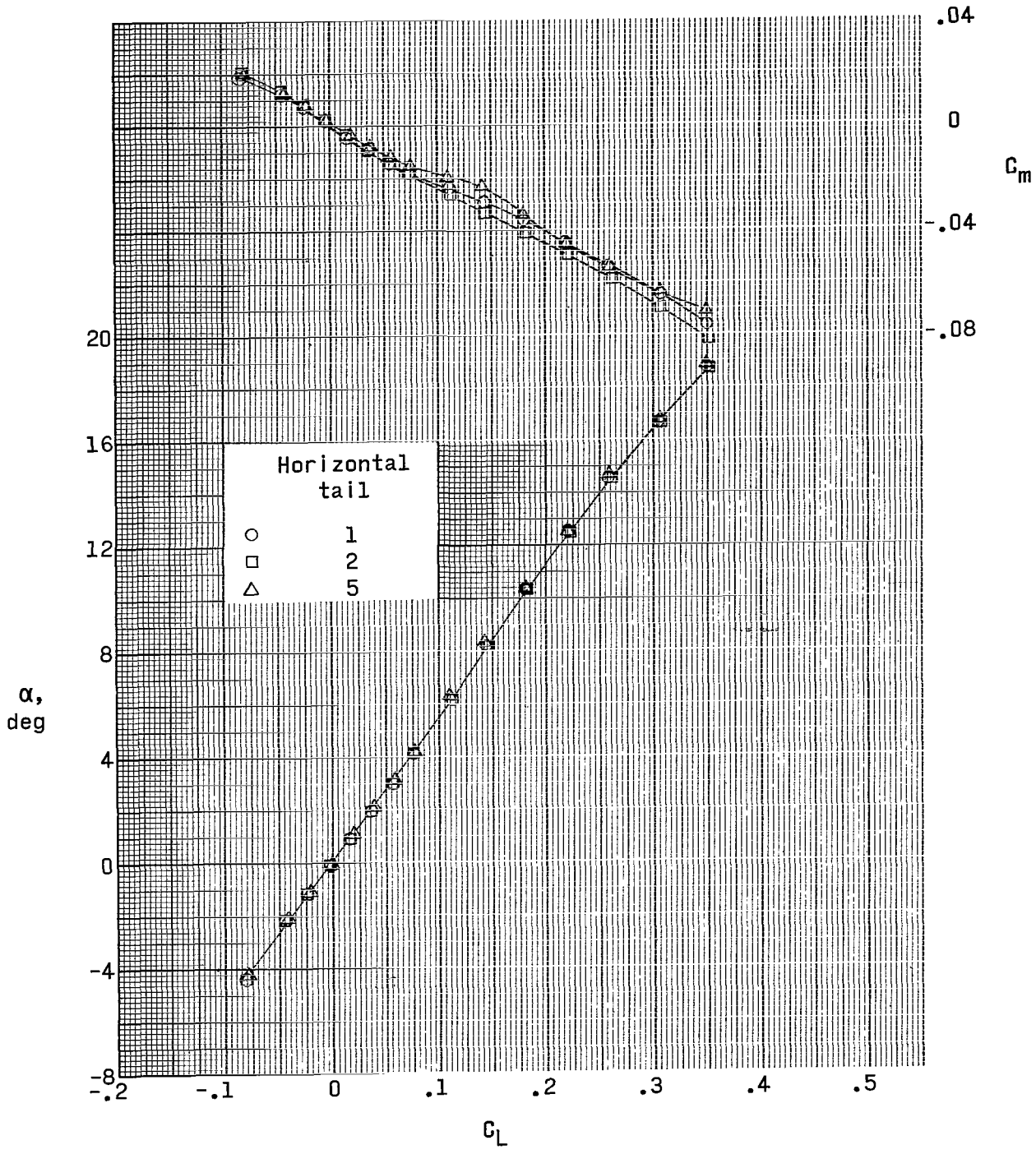

(d) M = 3.95.

Figure 5.- Continued.

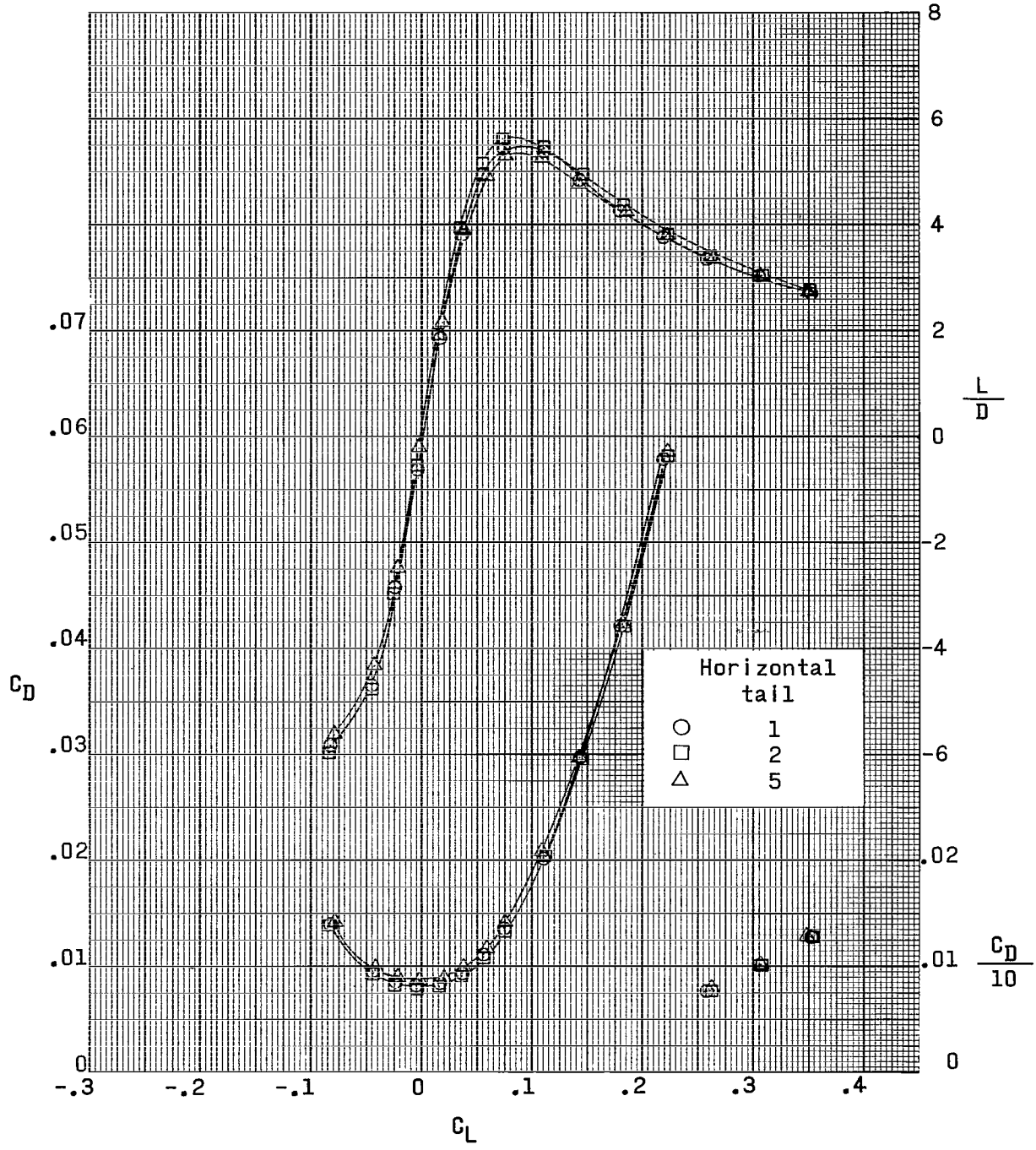

(d) Concluded.

Figure 5.- Continued.

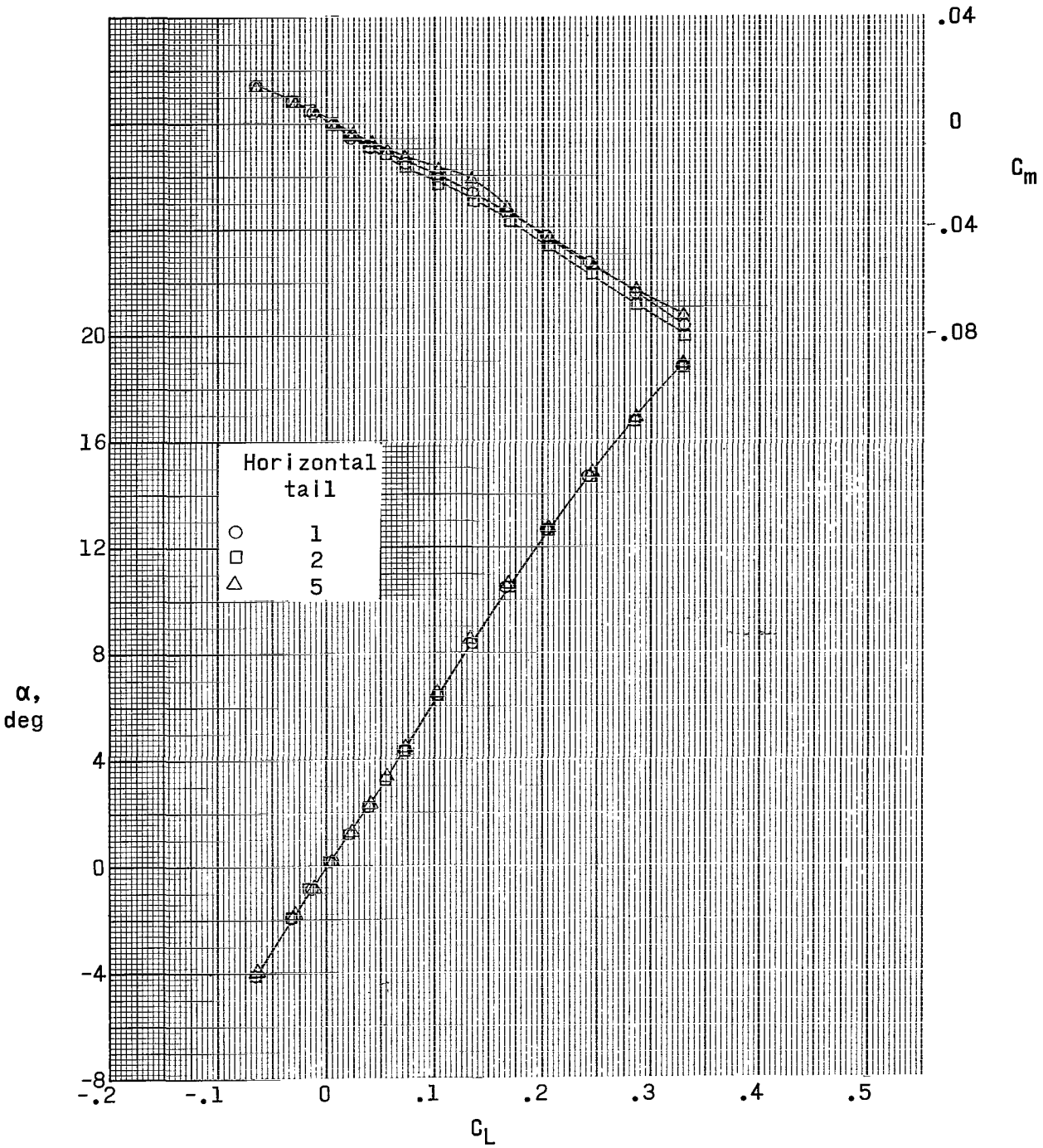

(e) M = 4.63.

Figure 5.- Continued.

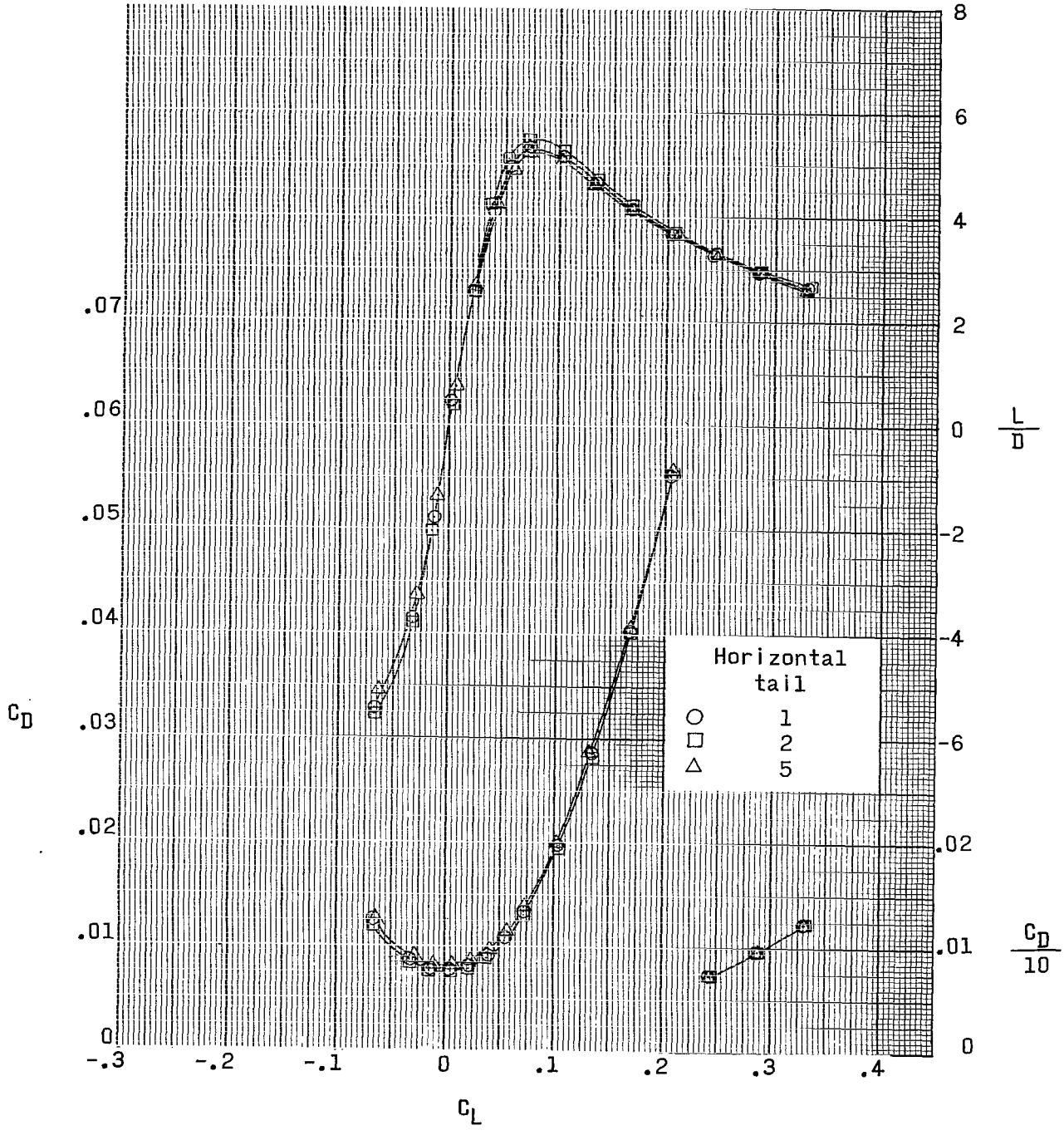

(e) Concluded.

Figure 5.- Concluded.

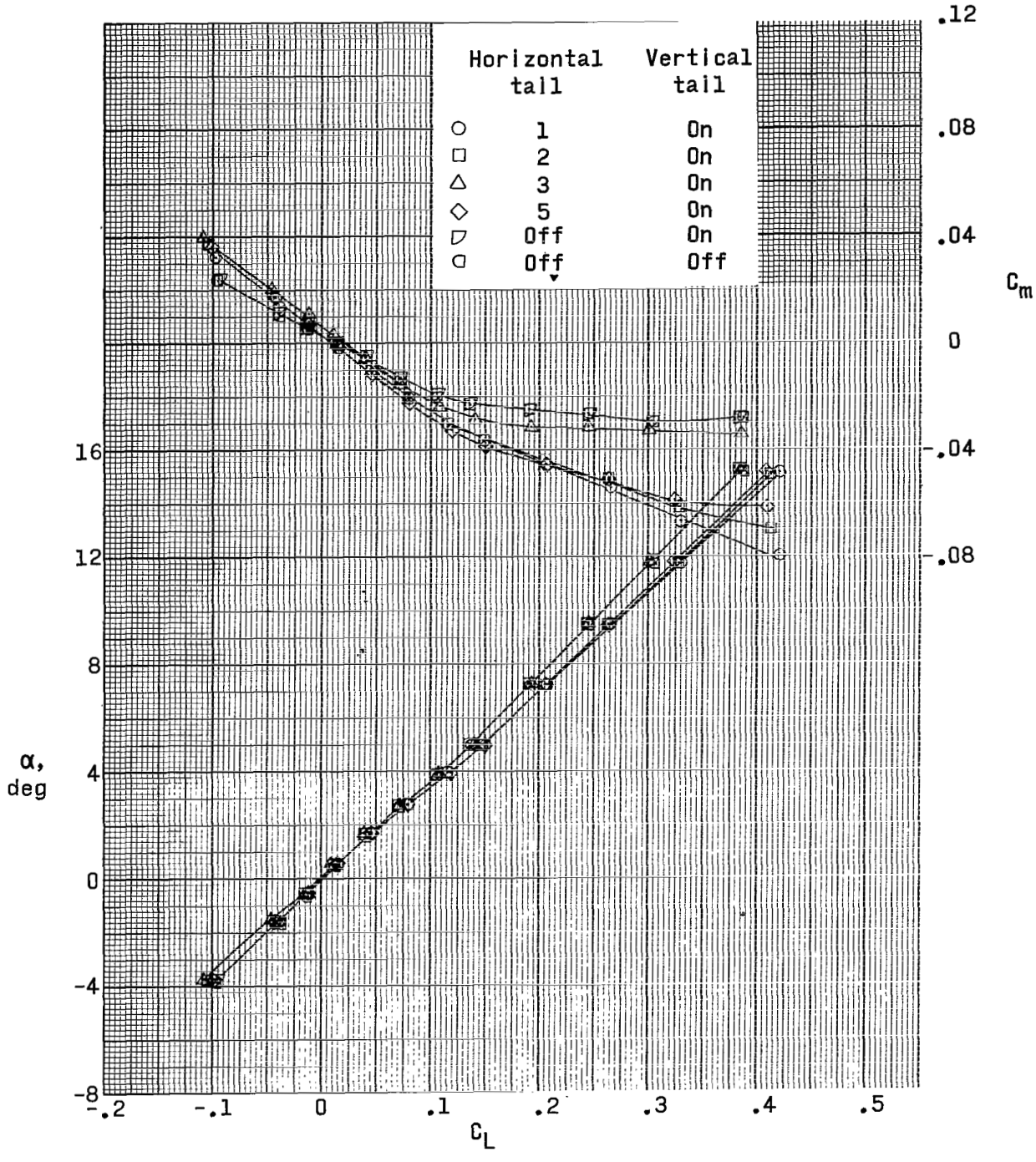

(a) M = 1.90.

Figure 6.- Effect of horizontal-tail height on aerodynamic characteristics in pitch. Low wing; 0° dihedral.

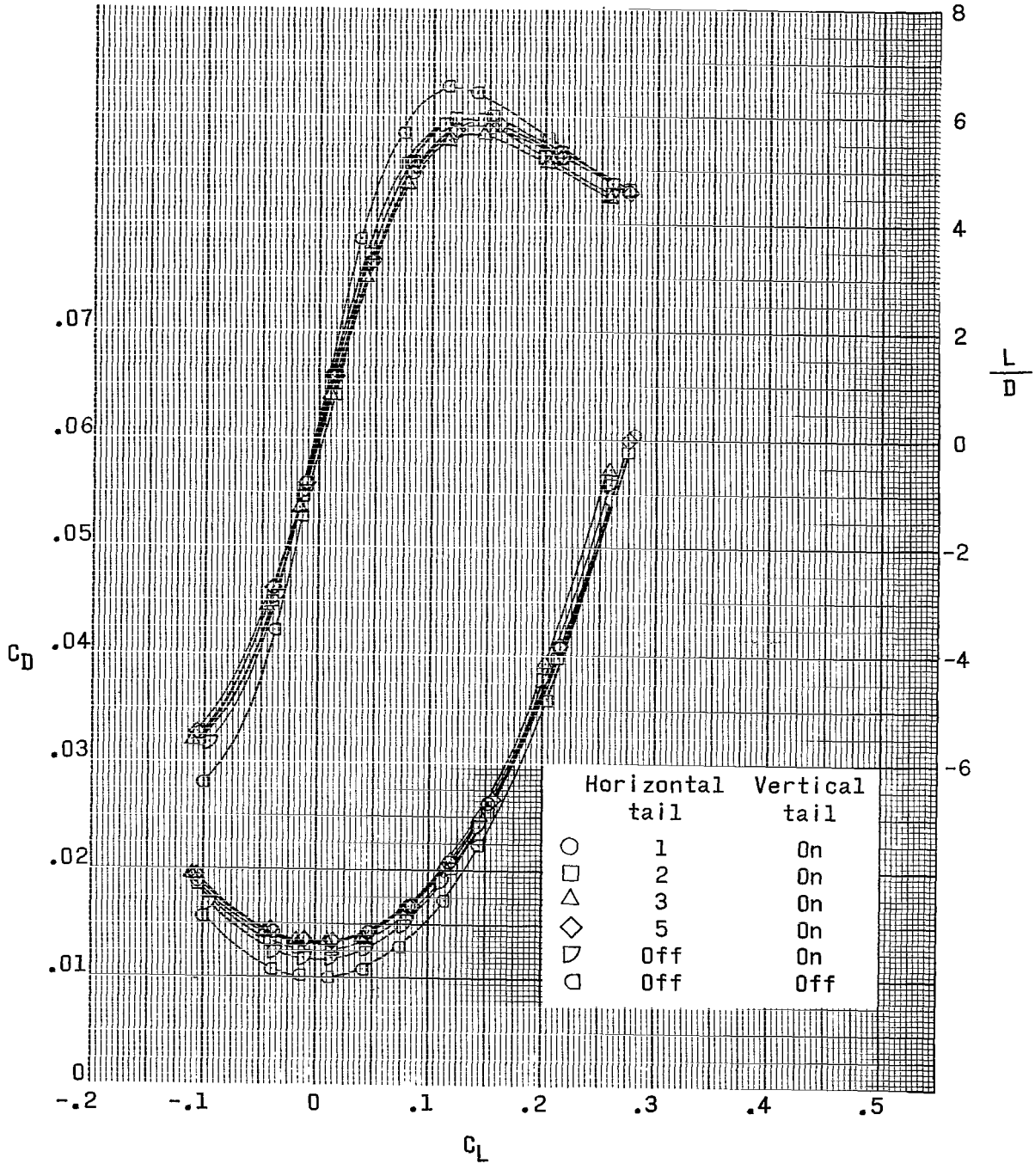

(a) Concluded.

Figure 6.- Continued.

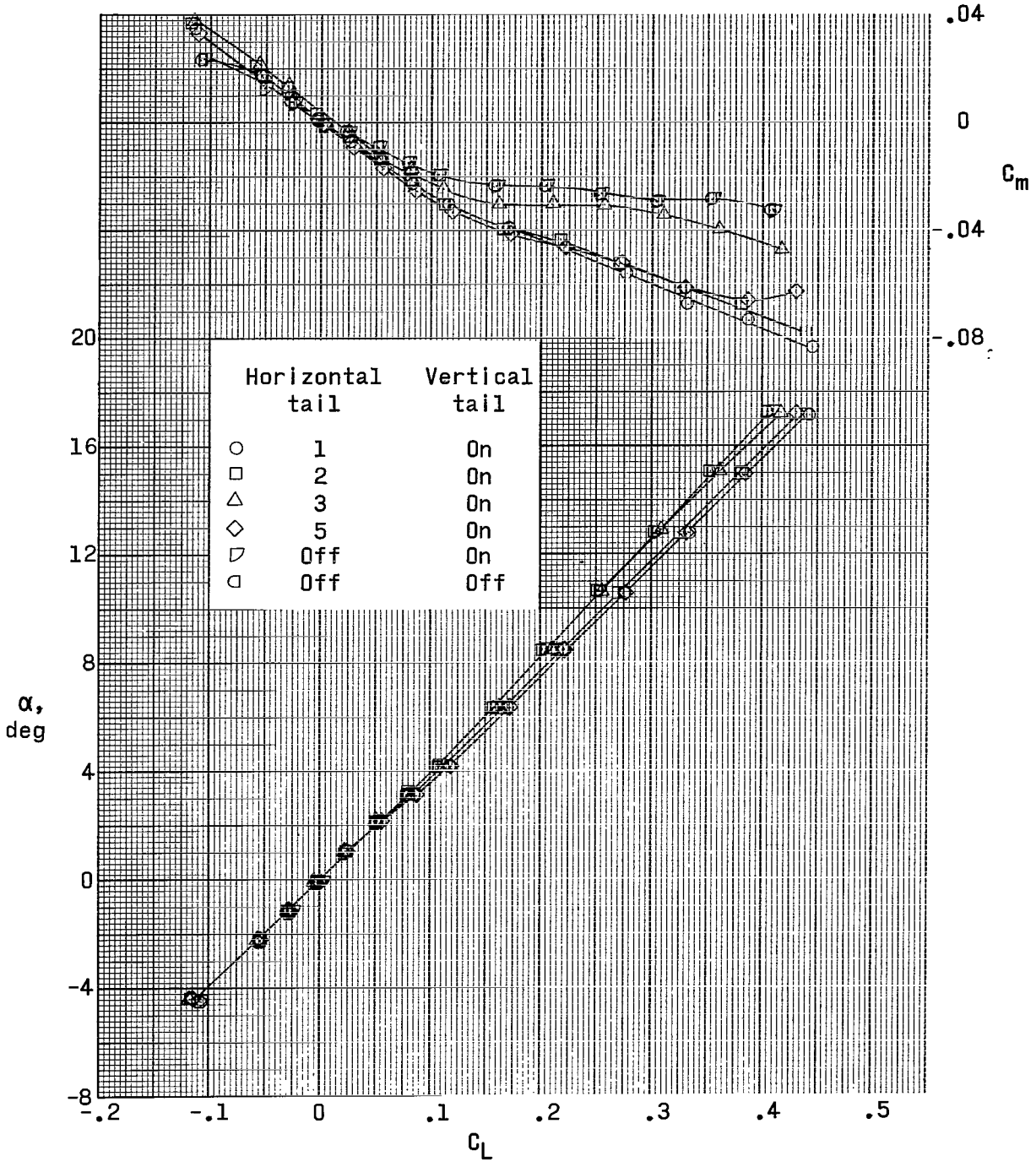

(b) M = 2.30.

Figure 6.- Continued.

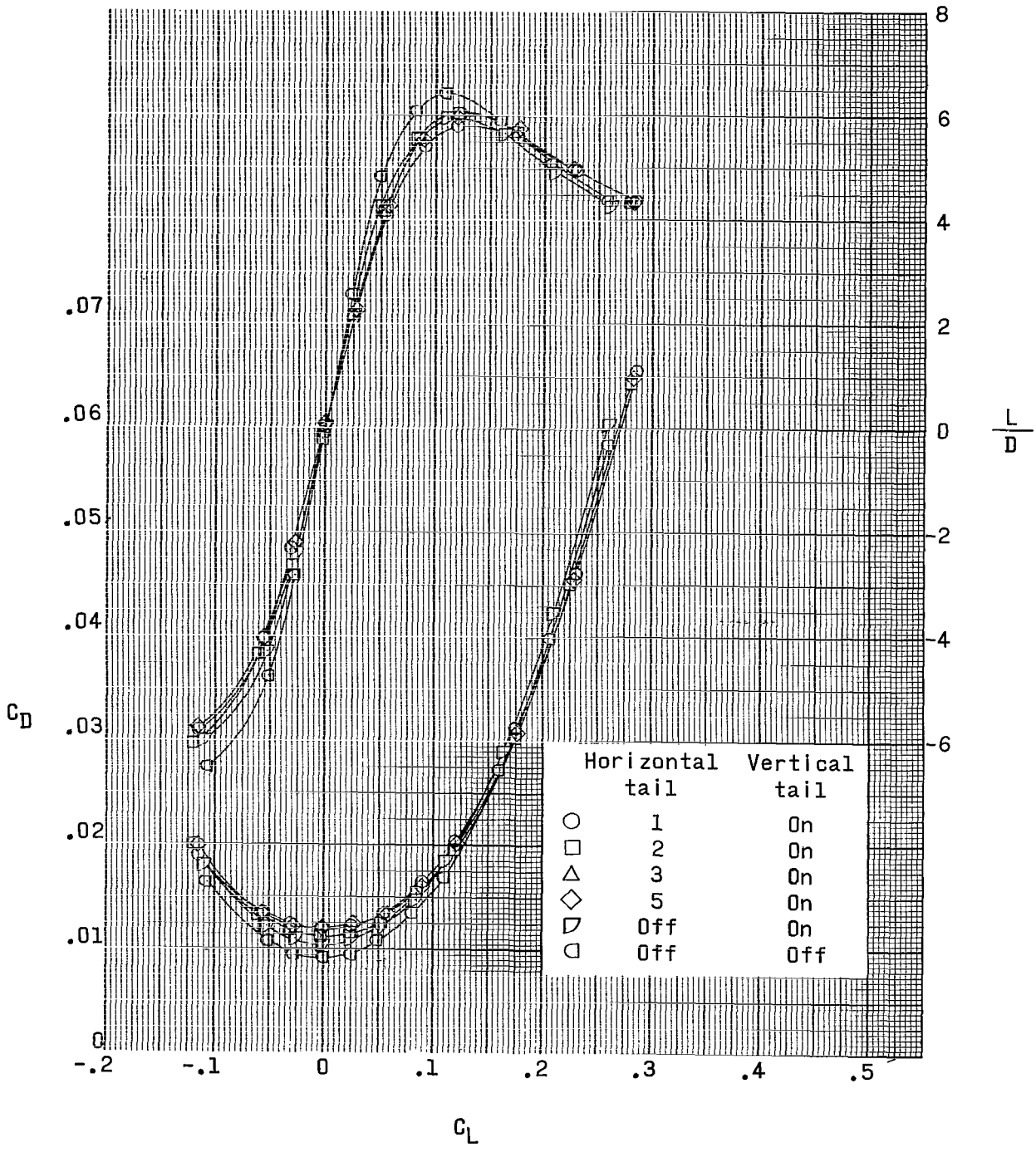

(b) Concluded.

Figure 6.- Continued.

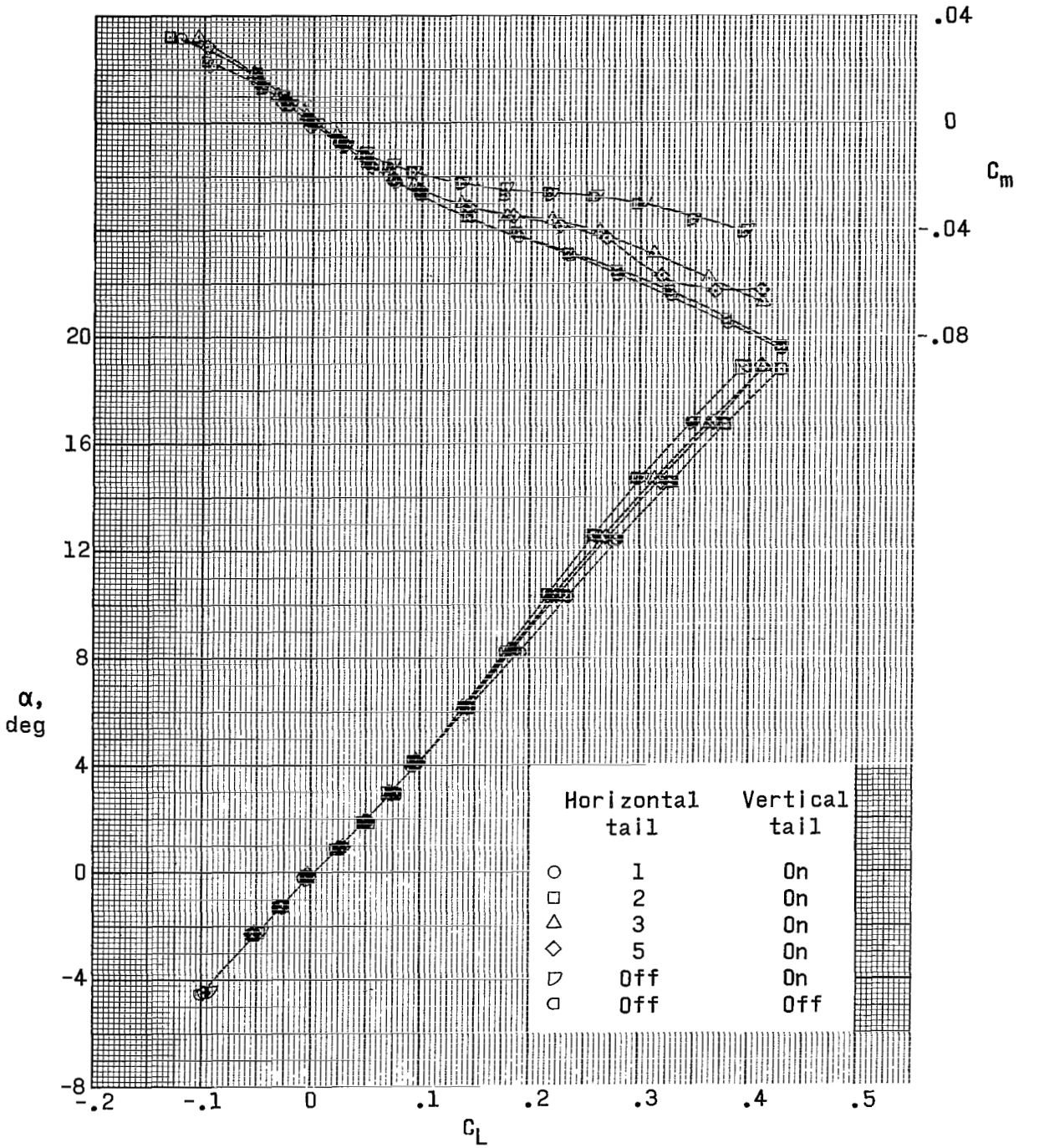

(c) M = 2.96.

Figure 6.- Continued.

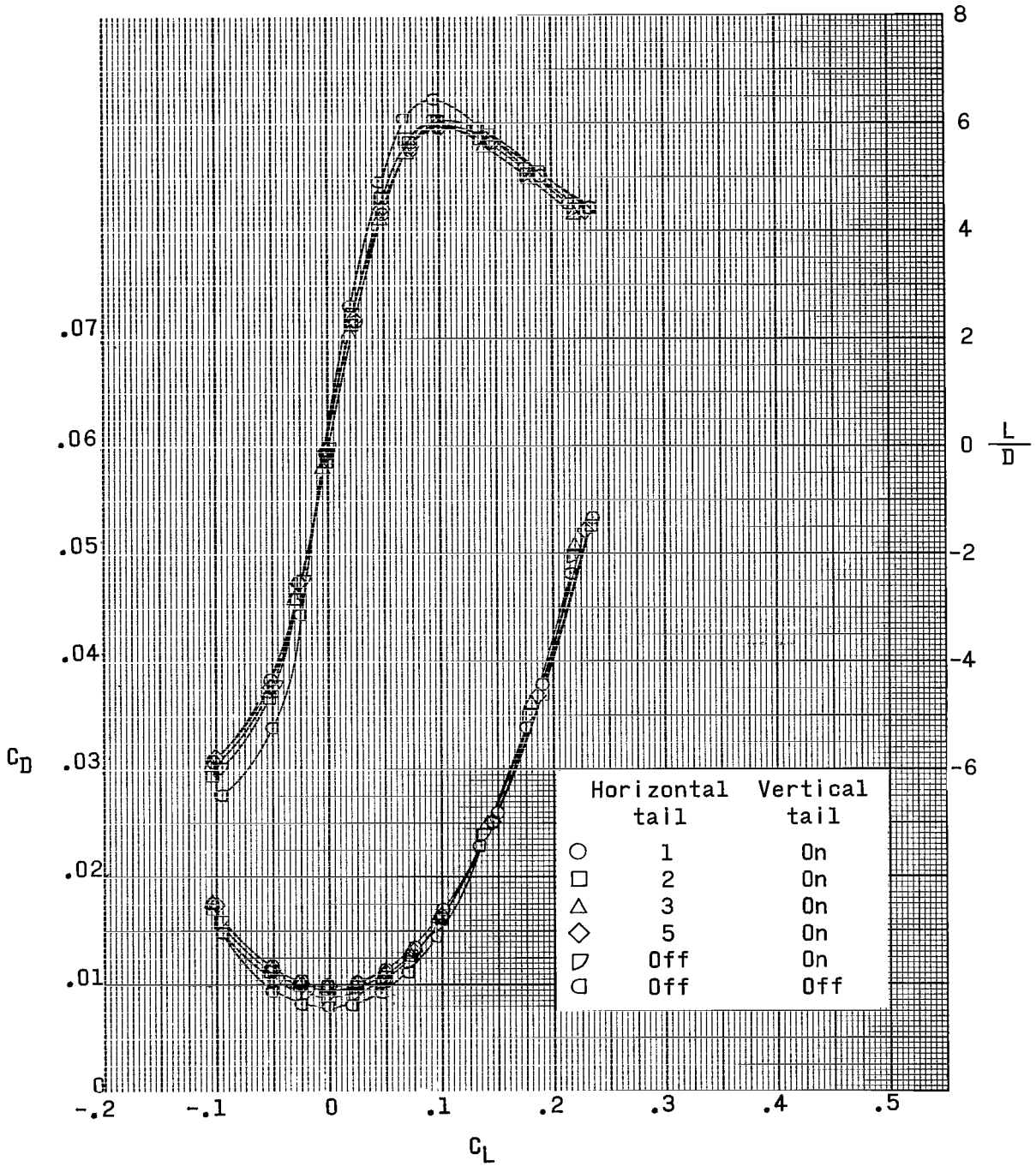

(c) Concluded.

Figure 6.- Continued.

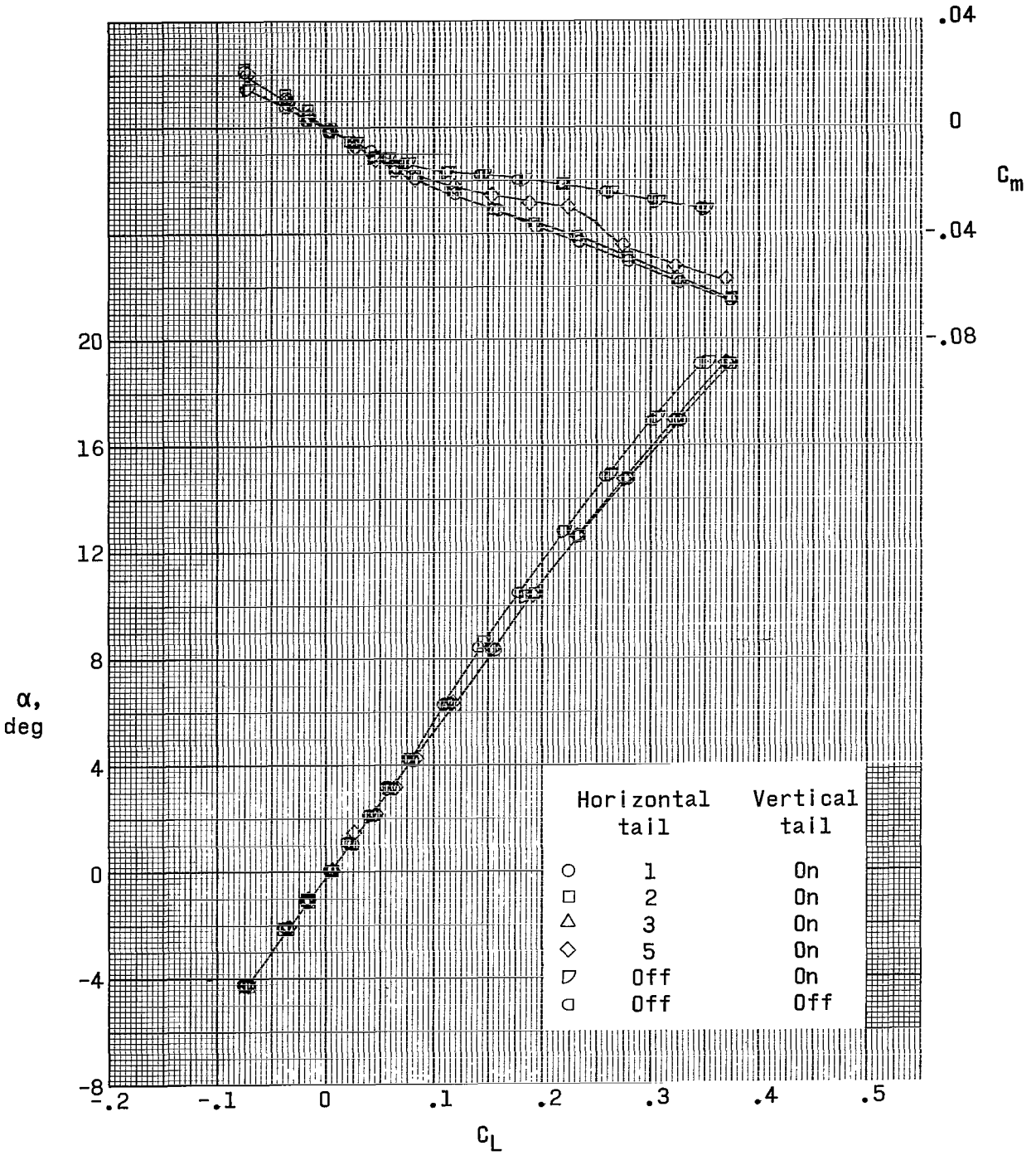

(d) M = 3.95.

Figure 6.- Continued.

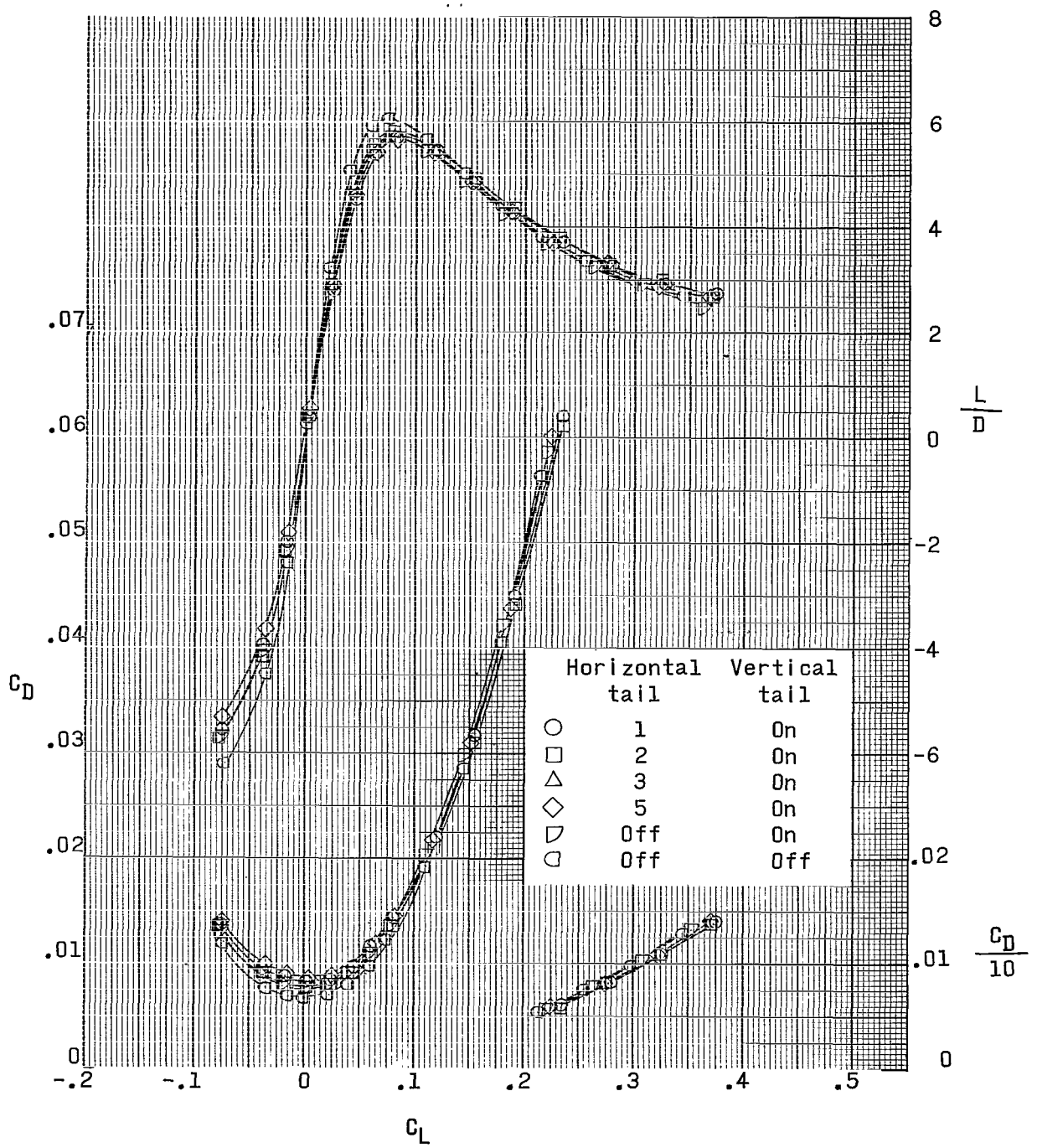

(d) Concluded.

Figure 6.- Continued.

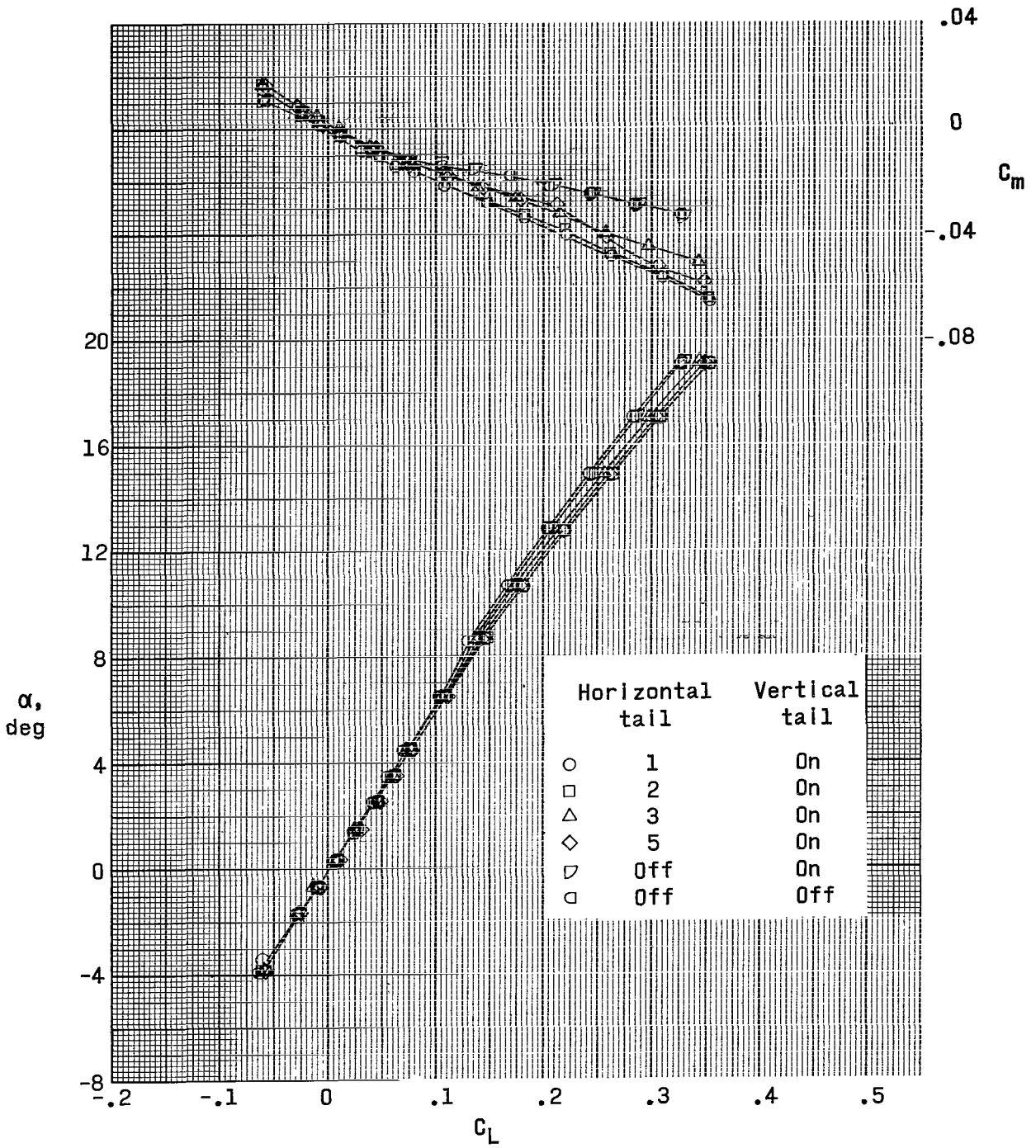

(e) M = 4.63.

Figure 6.- Continued.

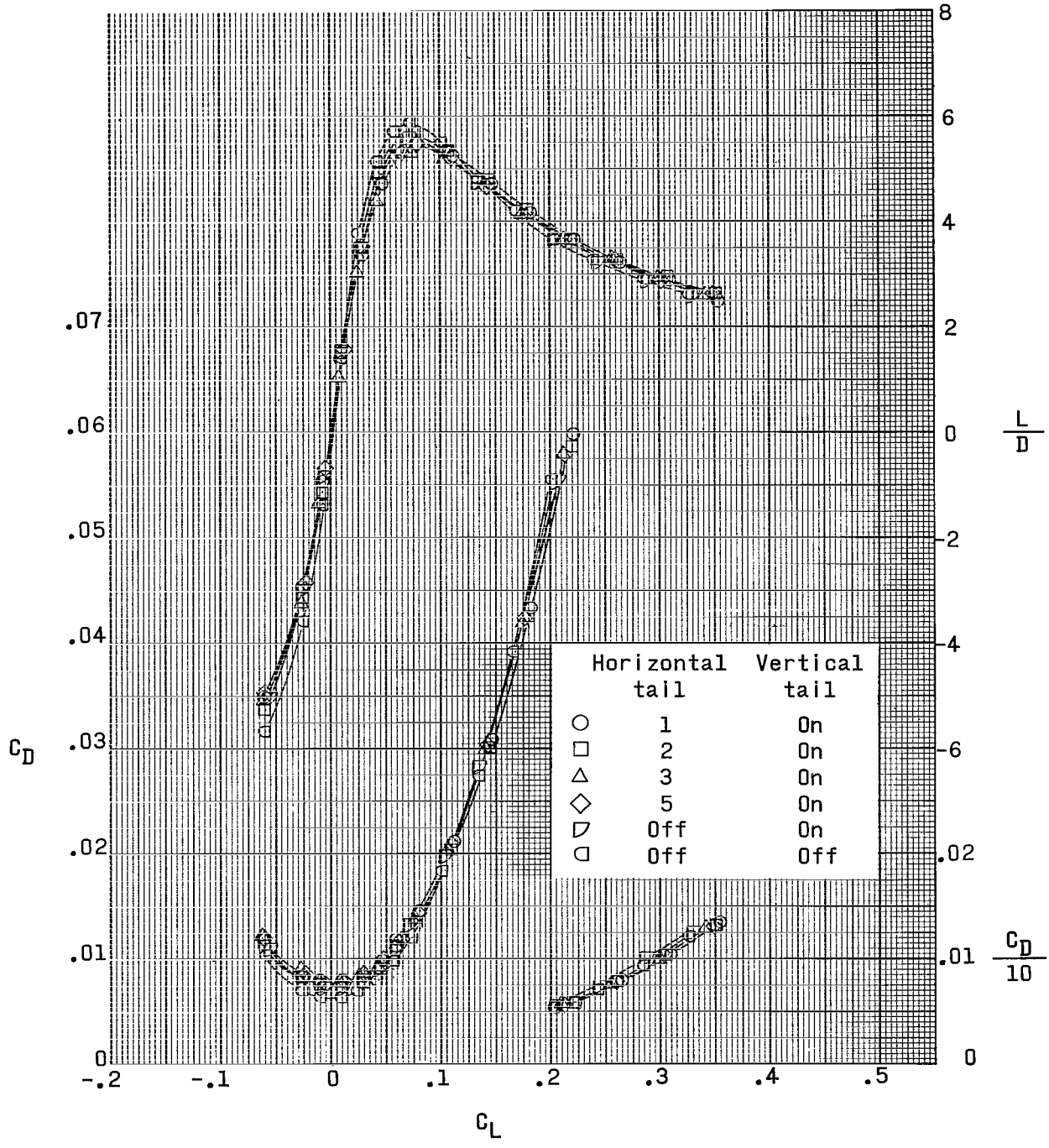

(e) Concluded.

Figure 6.- Concluded.

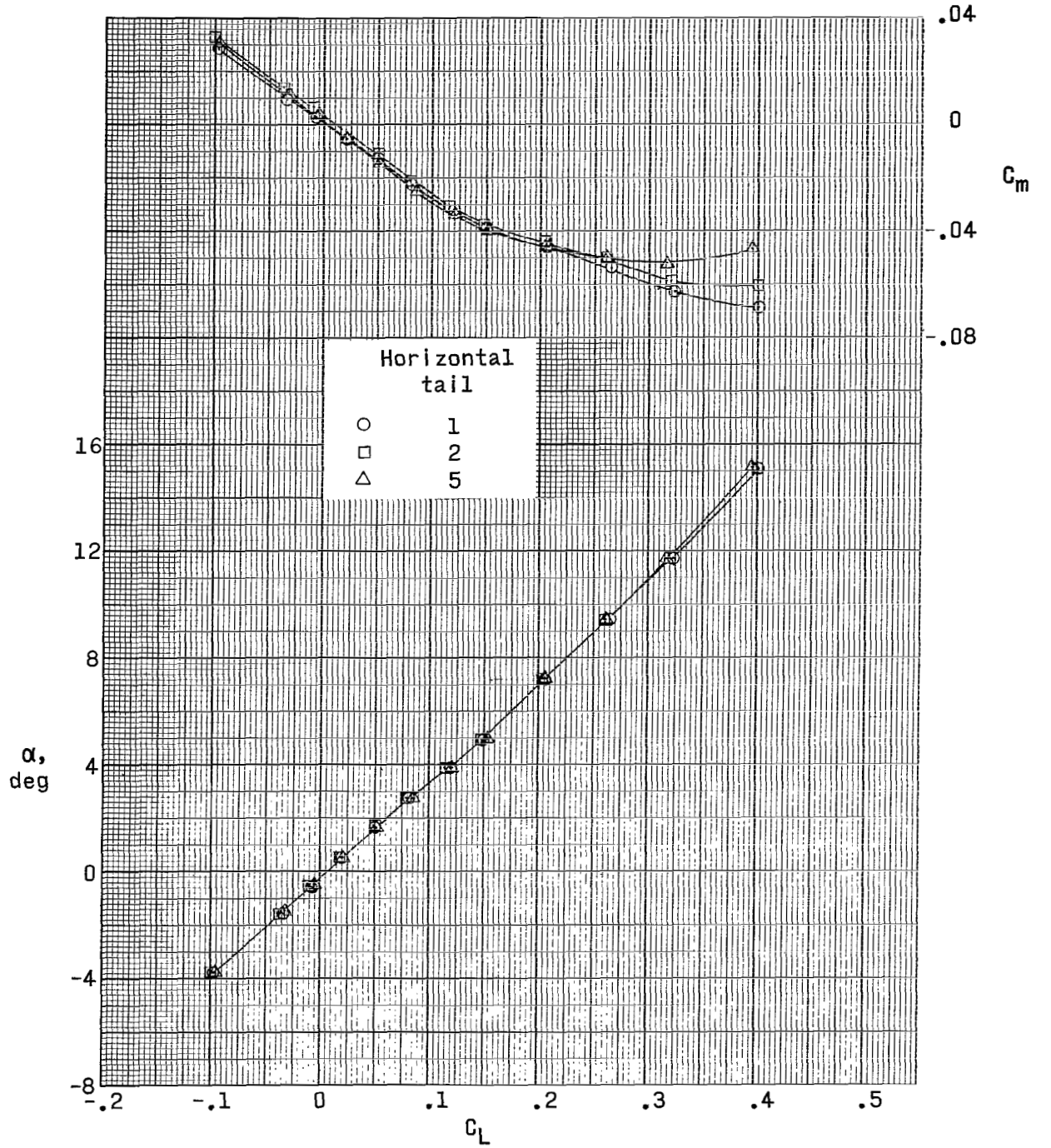

(a) M = 1.90.

Figure 7.- Effect of horizontal-tail height on aerodynamic characteristics in pitch. Low wing; 5° dihedral.

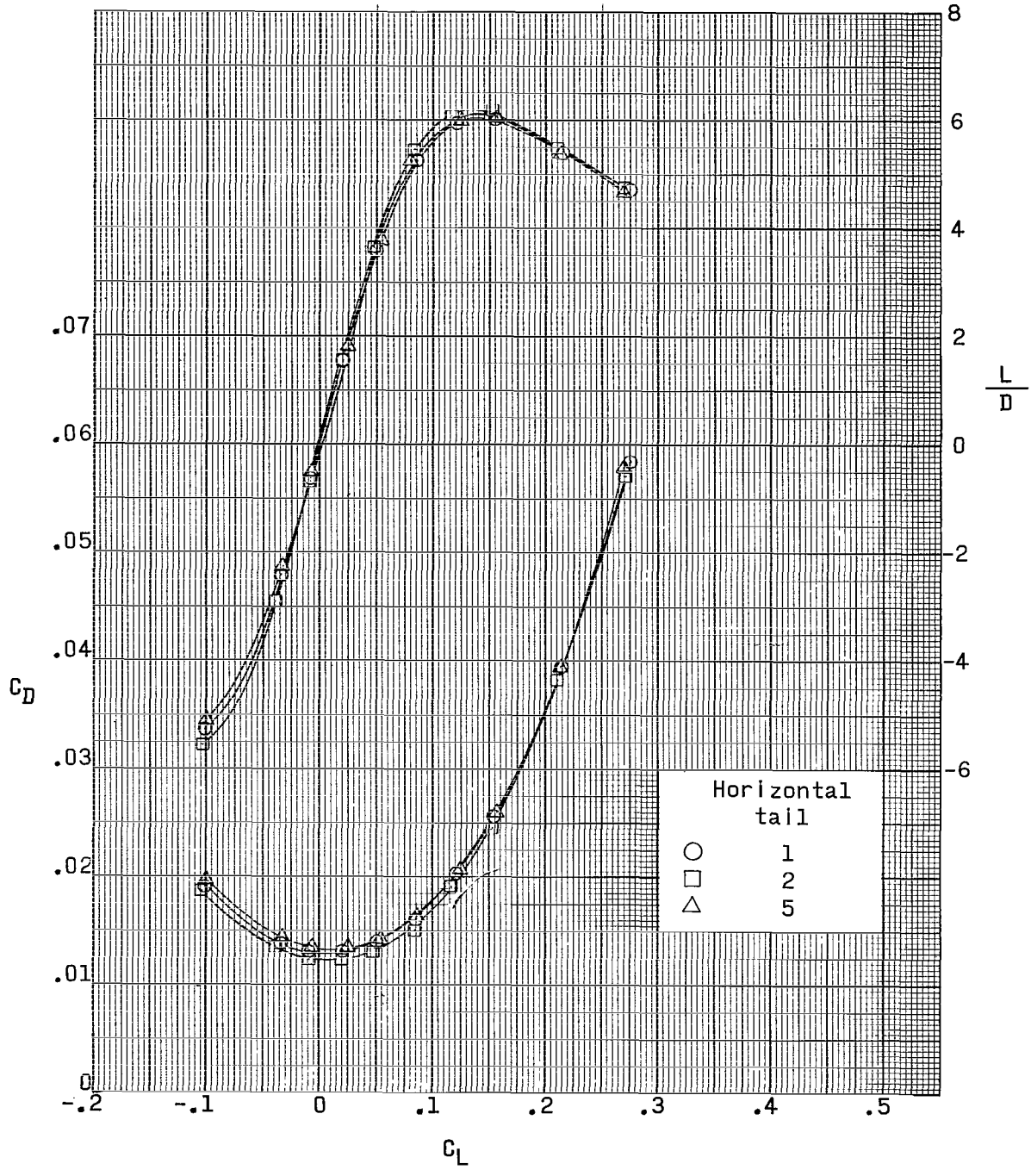

(a) Concluded.

Figure 7.- Continued.

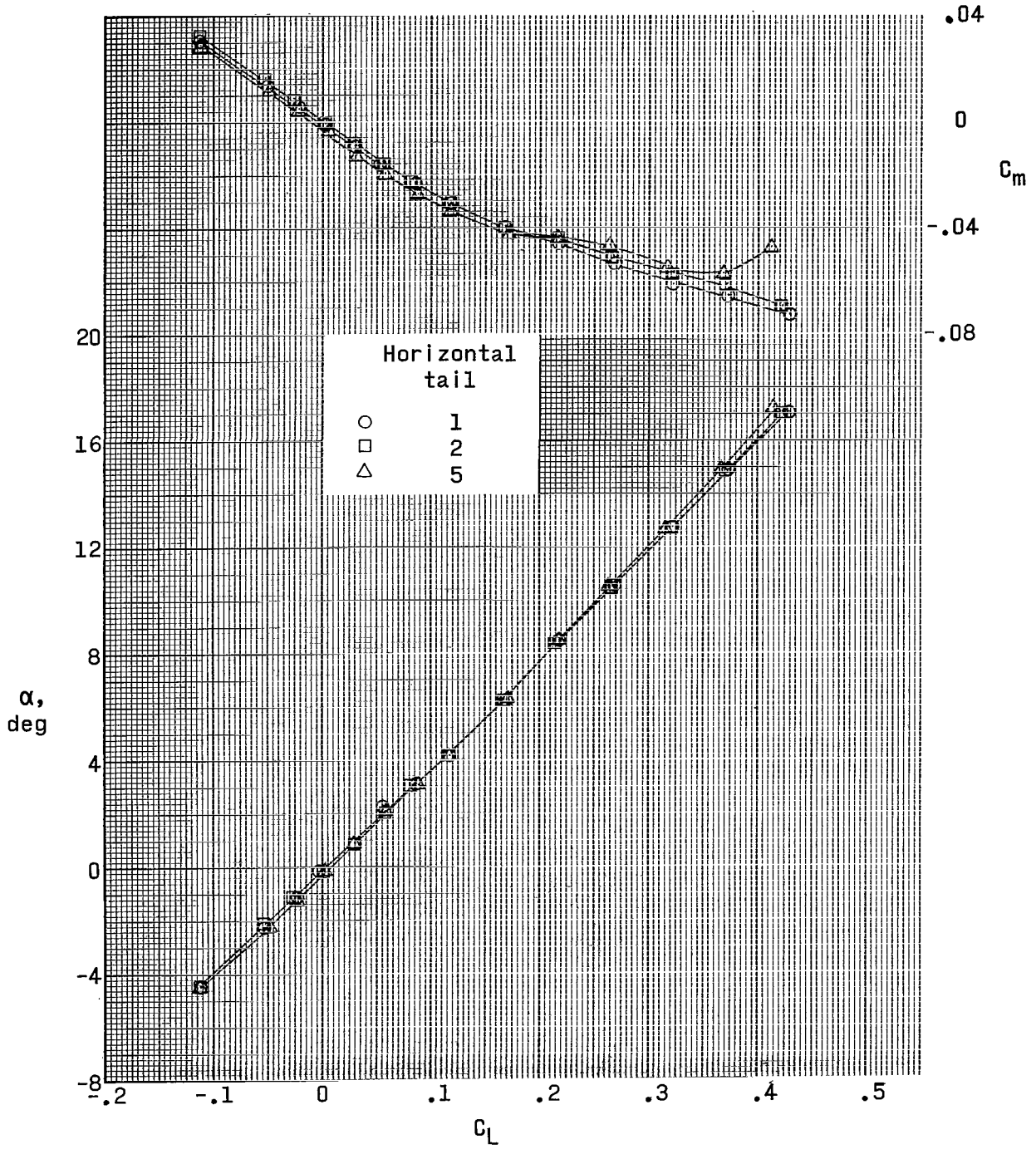

(b) M = 2.30.

Figure 7.- Continued.

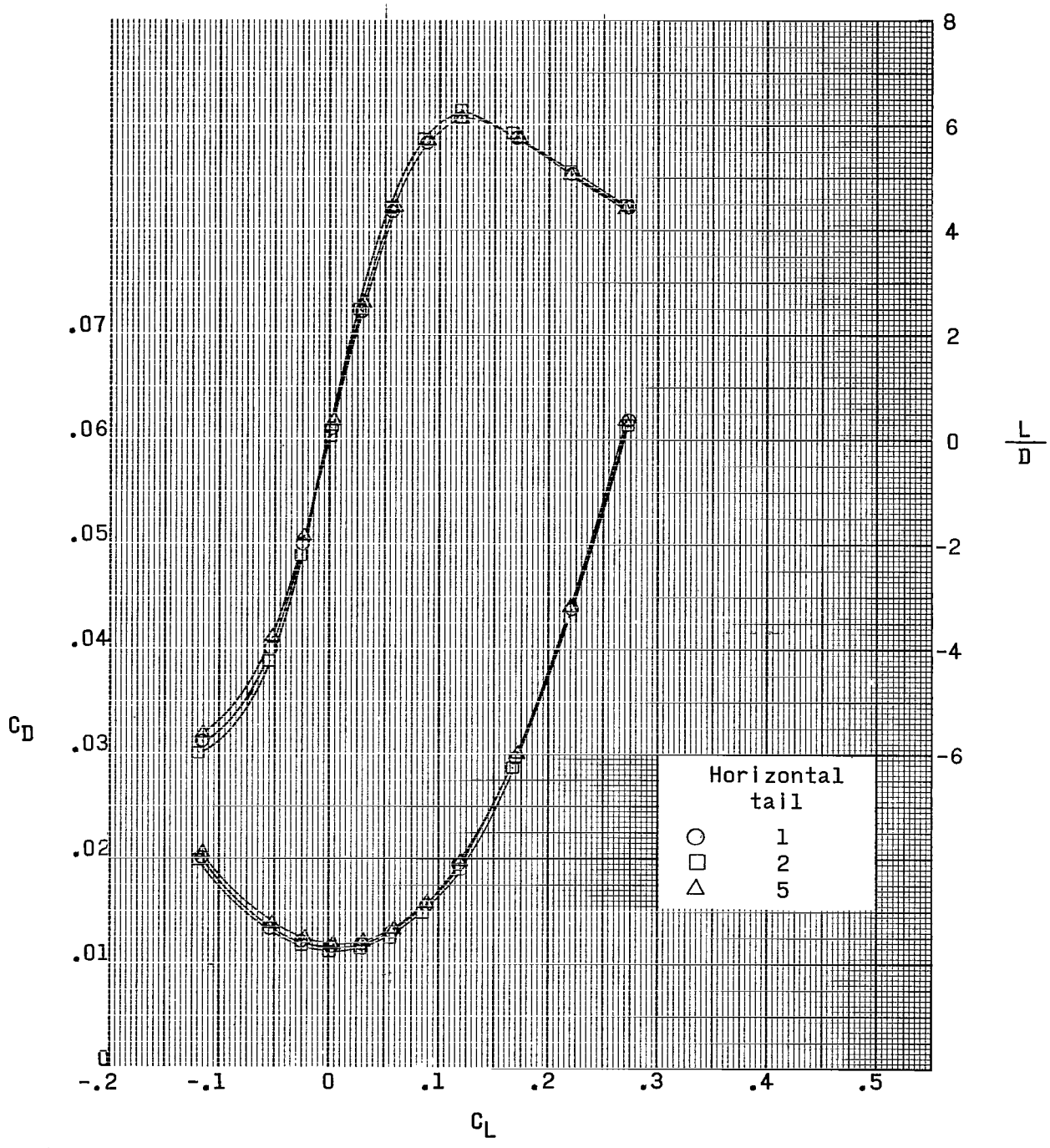

(b) Concluded.

Figure 7.- Continued.

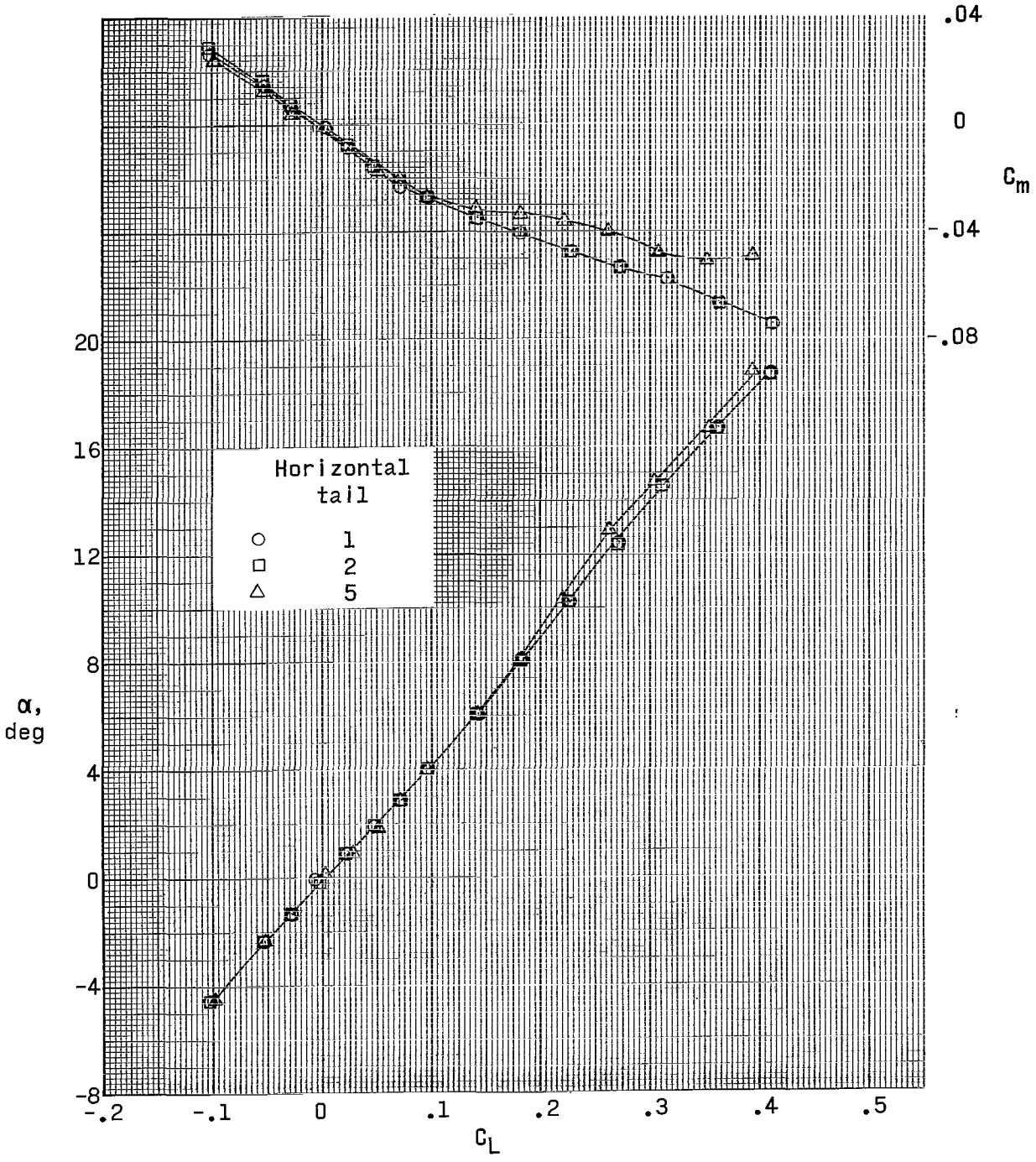

(c) M = 2.96.

Figure 7.- Continued.

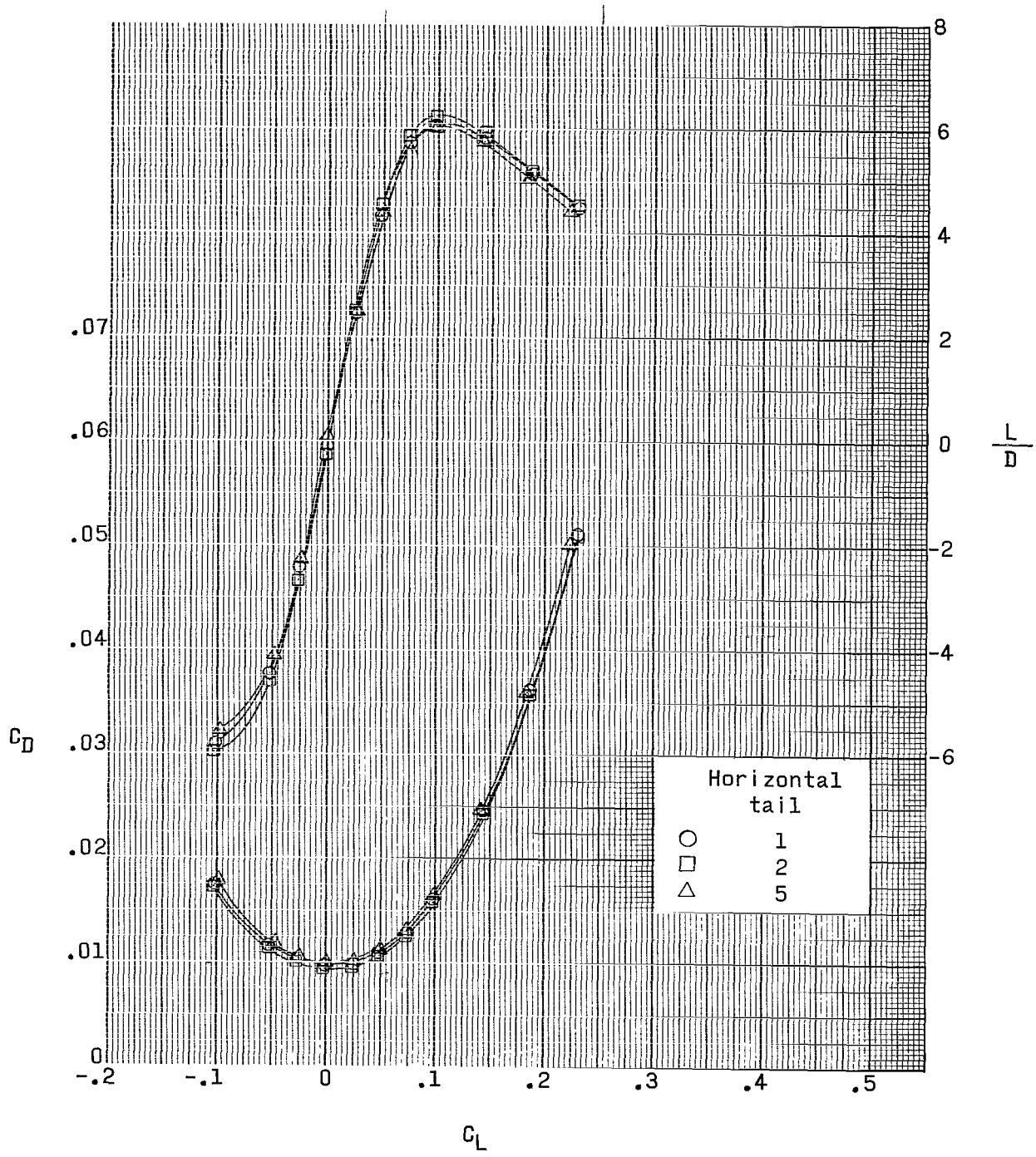

(c) Concluded.

Figure 7.- Continued.

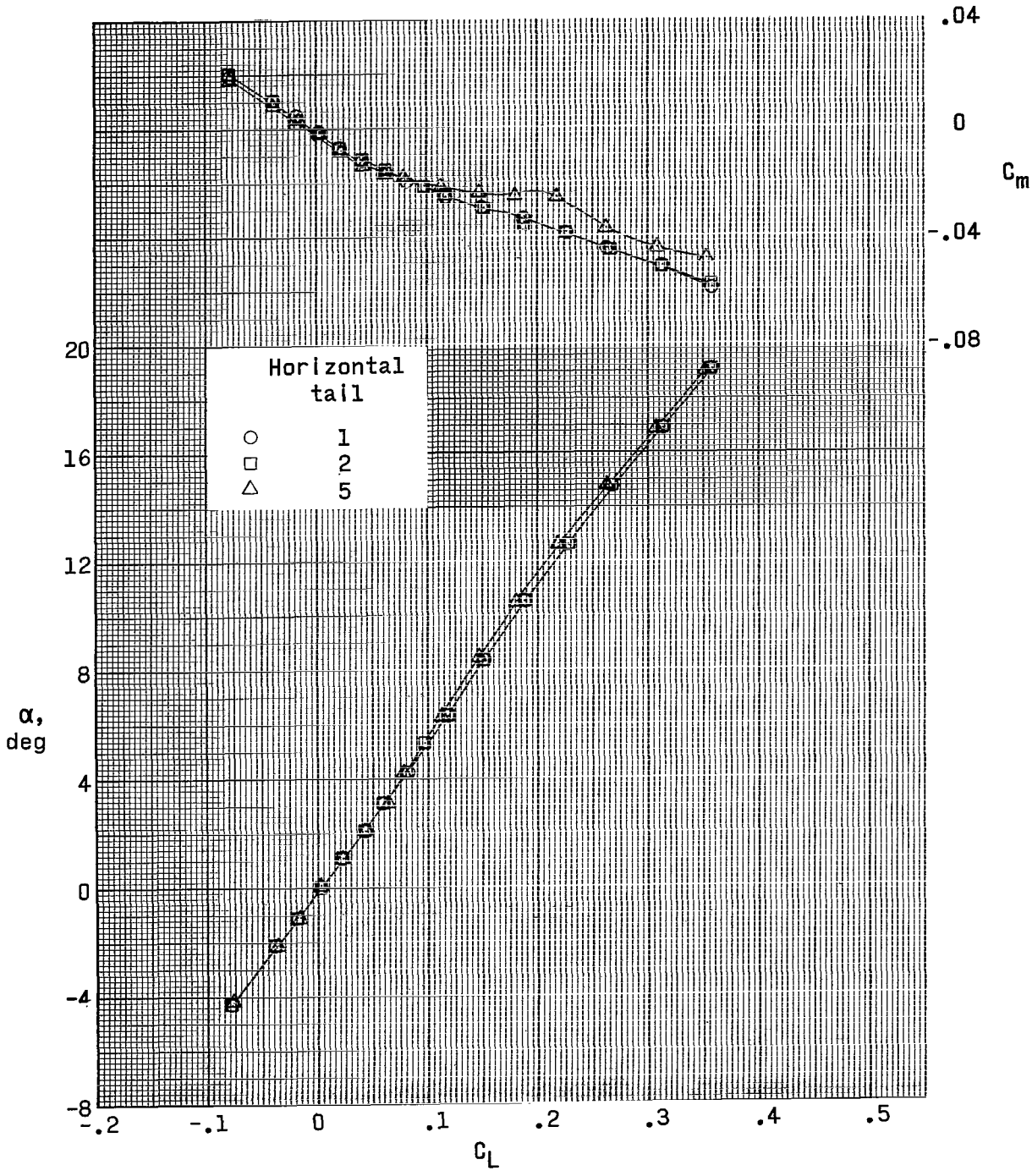

(d) M = 3.95.

Figure 7.- Continued.

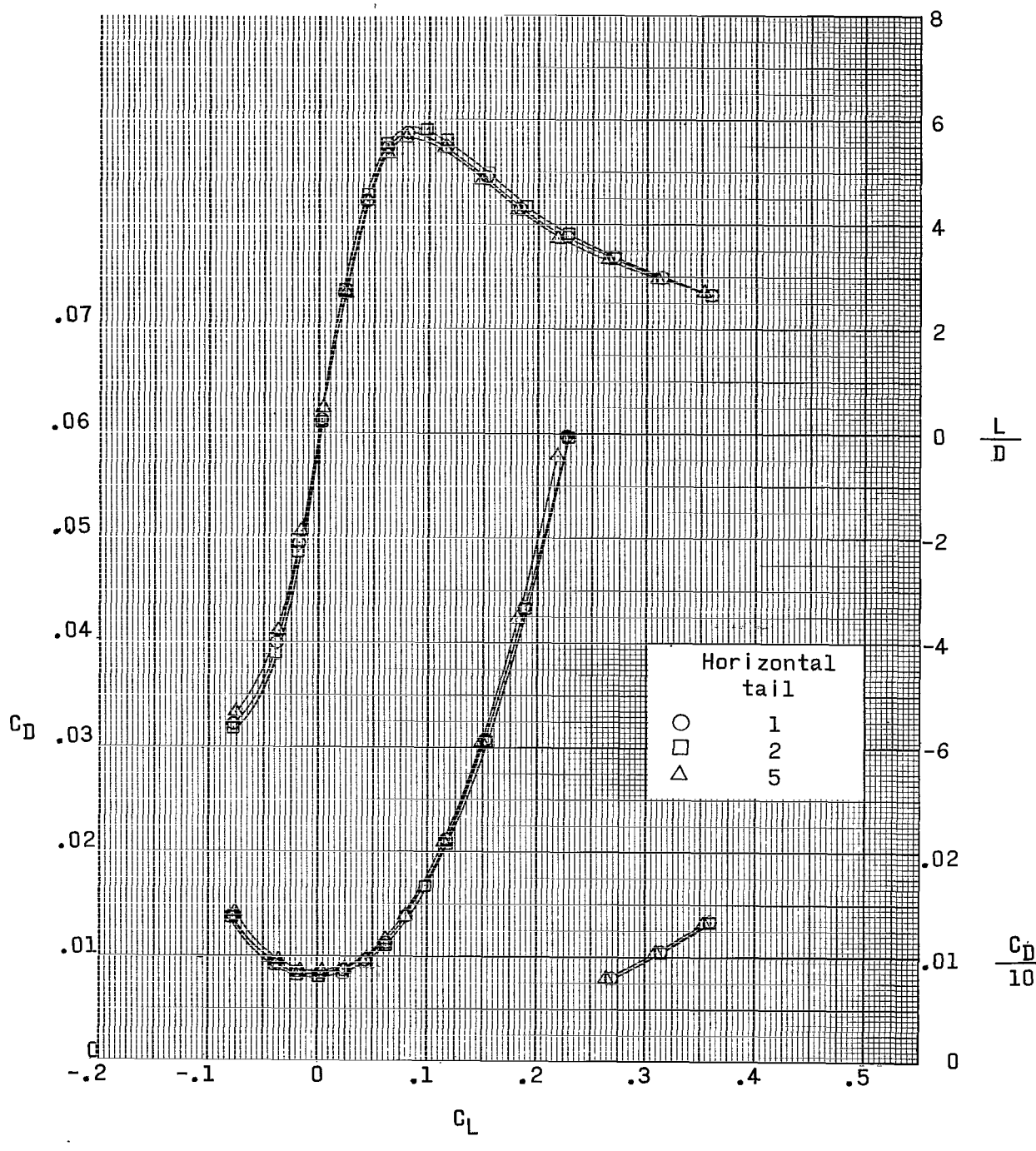

(d) Concluded.

Figure 7.- Continued.

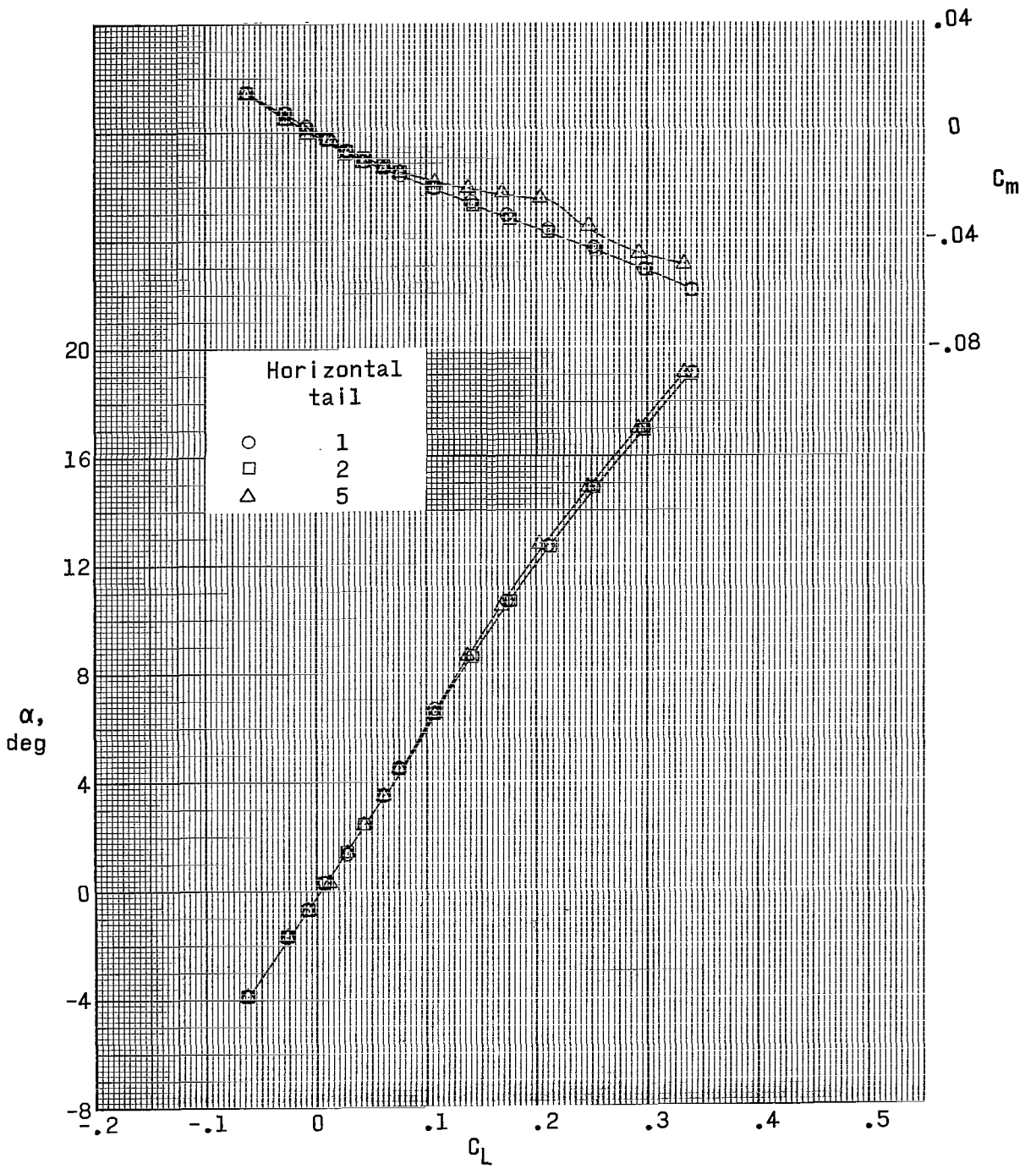

(e) M = 4.63.

Figure 7.- Continued.

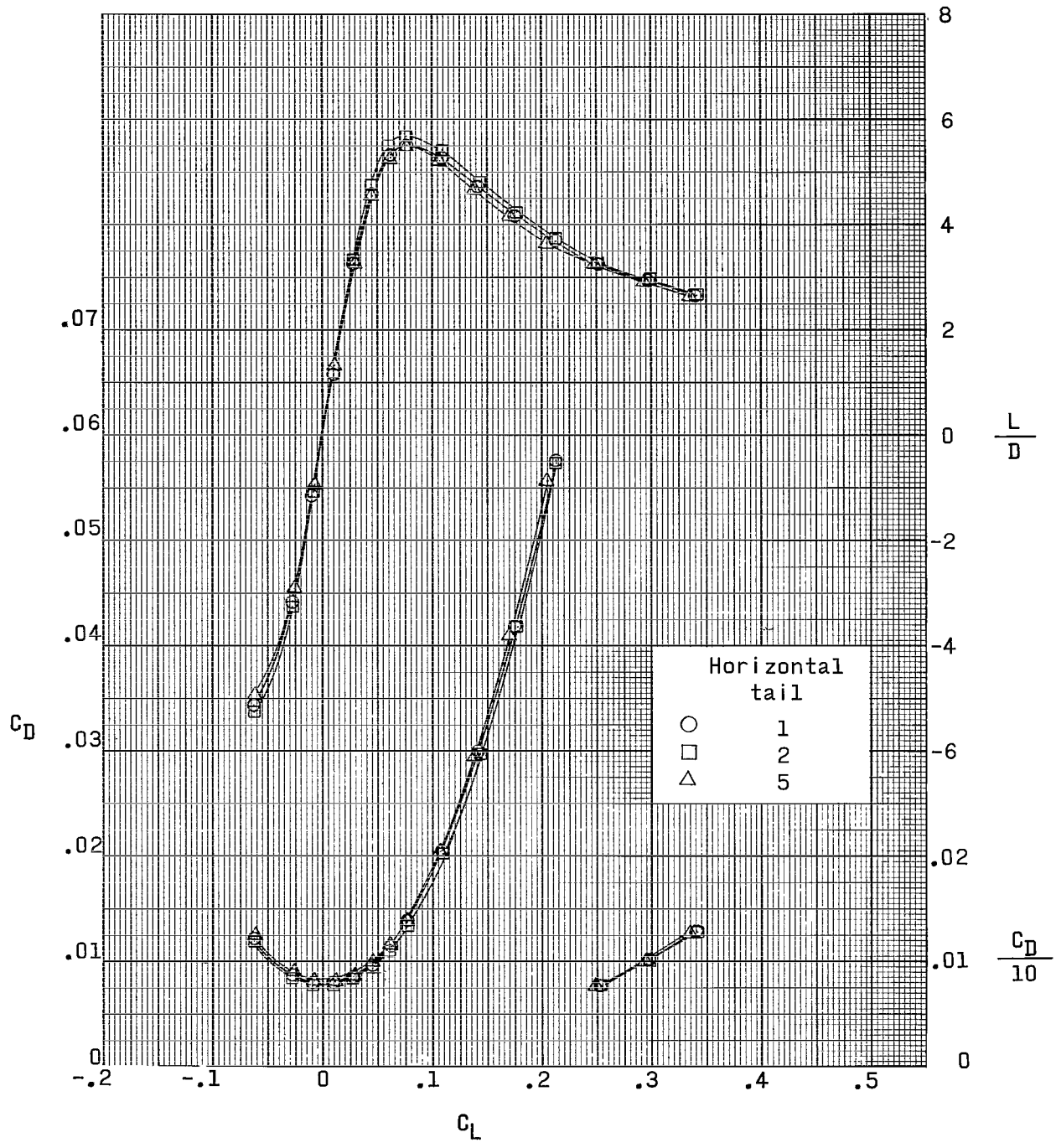

(e) Concluded.

Figure 7.- Concluded.

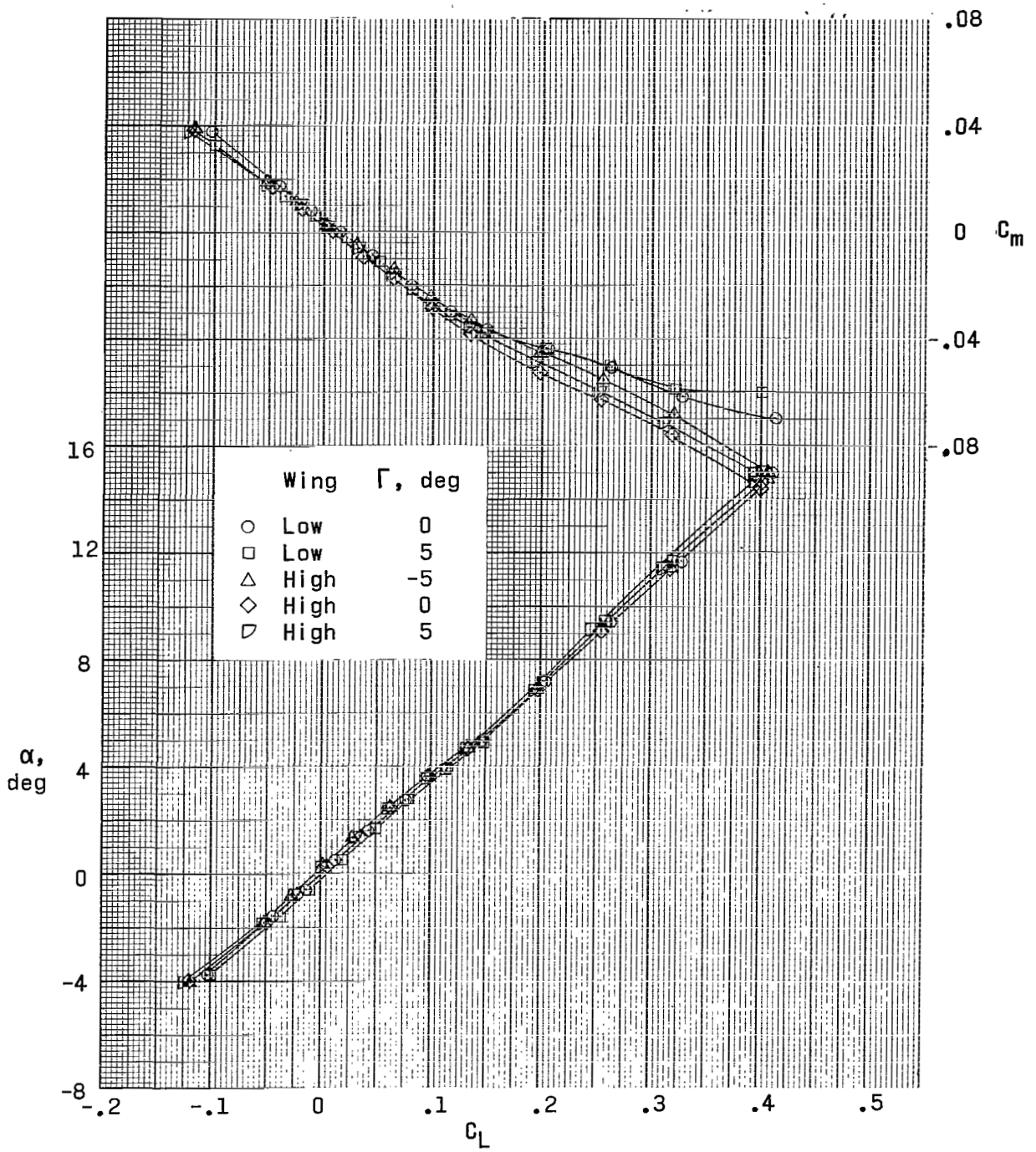

(a) M = 1.90.

Figure 8.- Effect of wing height and dihedral on aerodynamic characteristics in pitch. Horizontal-tail position 2.

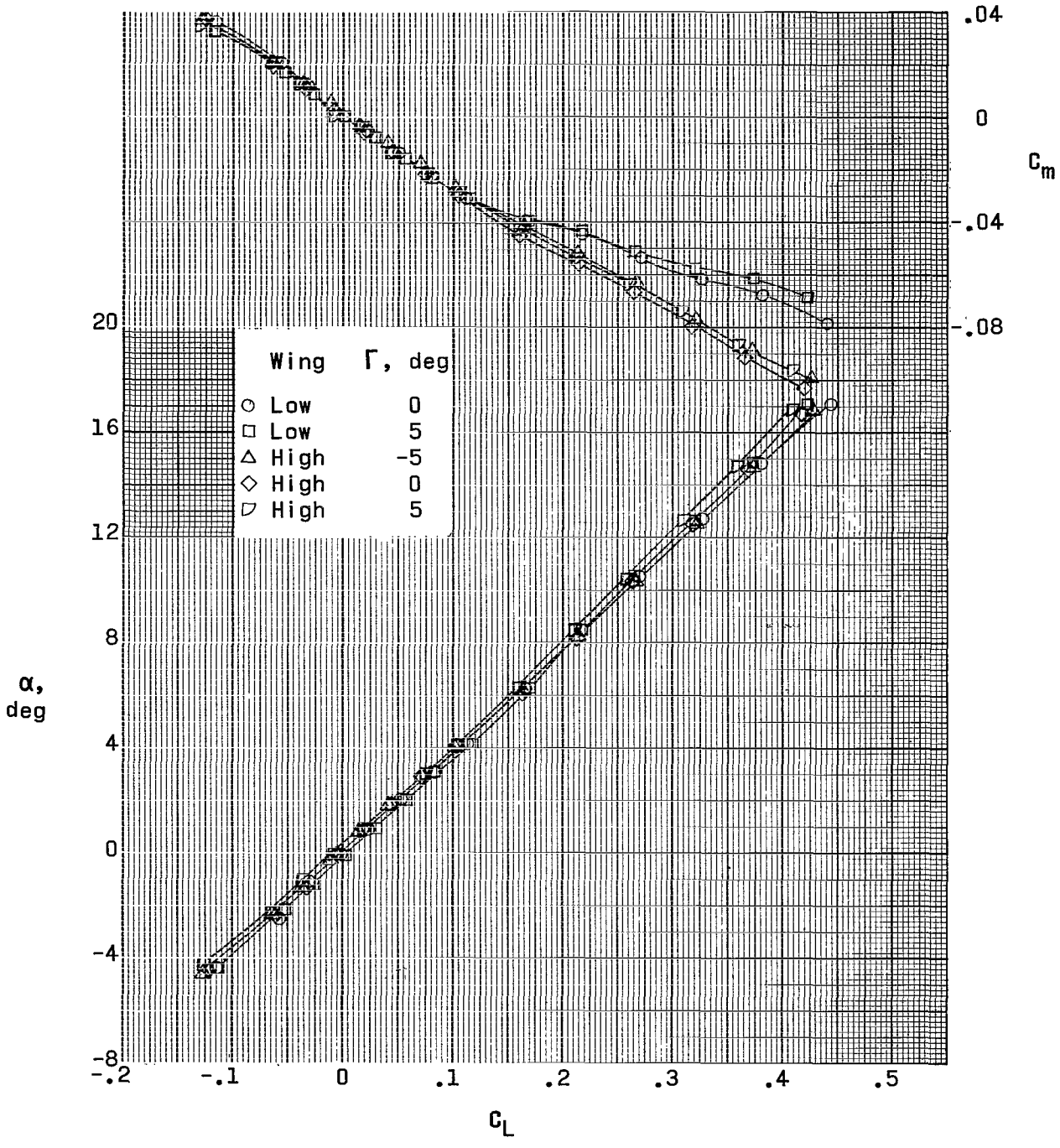

(b) M = 2.30.

Figure 8.- Continued.

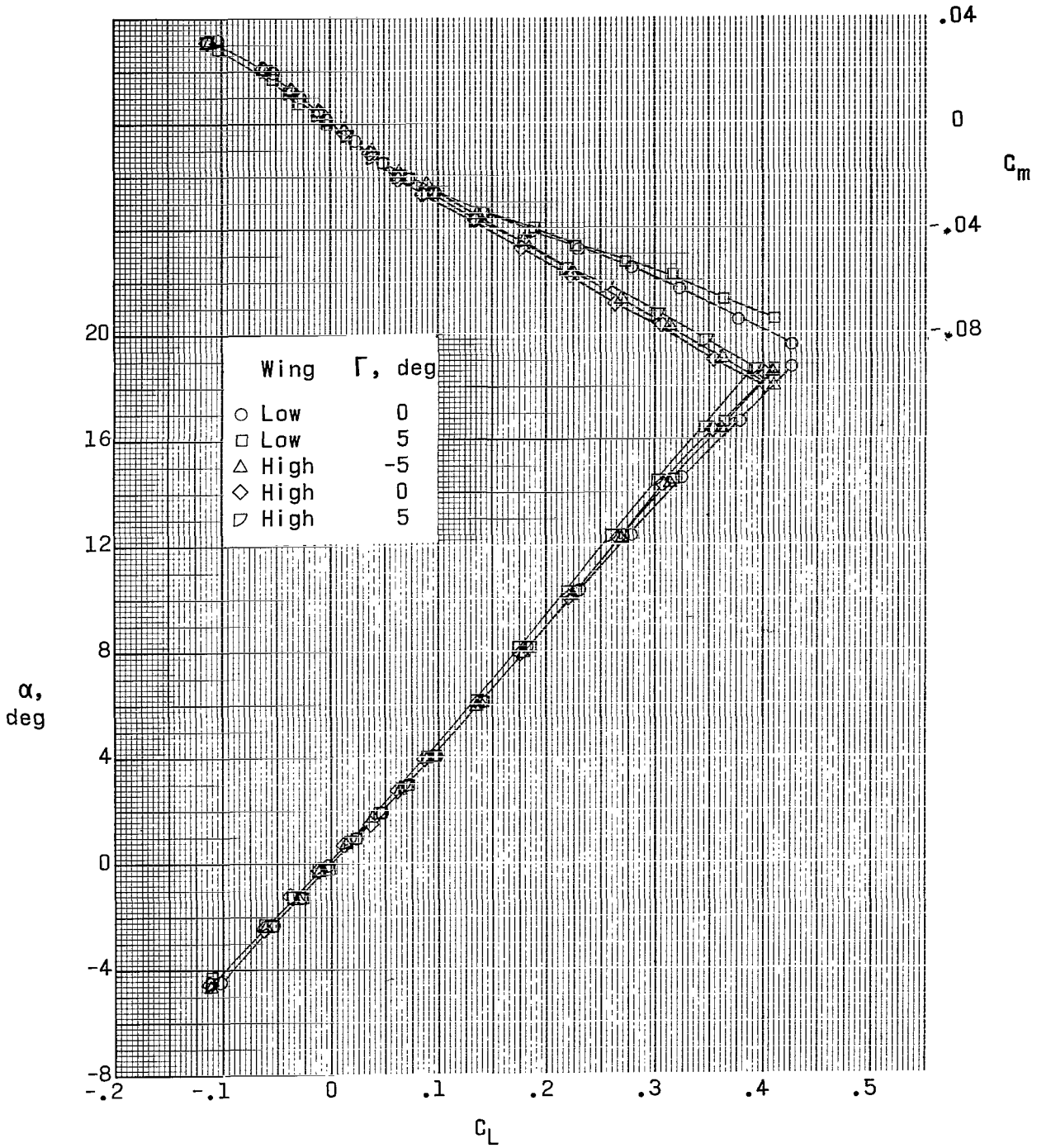

(c) M = 2.96.

Figure 8.- Continued.

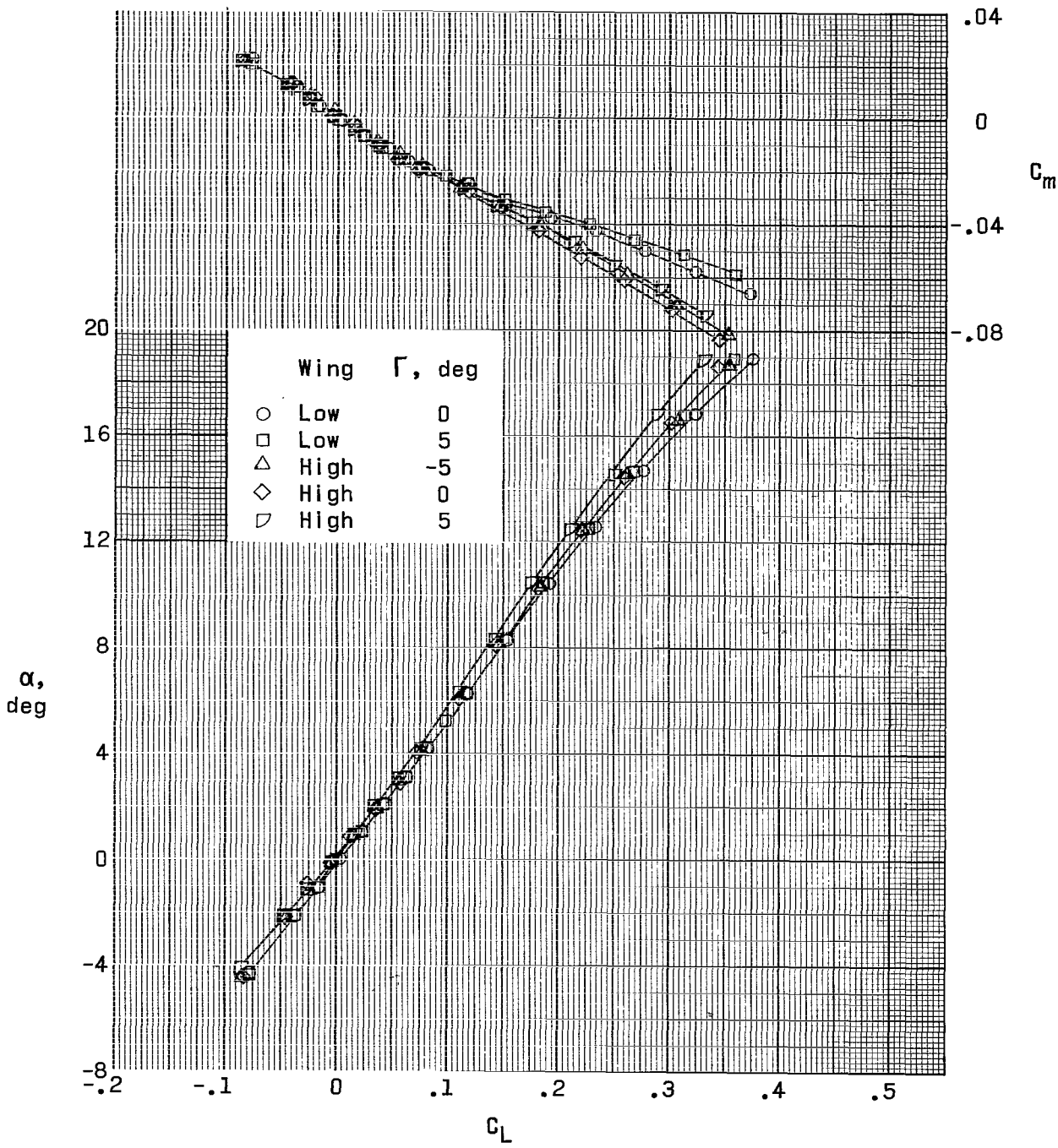

(d) M = 3.95.

Figure 8.- Continued.

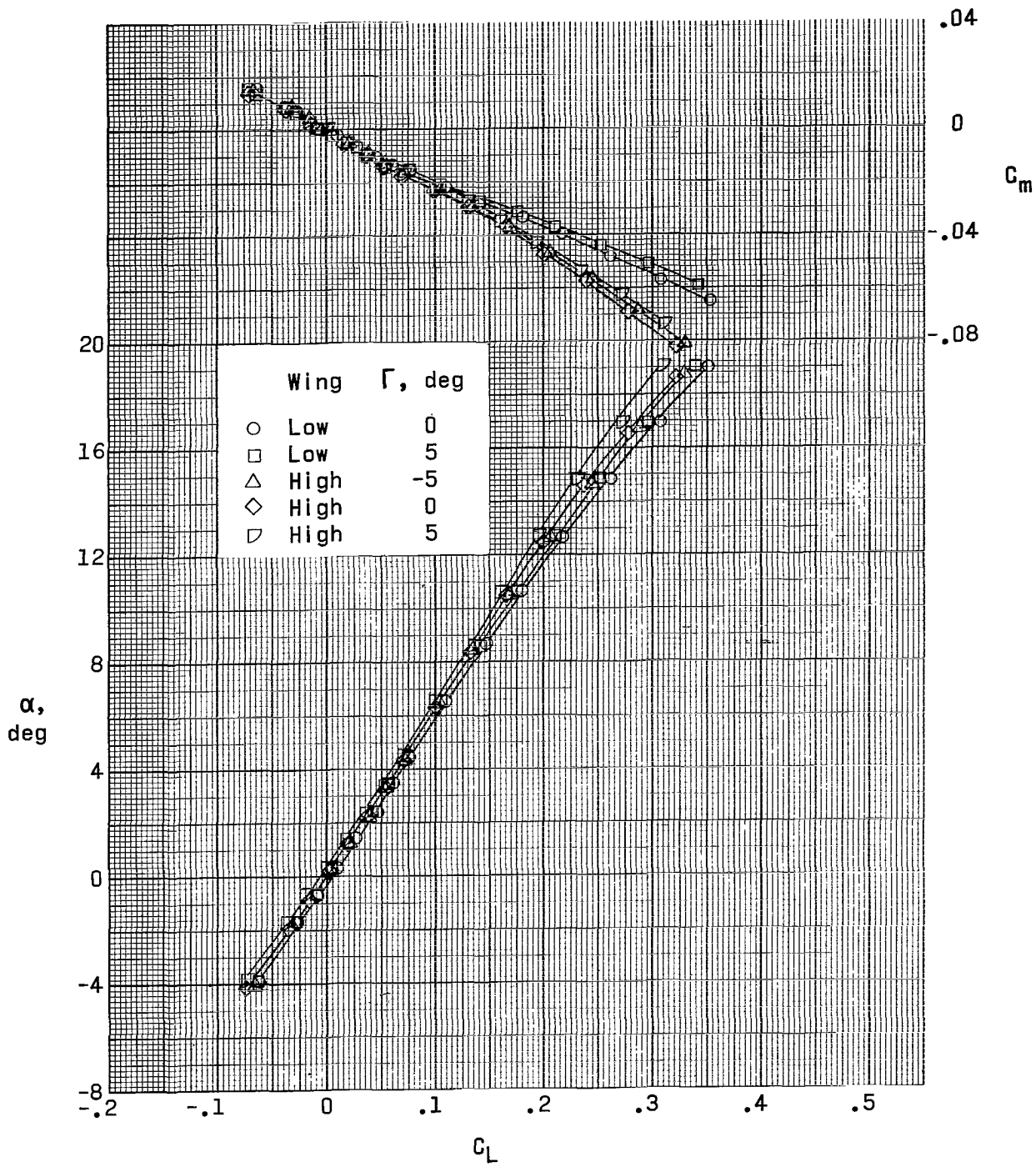

(e) M = 4.63.

Figure 8.- Concluded.

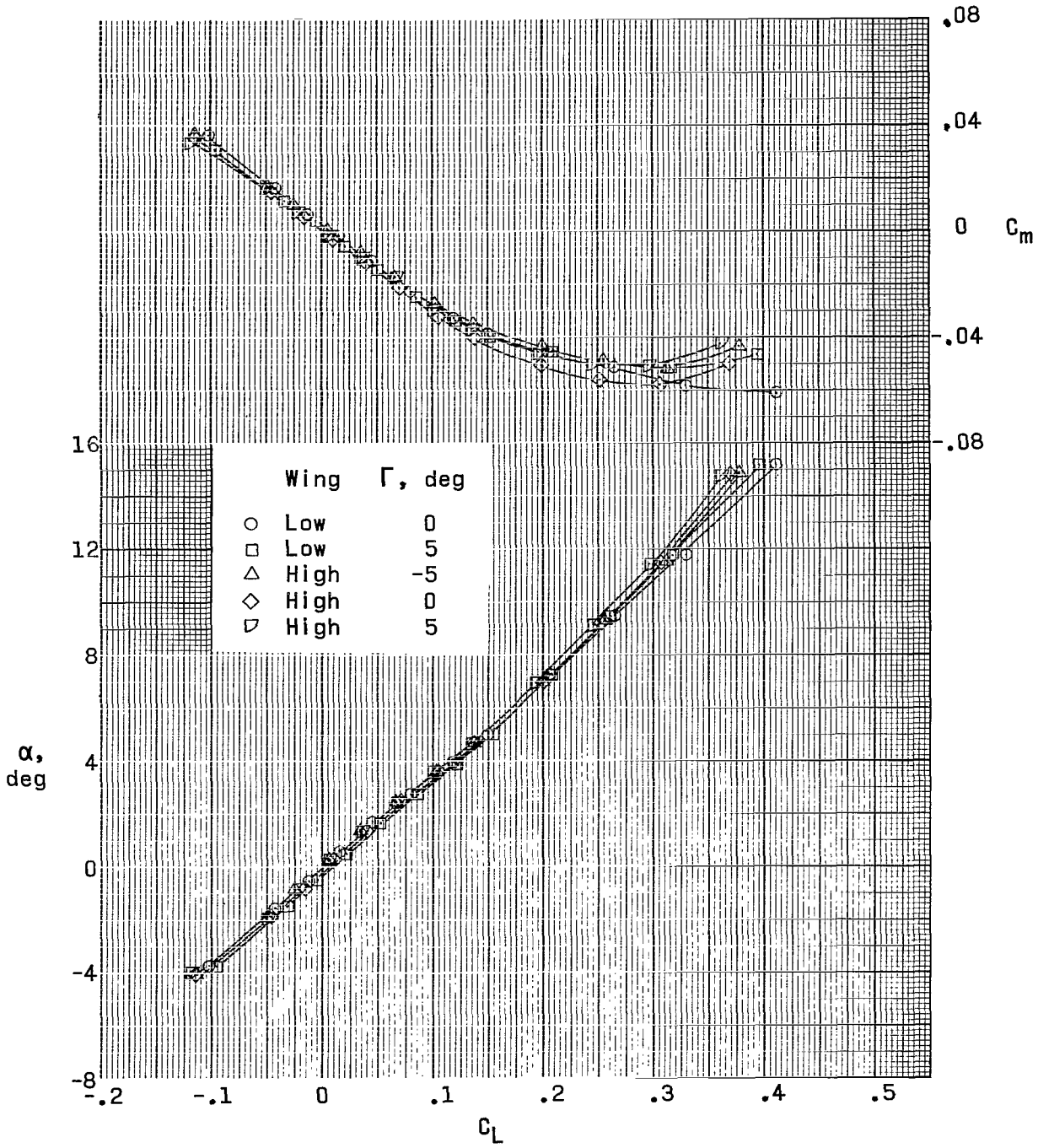

(a) M = 1.90.

Figure 9.- Effect of wing height and dihedral on aerodynamic characteristics in pitch. Horizontal-tail position 5.

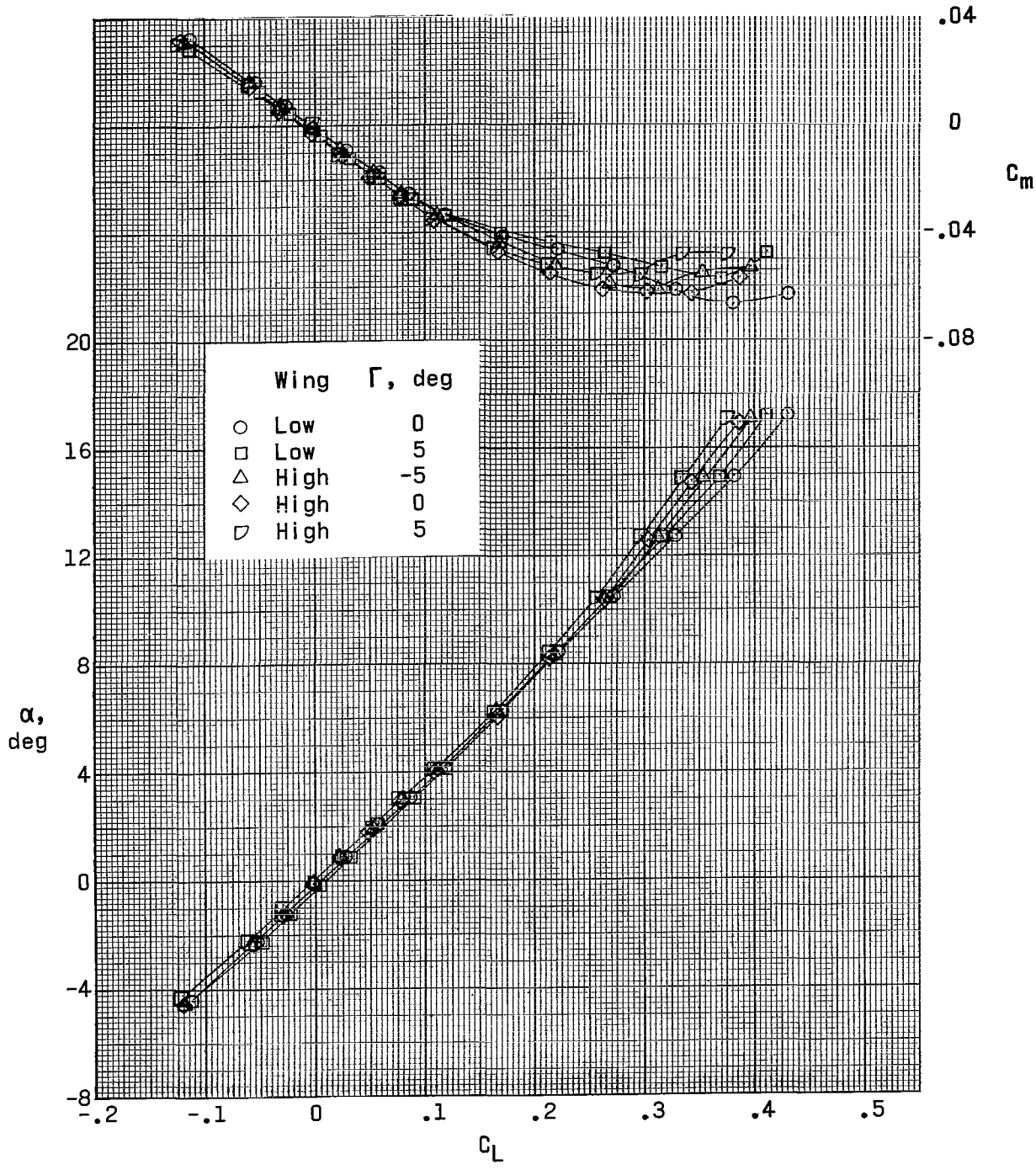

(b) M = 2.30.

Figure 9.- Continued.

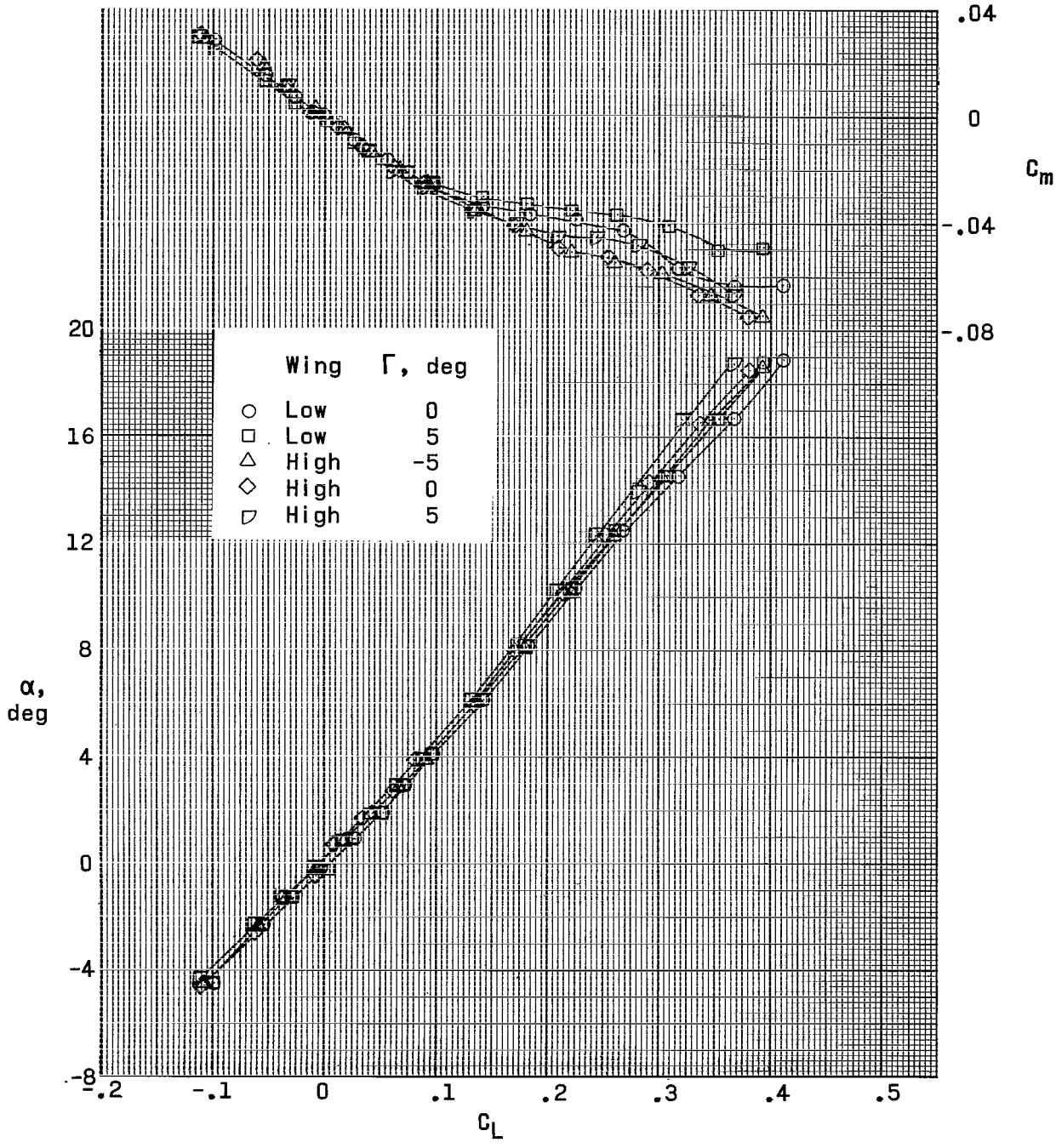

(c) M = 2.96.

Figure 9.- Continued.

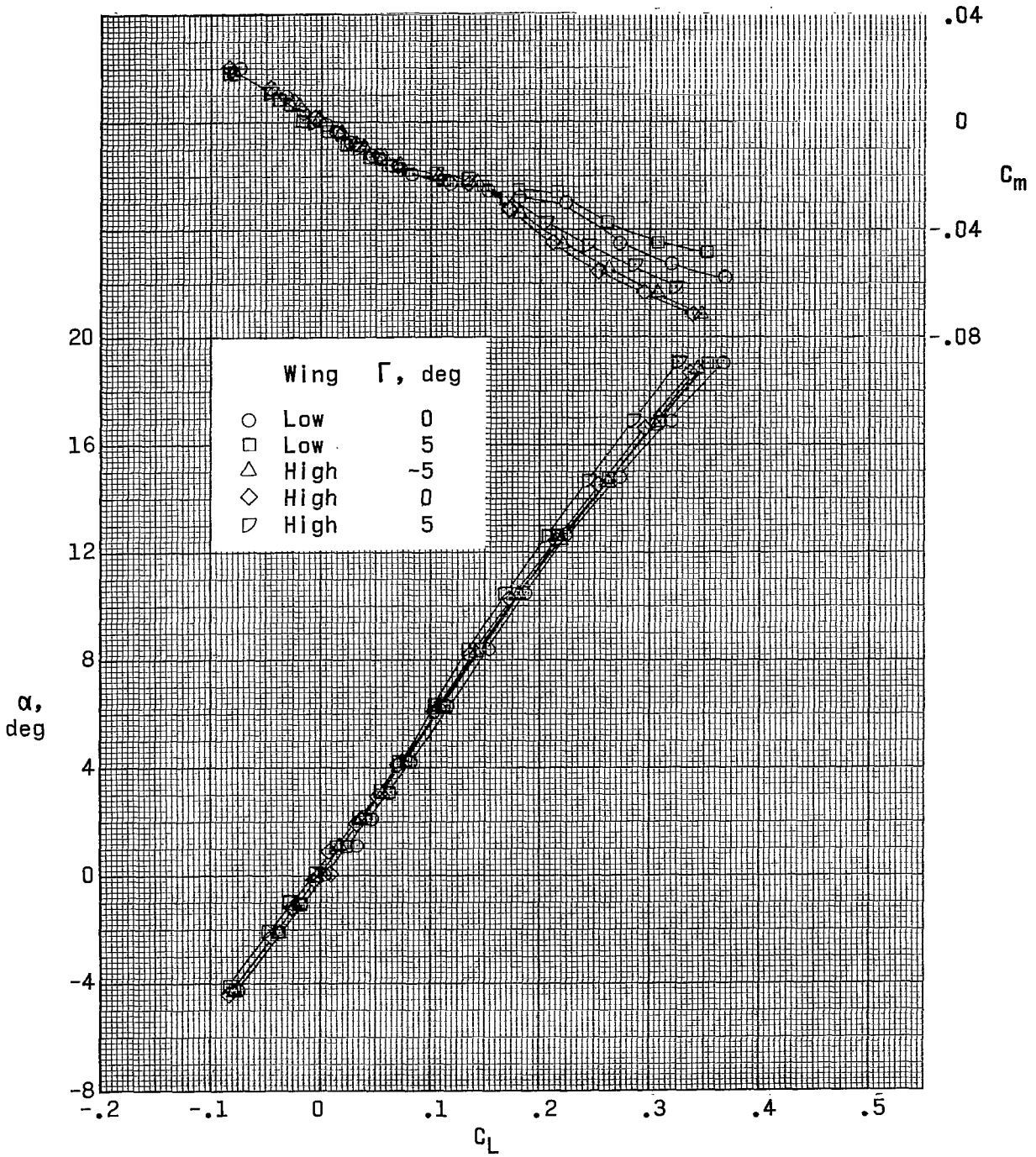

(d) M = 3.95.

Figure 9.- Continued.

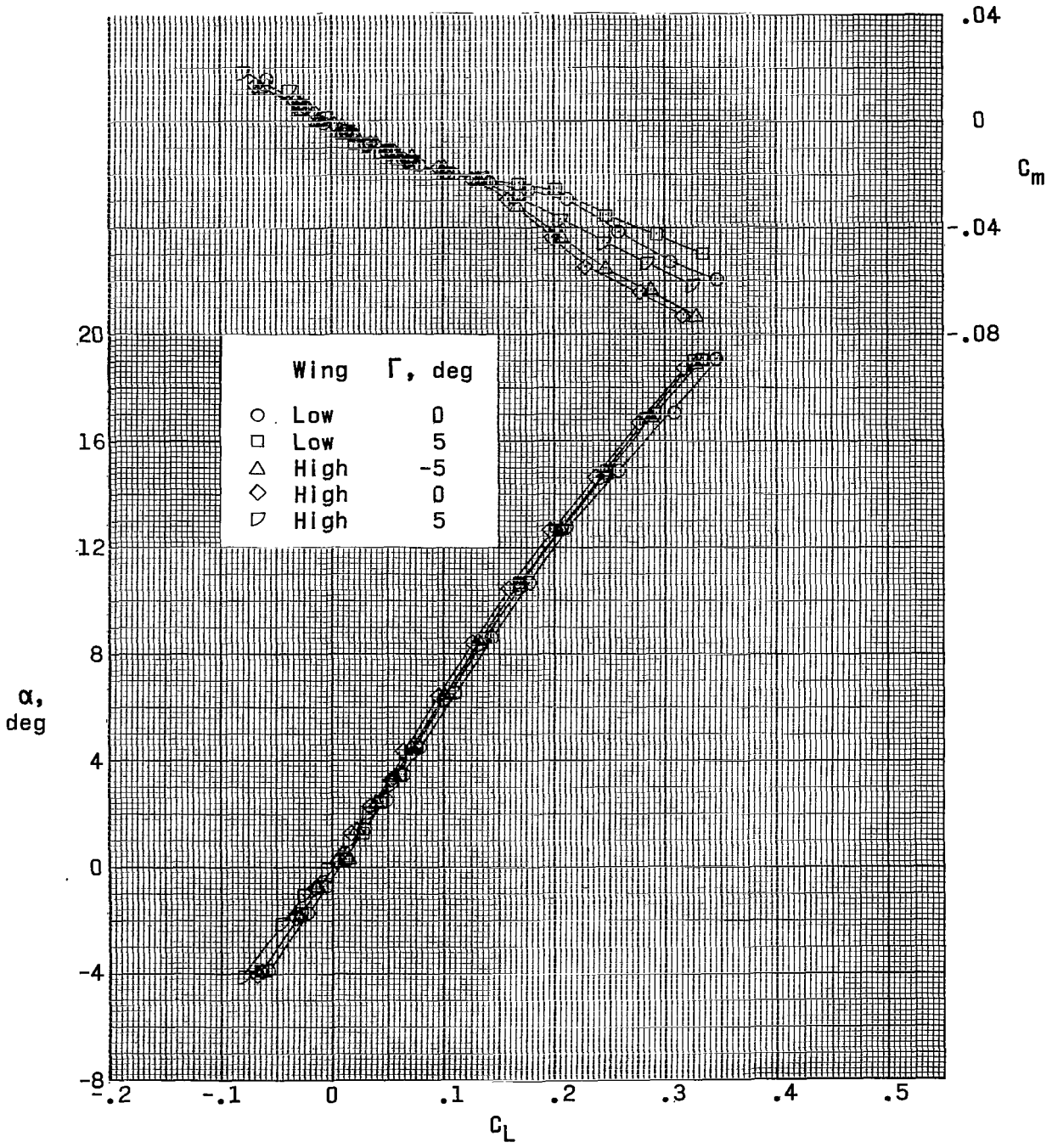

(e) M = 4.63.

Figure 9.- Concluded.

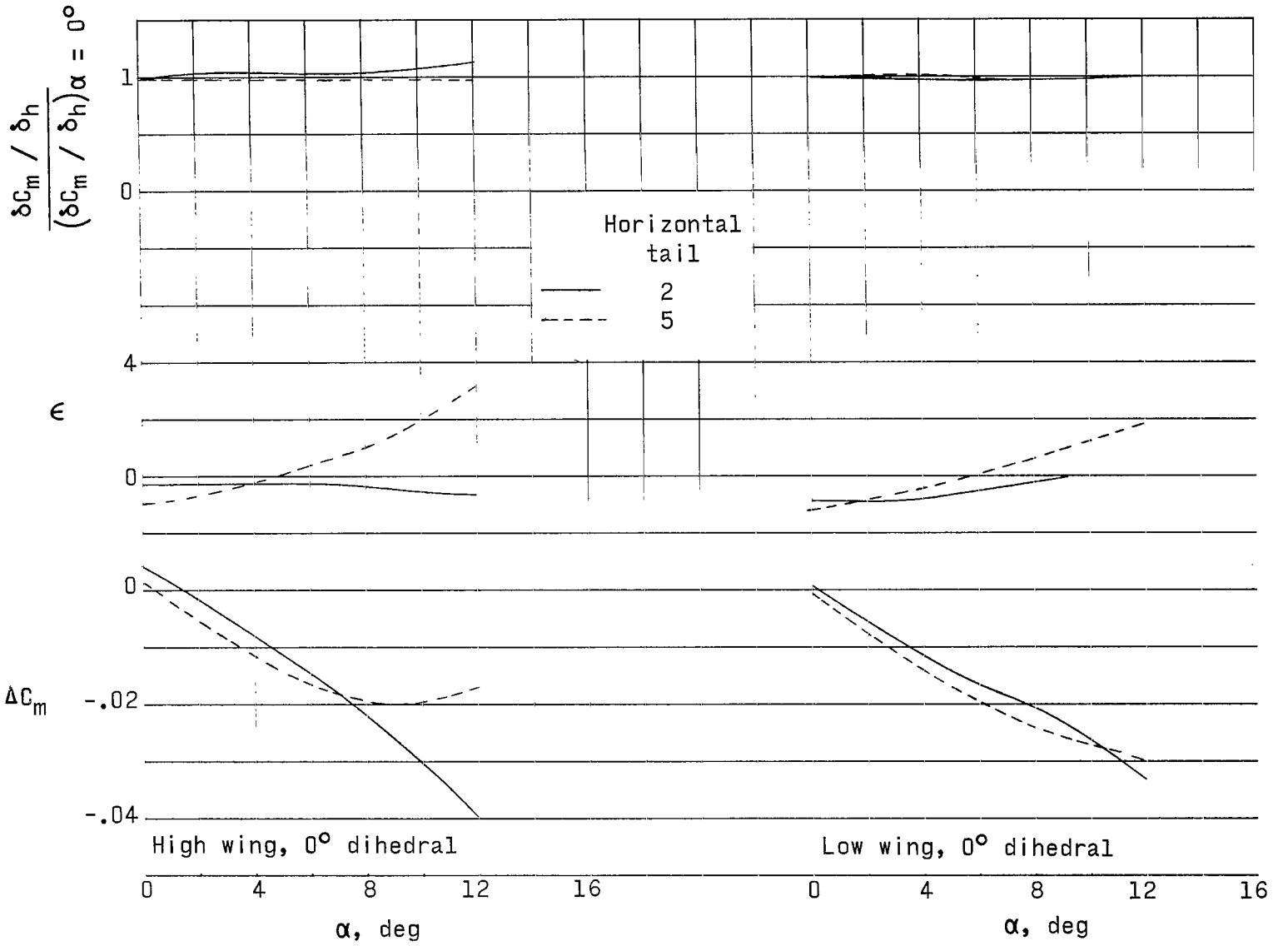

(a) M = 1.90.

Figure 10.- Summary of horizontal-tail and downwash characteristics.

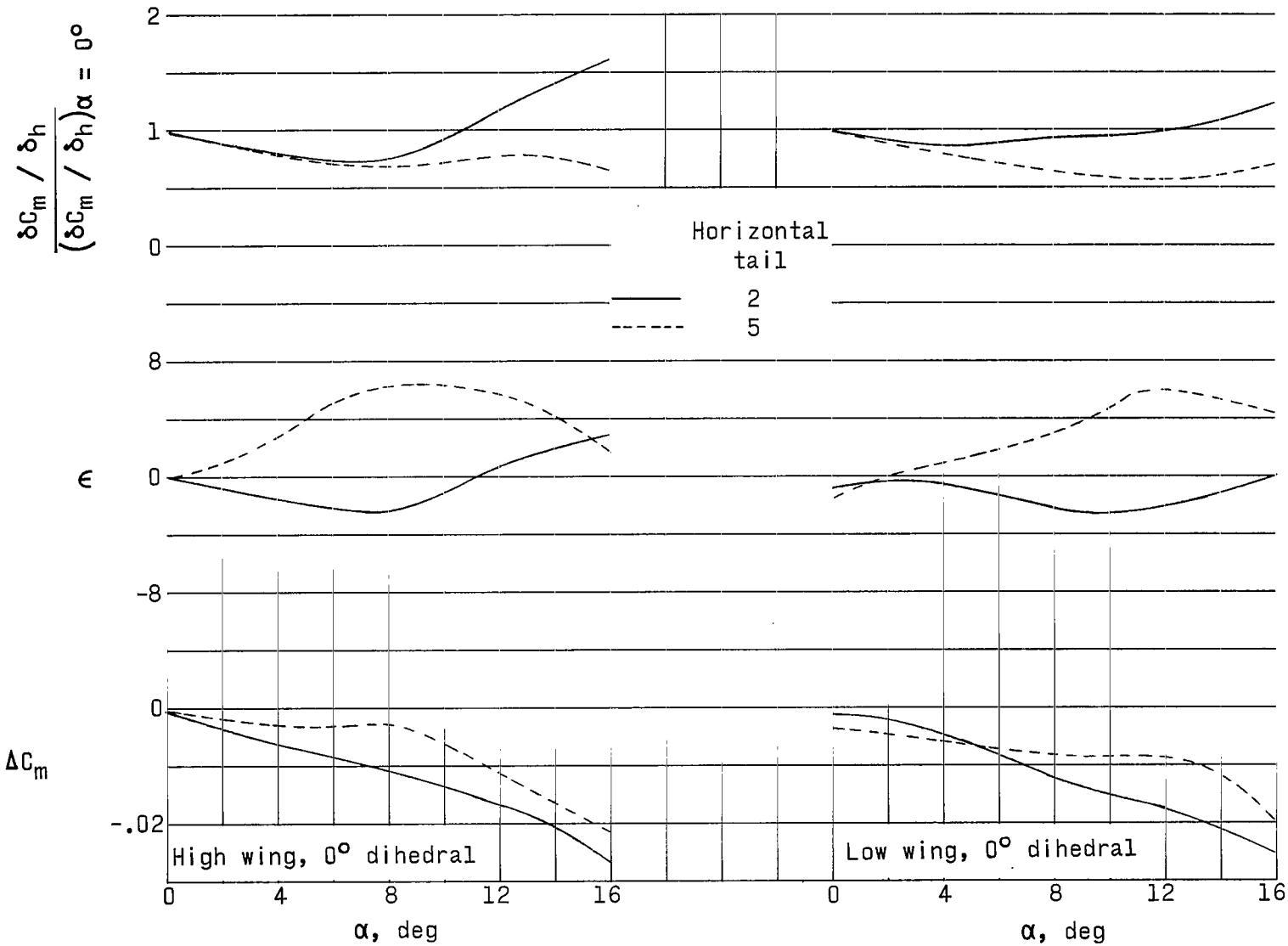

(b) M = 4.63.

Figure 10.- Concluded.

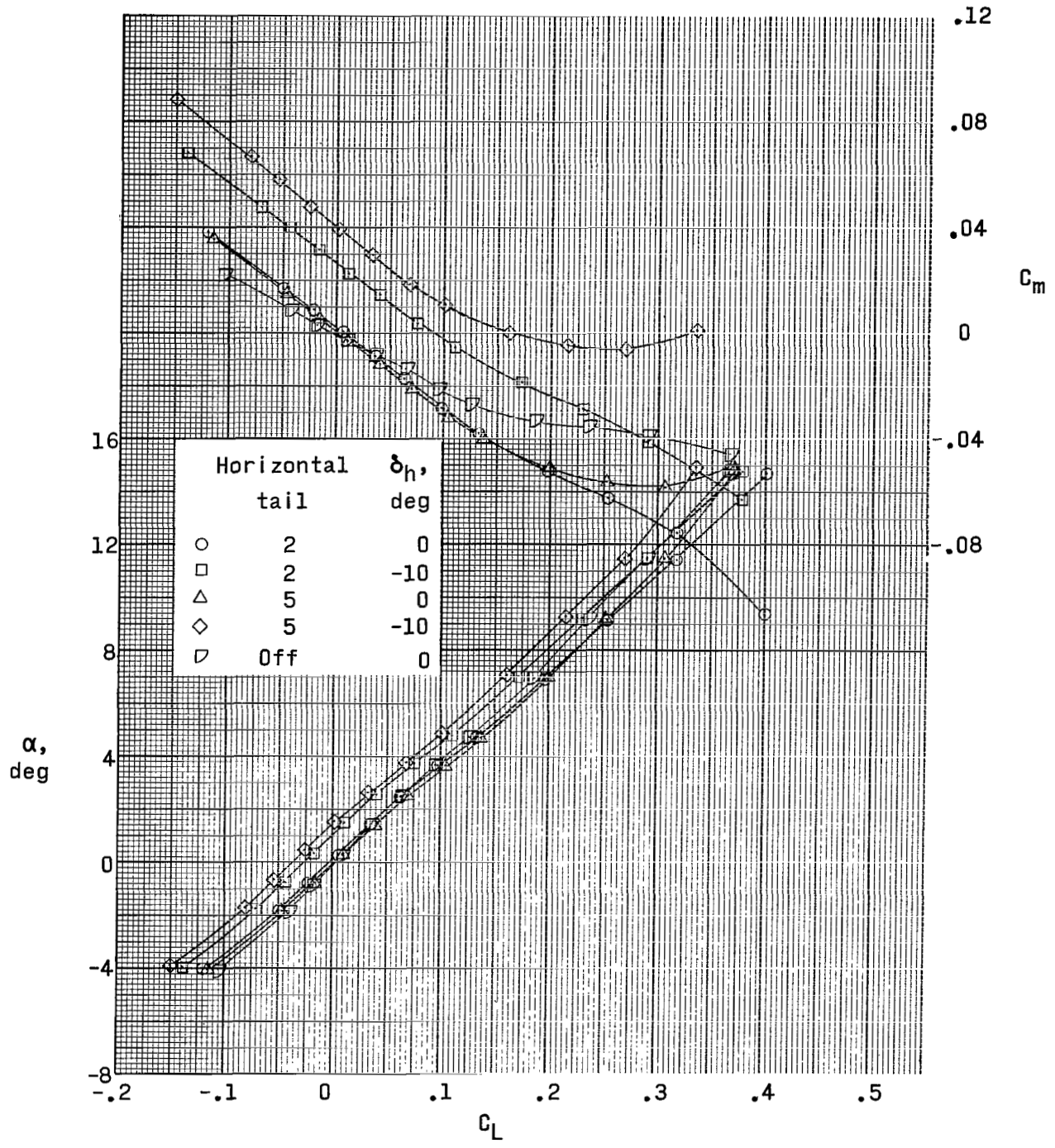

(a) M = 1.90.

Figure 11.- Effect of horizontal-tail deflection on aerodynamic characteristics in pitch. High wing; 0° dihedral.

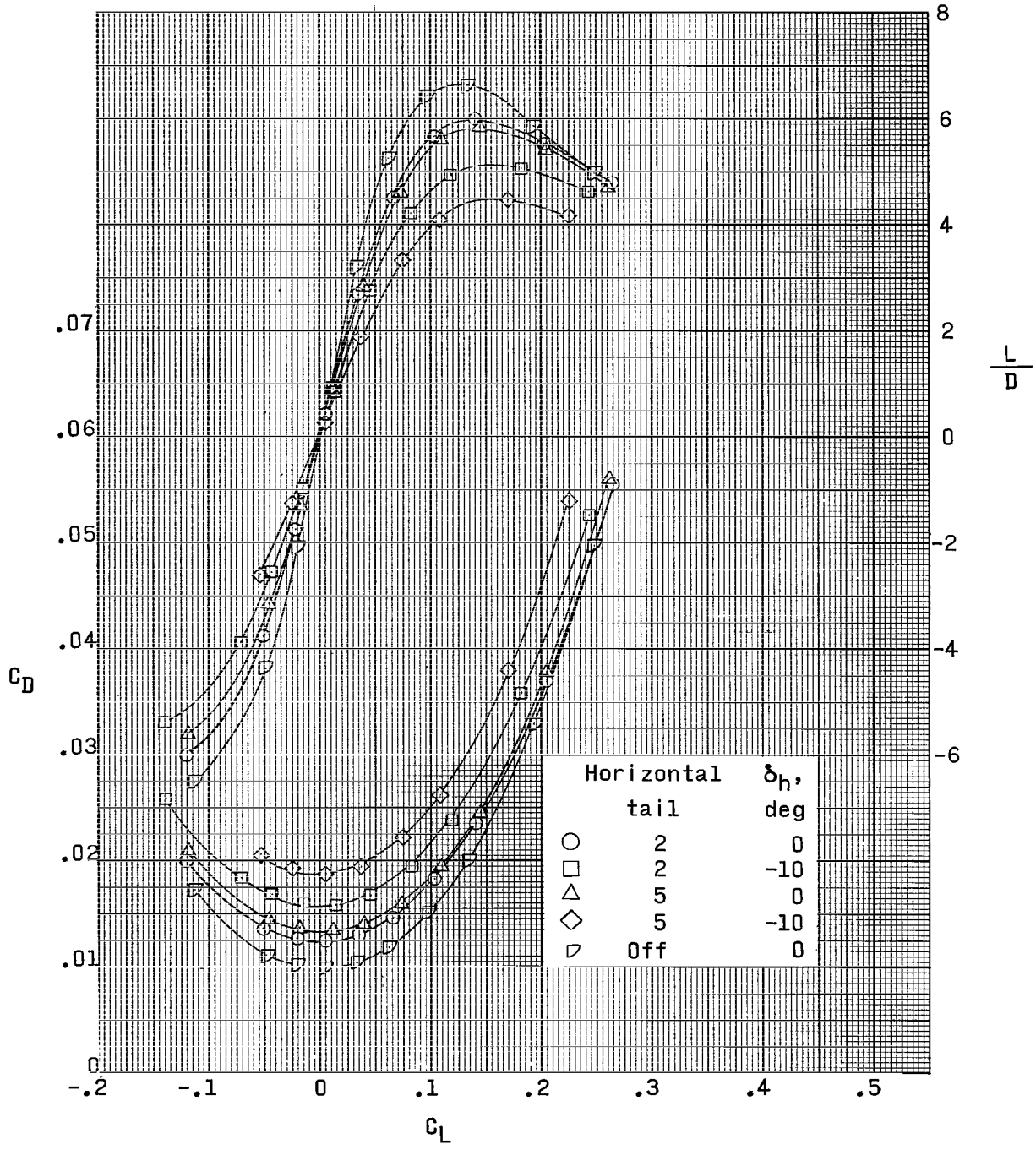

(a) Concluded.

Figure 11.- Continued.

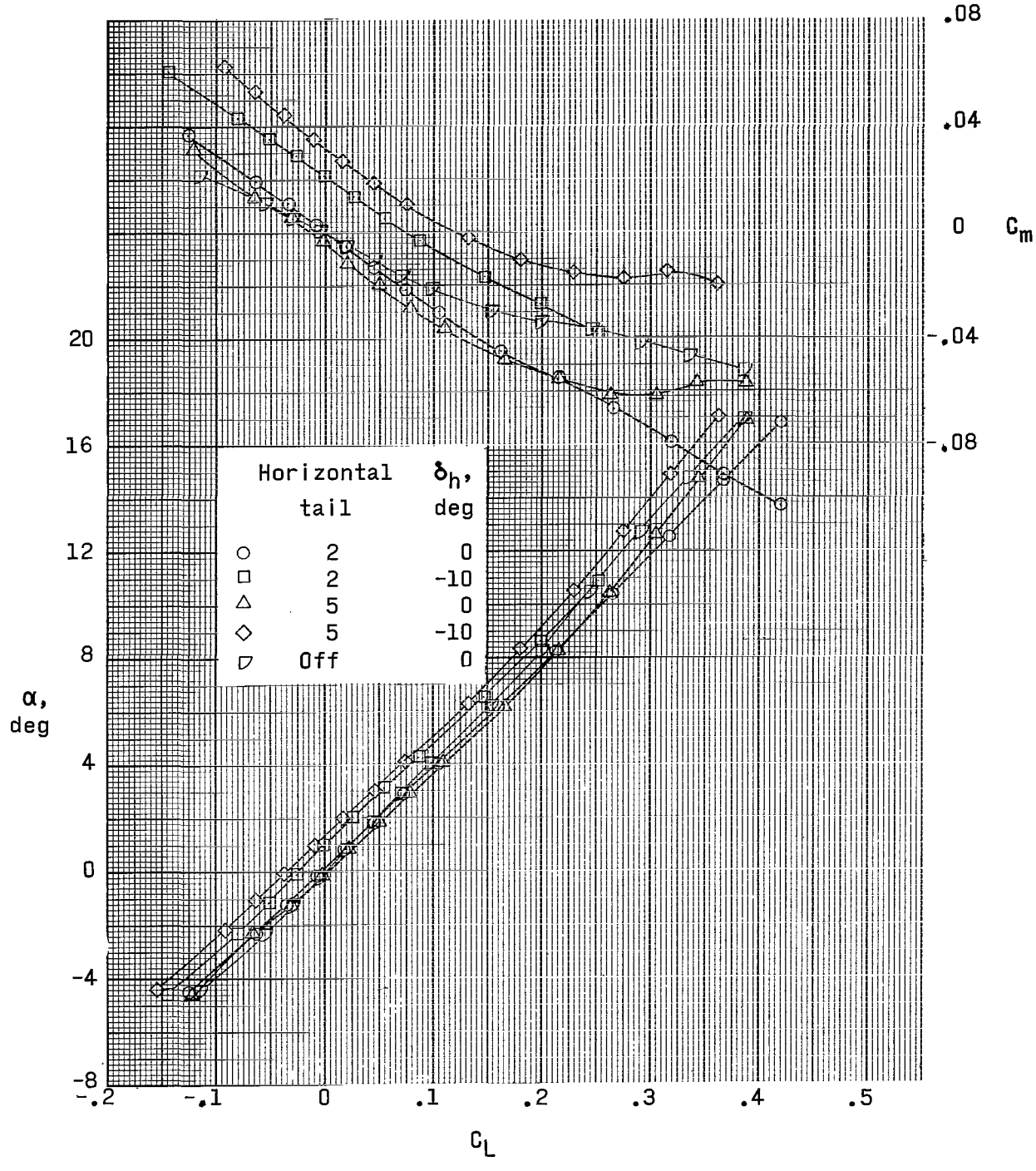

(b) M = 2.30.

Figure 11.- Continued.

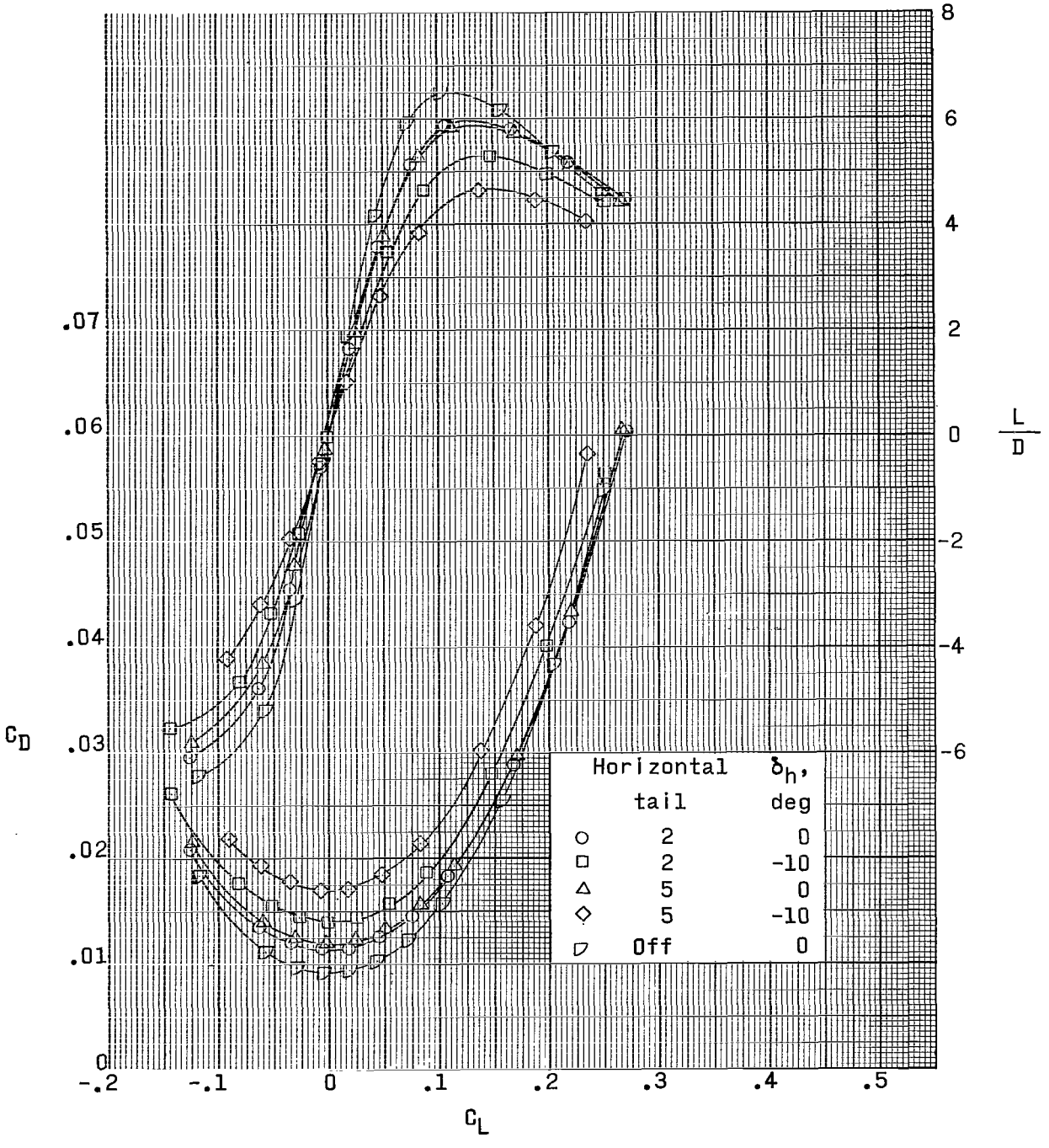

(b) Concluded.

Figure 11.- Continued.

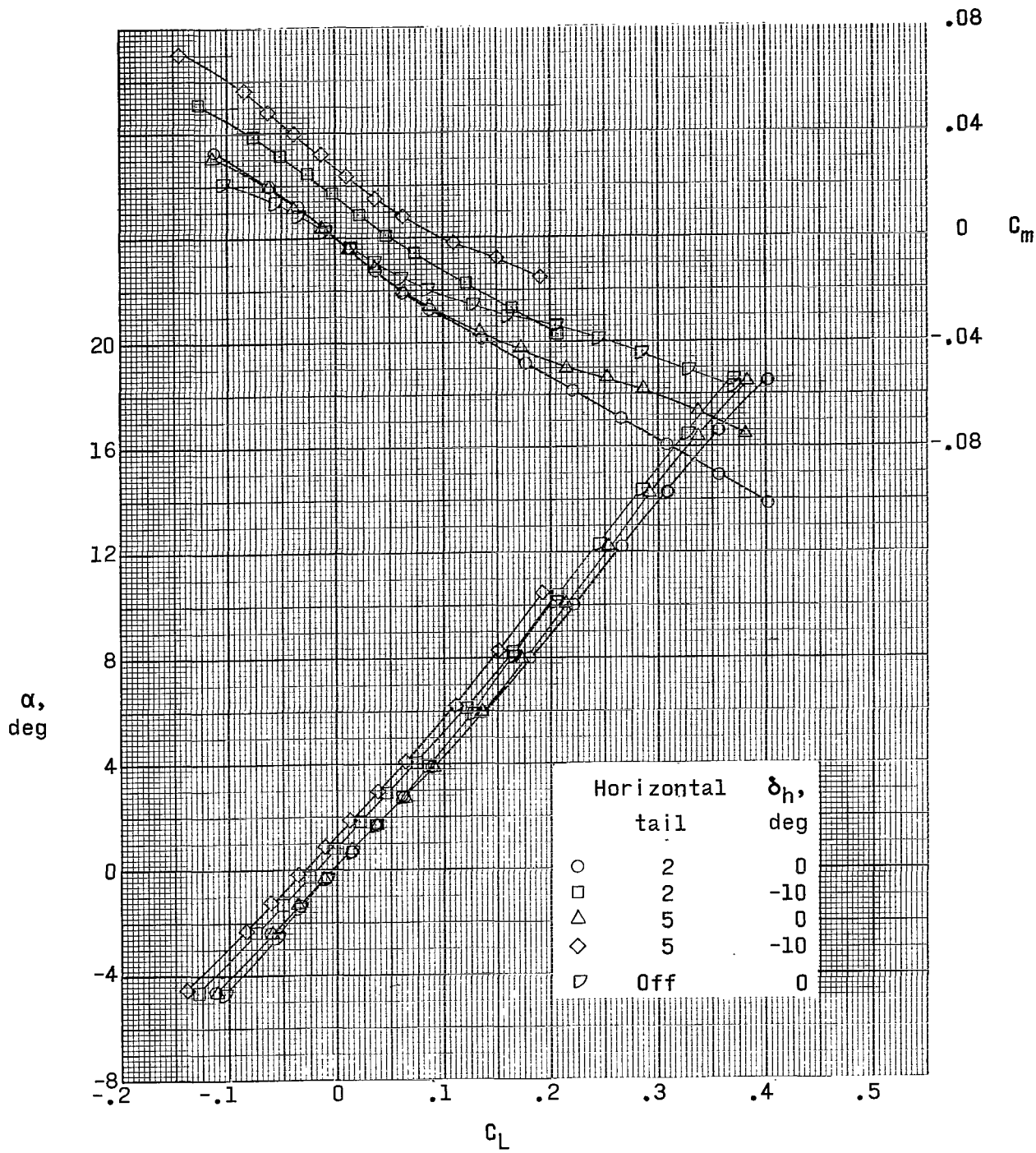

(c) M = 2.96.

Figure 11.- Continued.

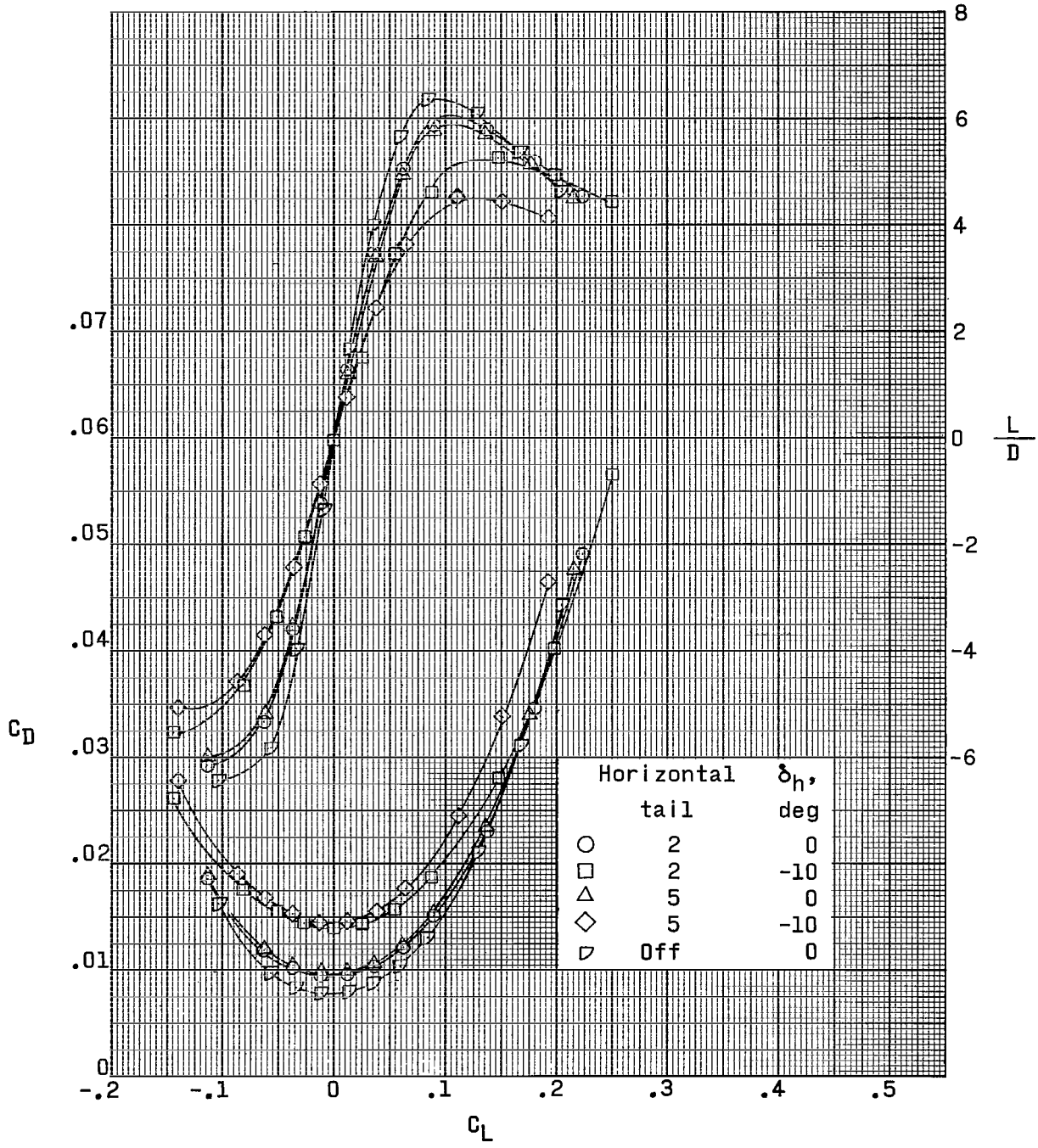

(c) Concluded.

Figure 11.- Continued.

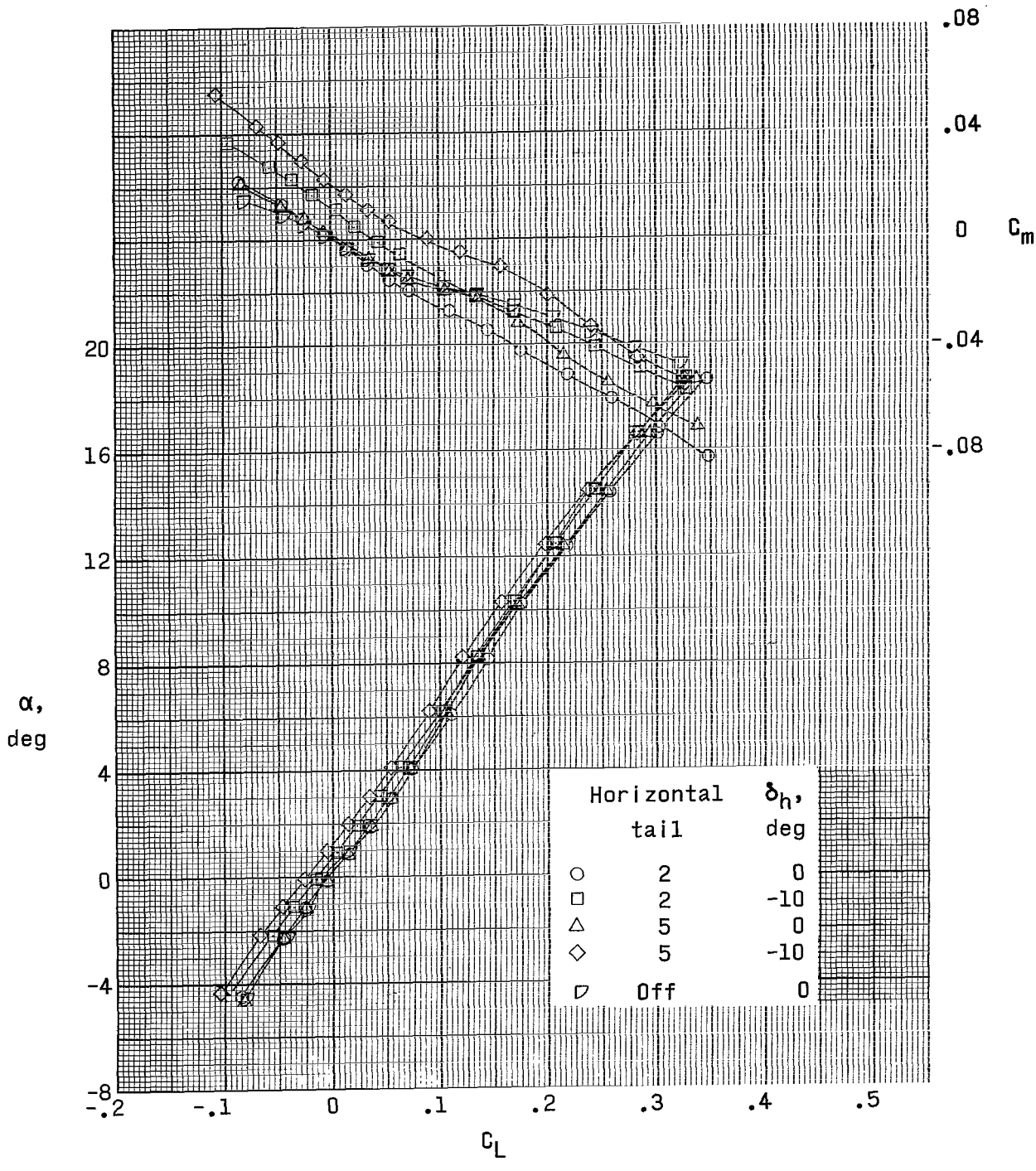

(d) M = 3.95.

Figure 11.- Continued.

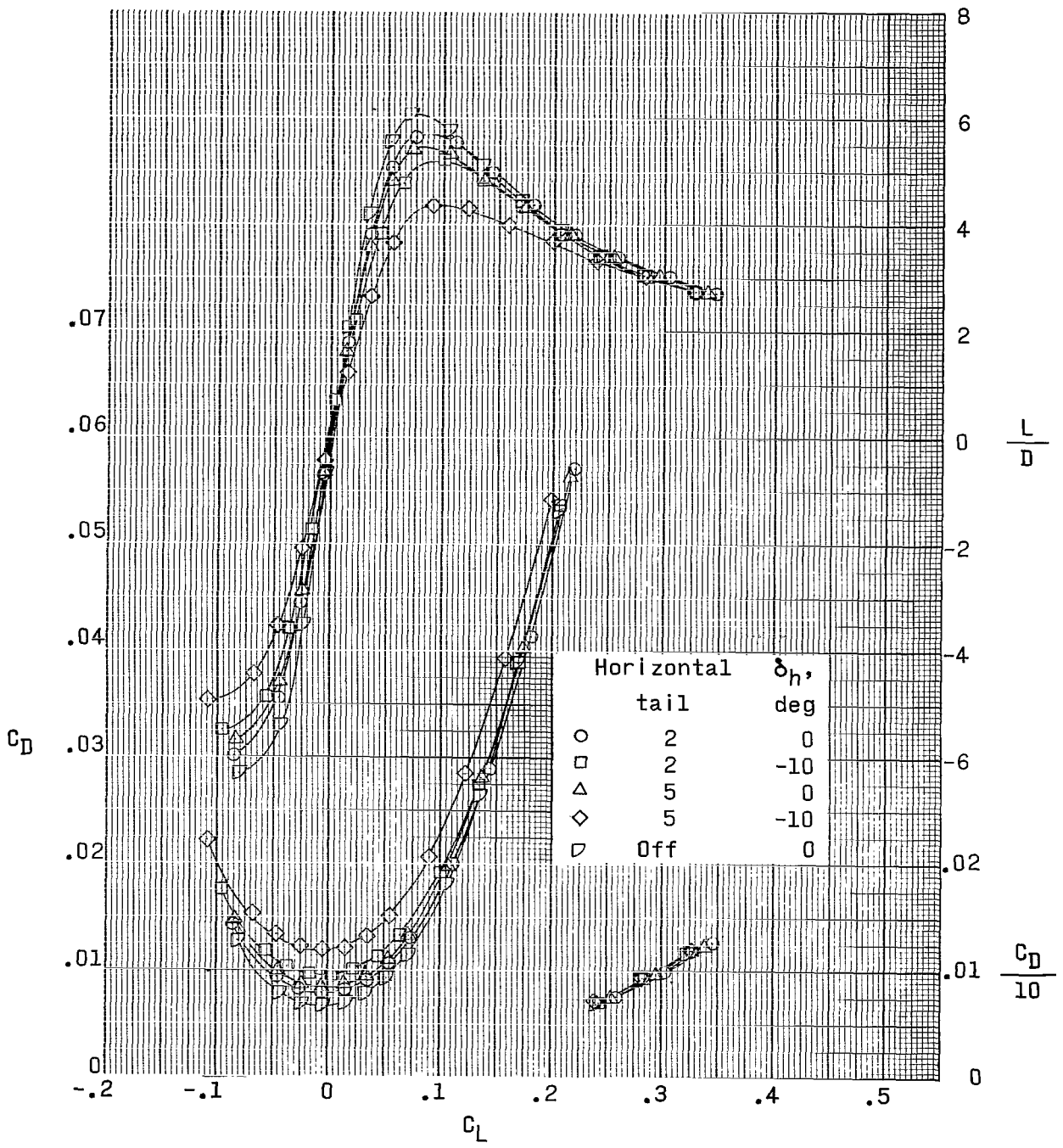

(d) Concluded.

Figure 11.- Continued.

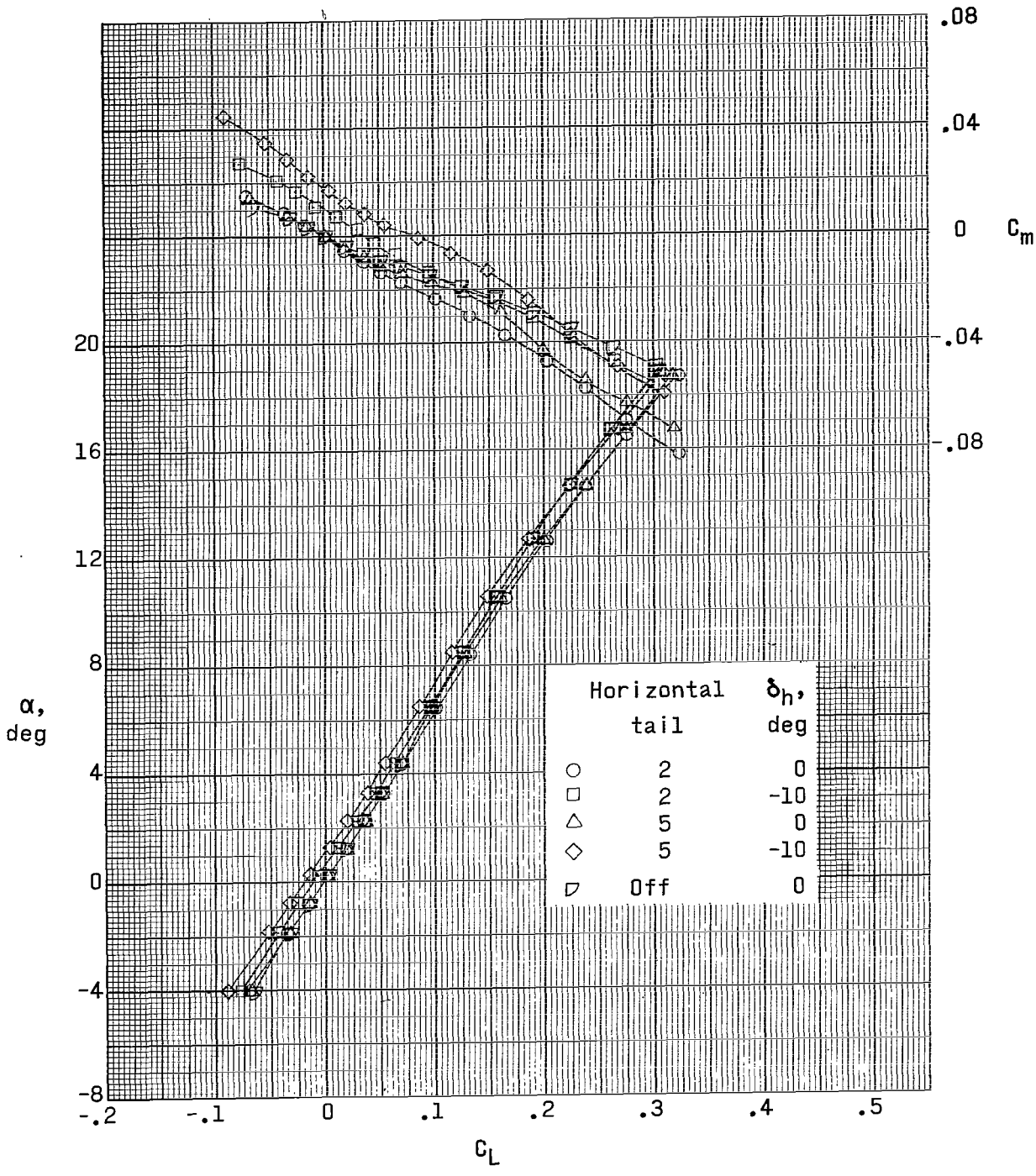

(e) M = 4.63.

Figure 11.- Continued.

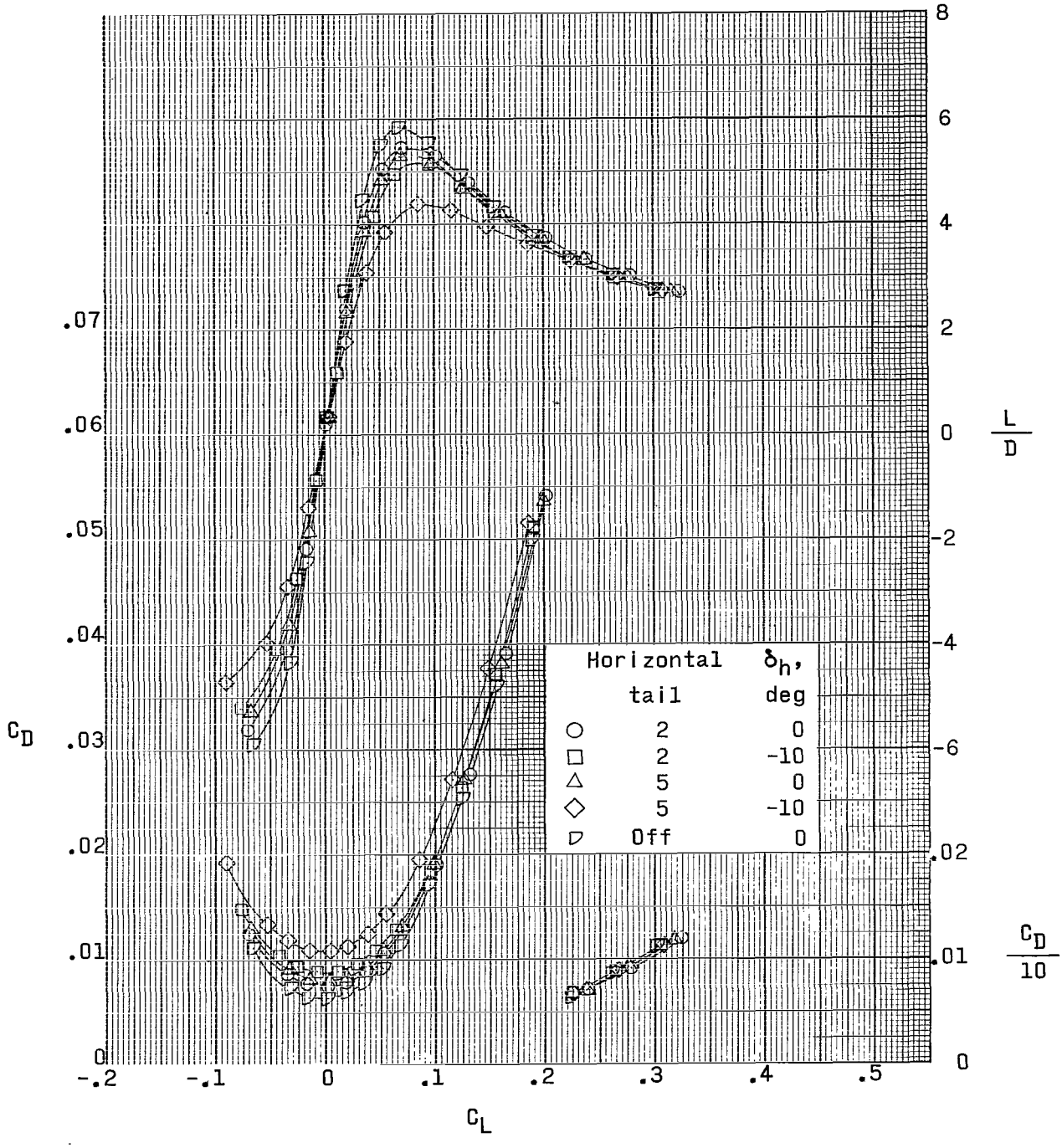

(e) Concluded.

Figure 11.- Concluded.

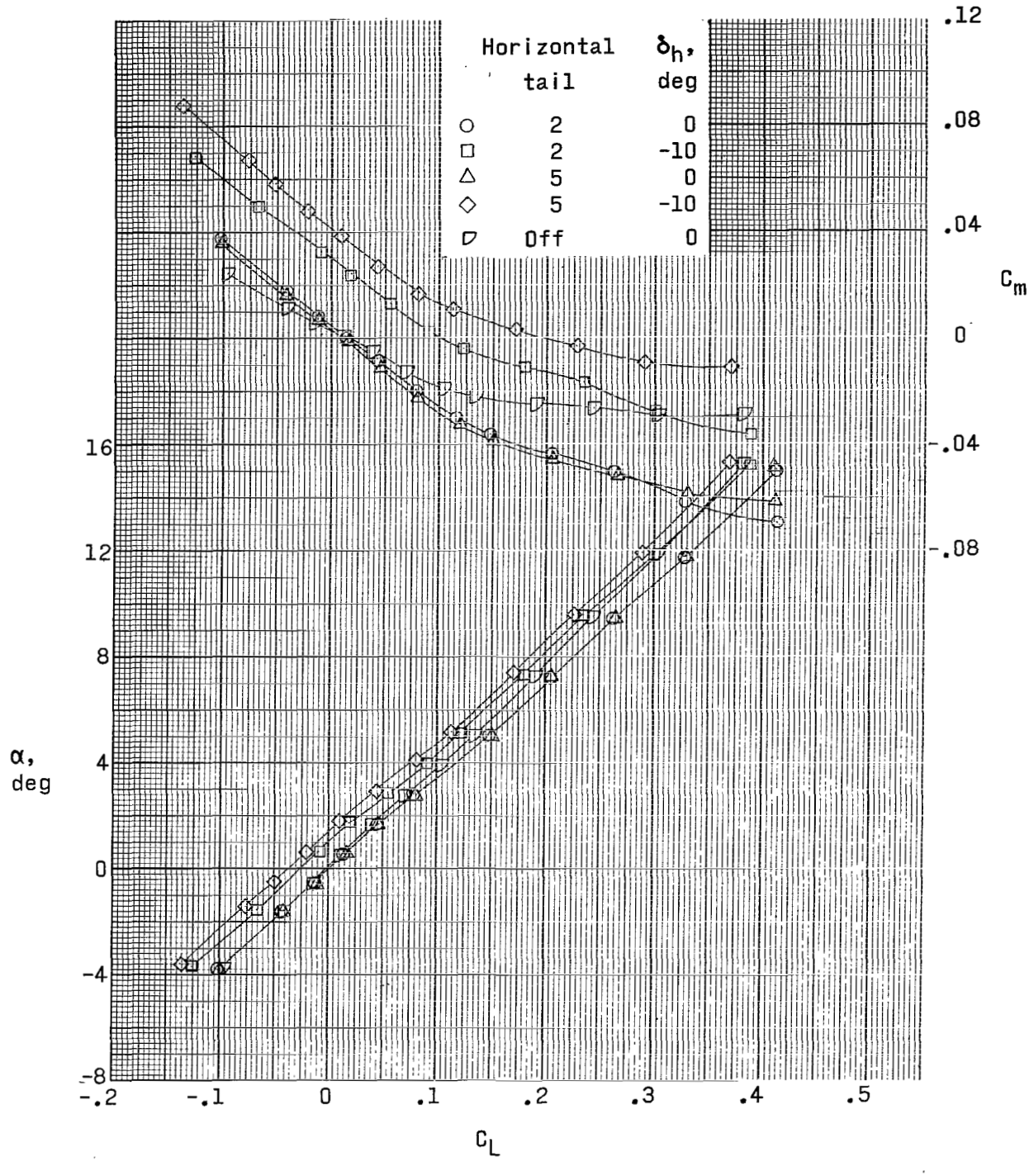

(a) M = 1.90.

Figure 12.- Effect of horizontal-tail deflection on aerodynamic characteristics in pitch. Low wing; 0^0 dihedral.

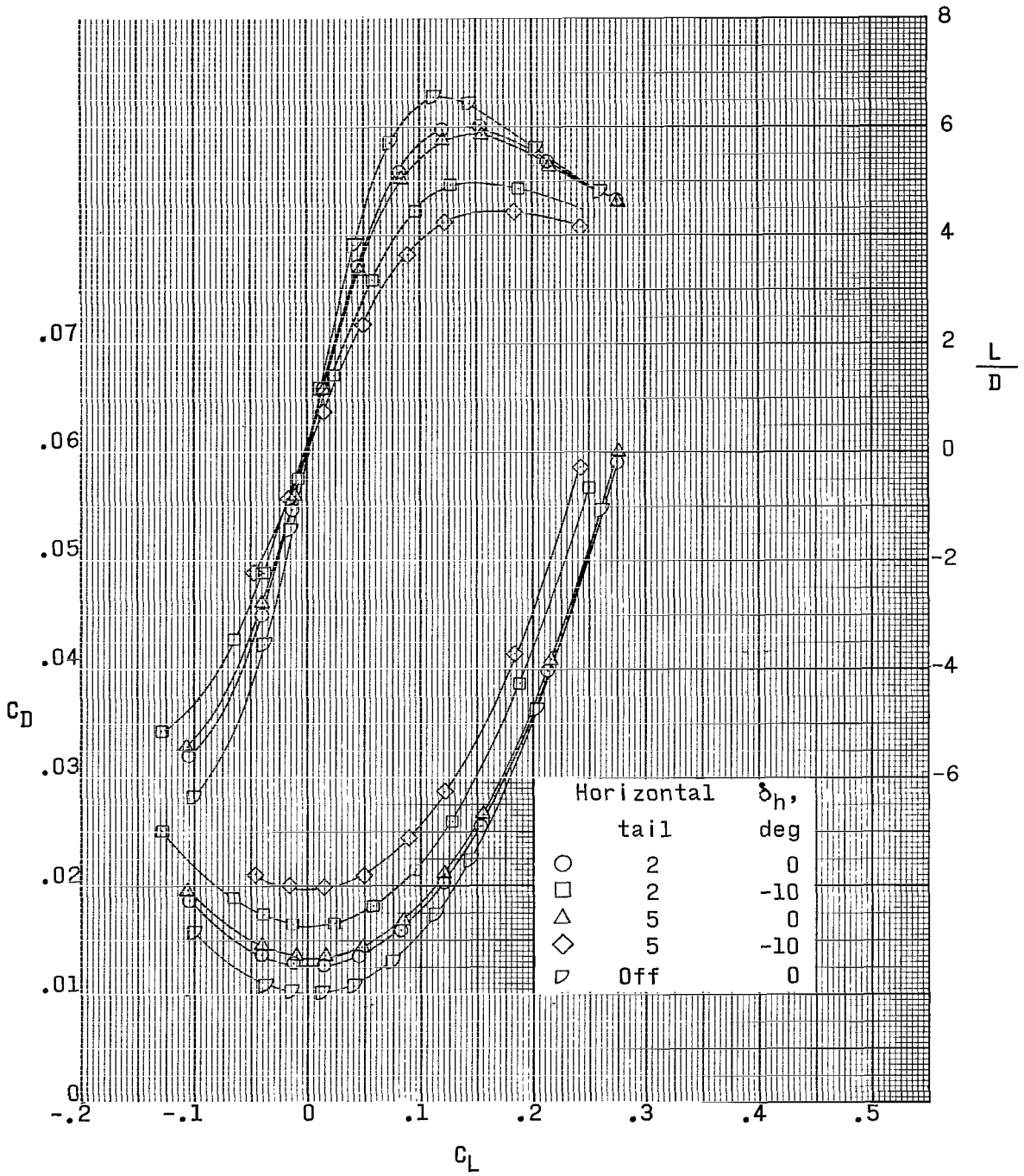

(a) Concluded.

Figure 12.- Continued.

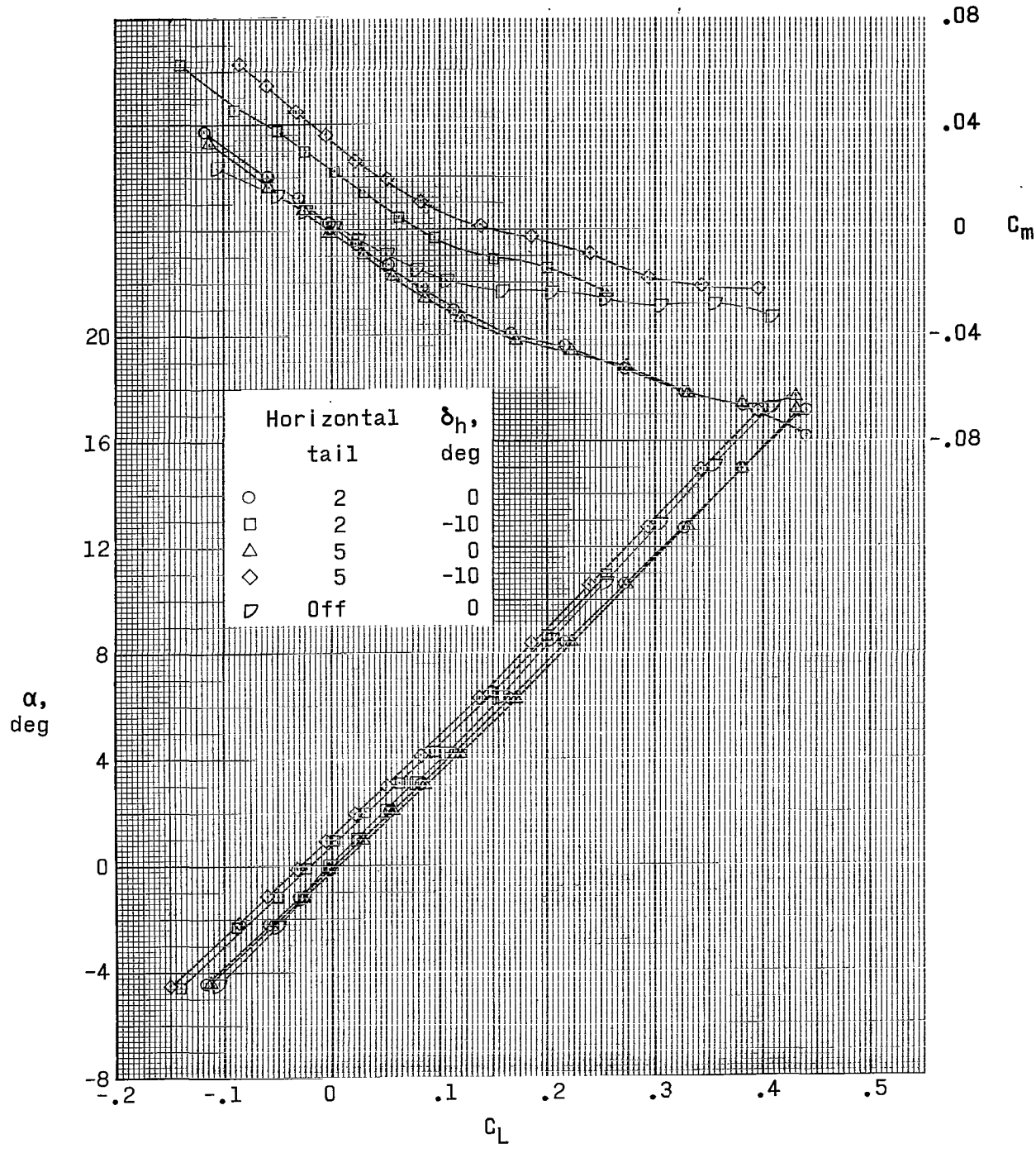

(b) M = 2.30.

Figure 12.- Continued.

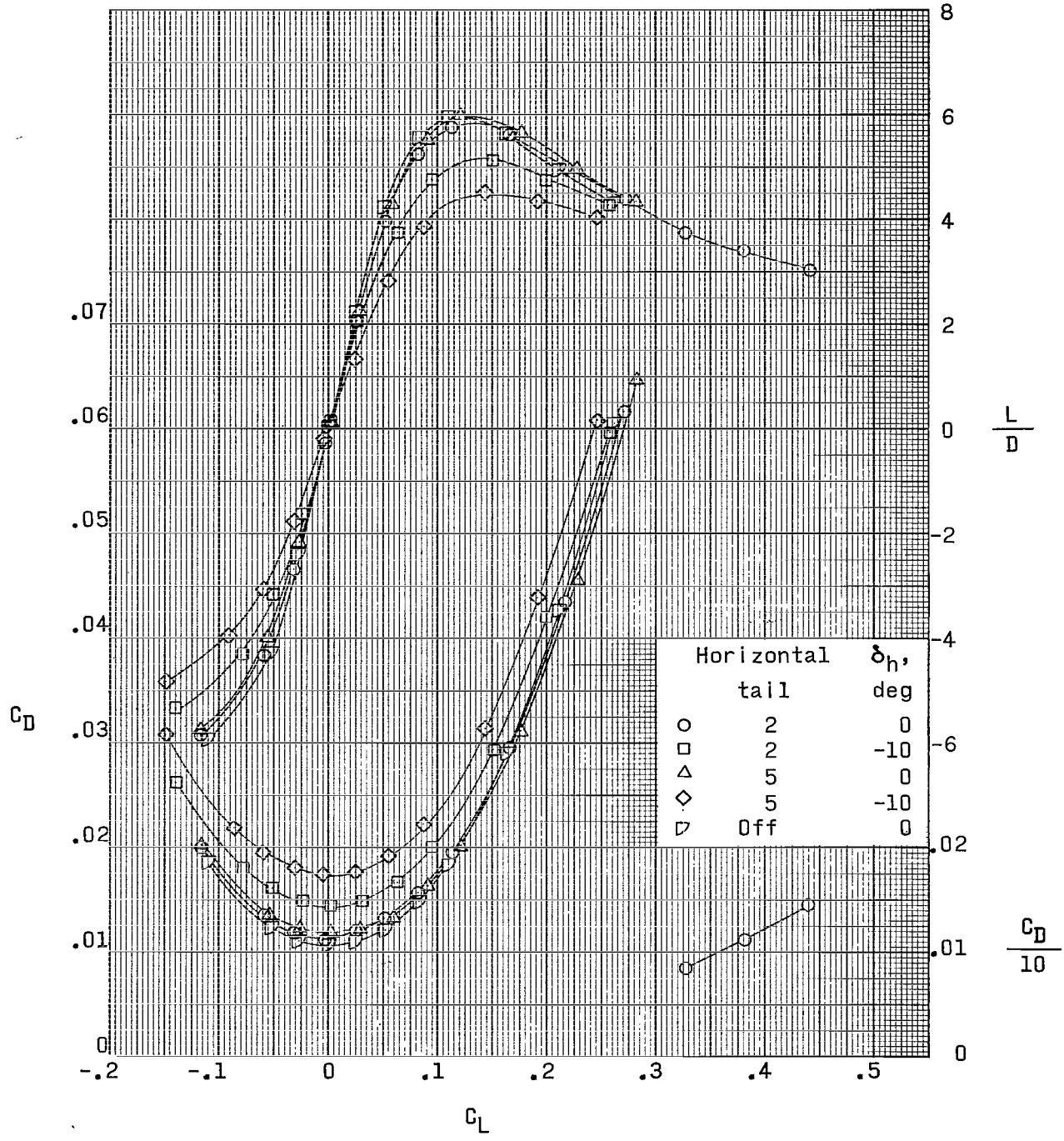

(b) Concluded.

Figure 12.- Continued.

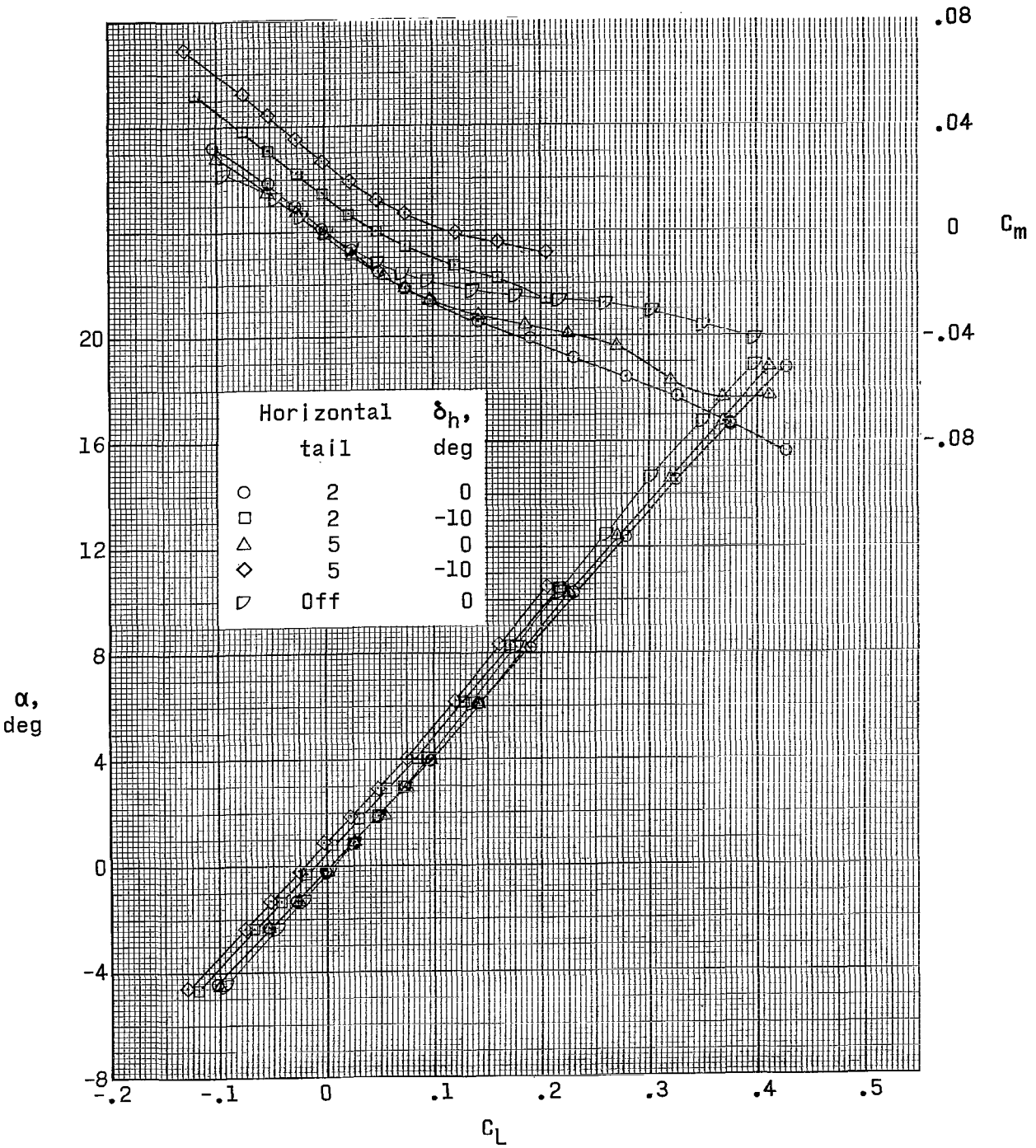

(c) M = 2.96 .

Figure 12.- Continued.

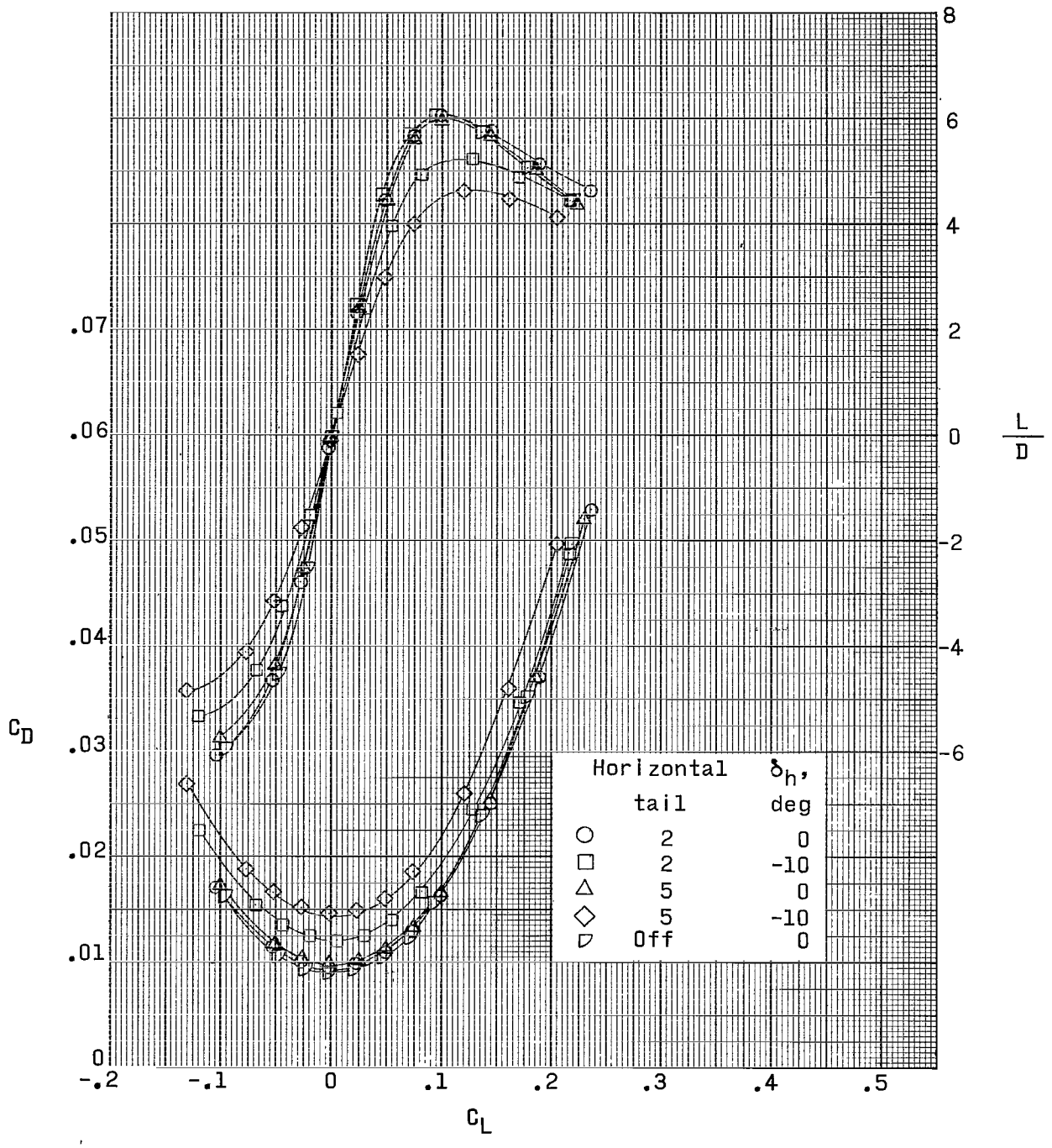

(c) Concluded.

Figure 12.- Continued.

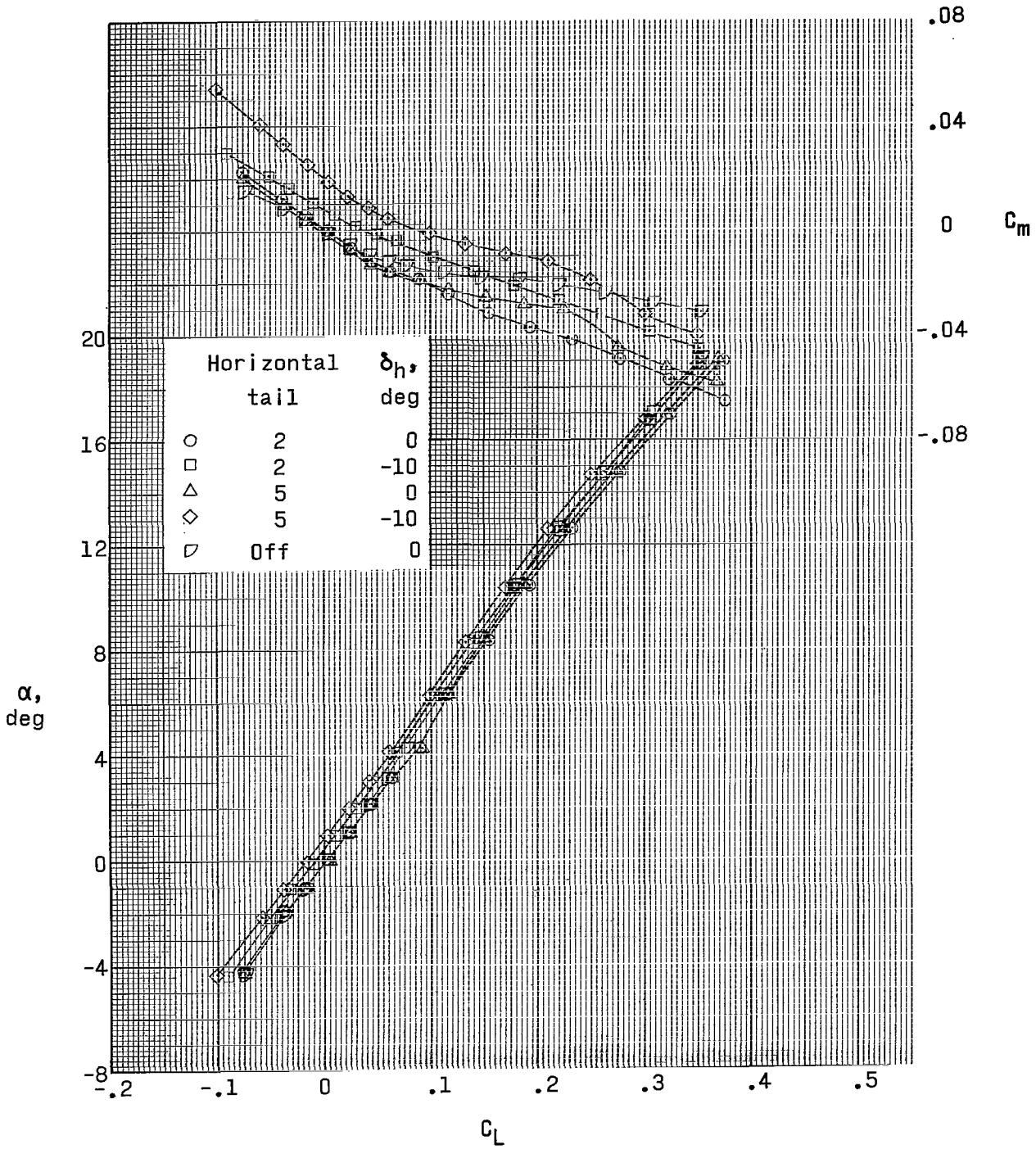

(d) M = 3.95.

Figure 12.- Continued.

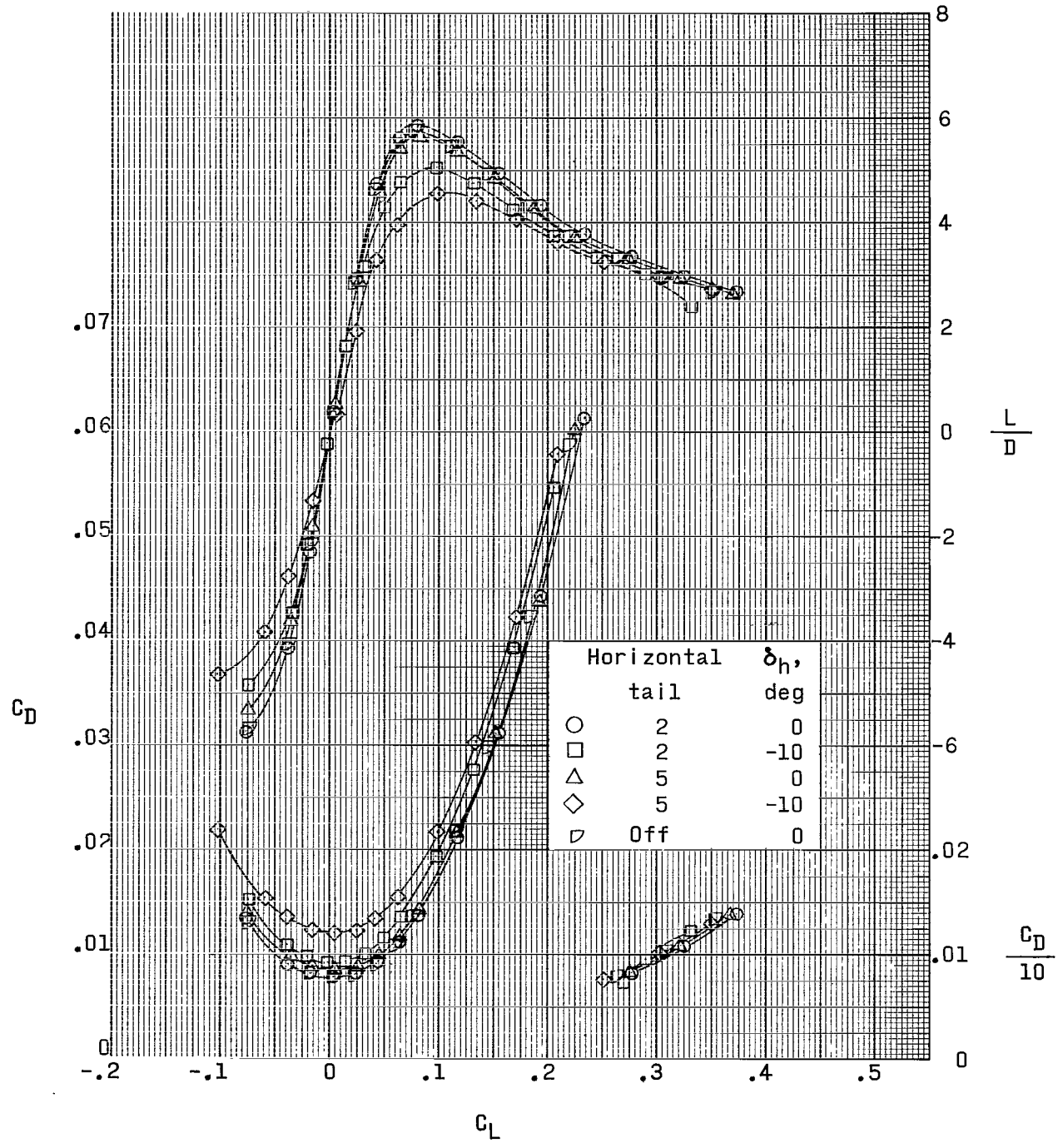

(d) Concluded.

Figure 12.- Continued.

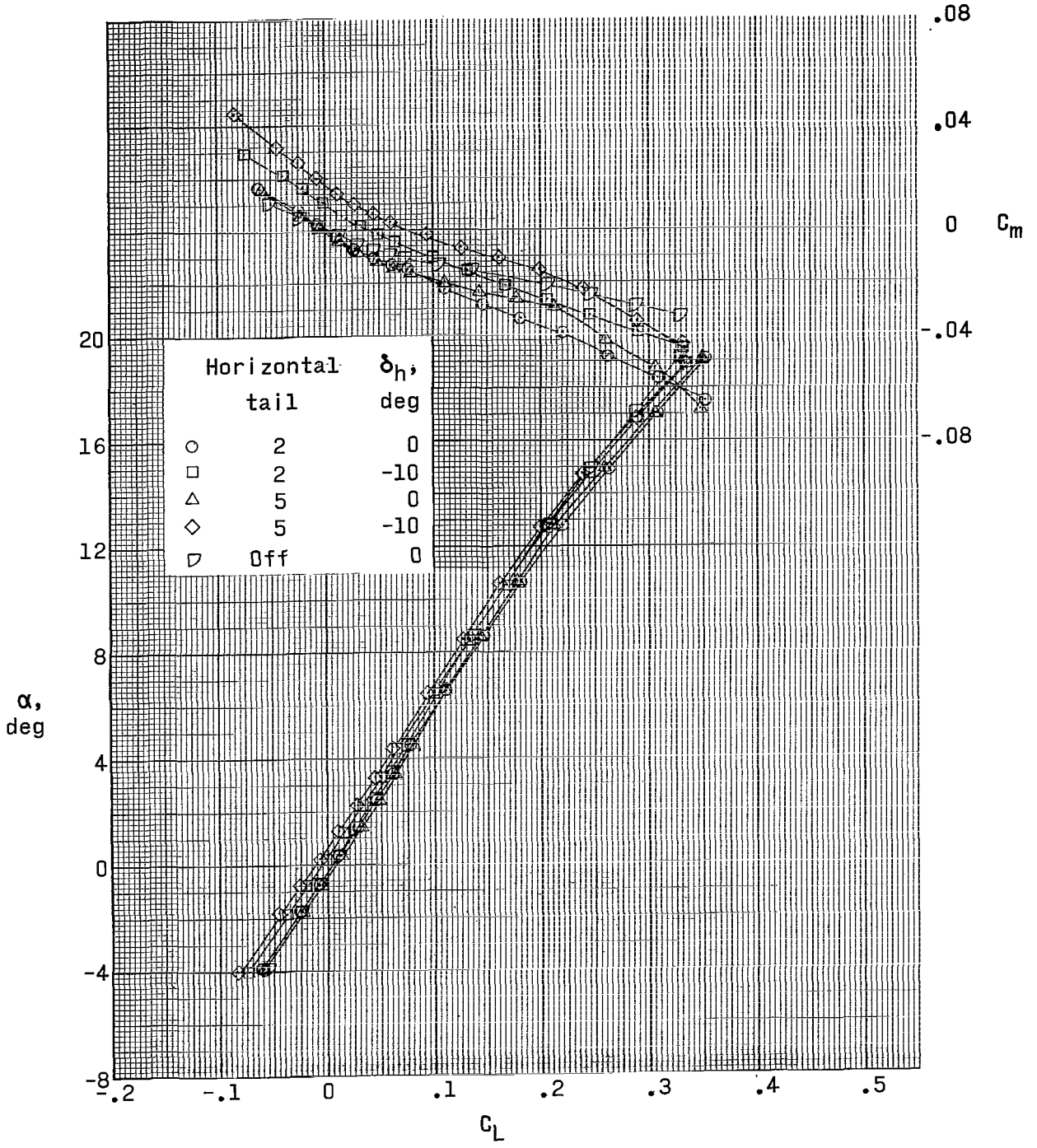

(e) M = 4.63.

Figure 12.- Continued.

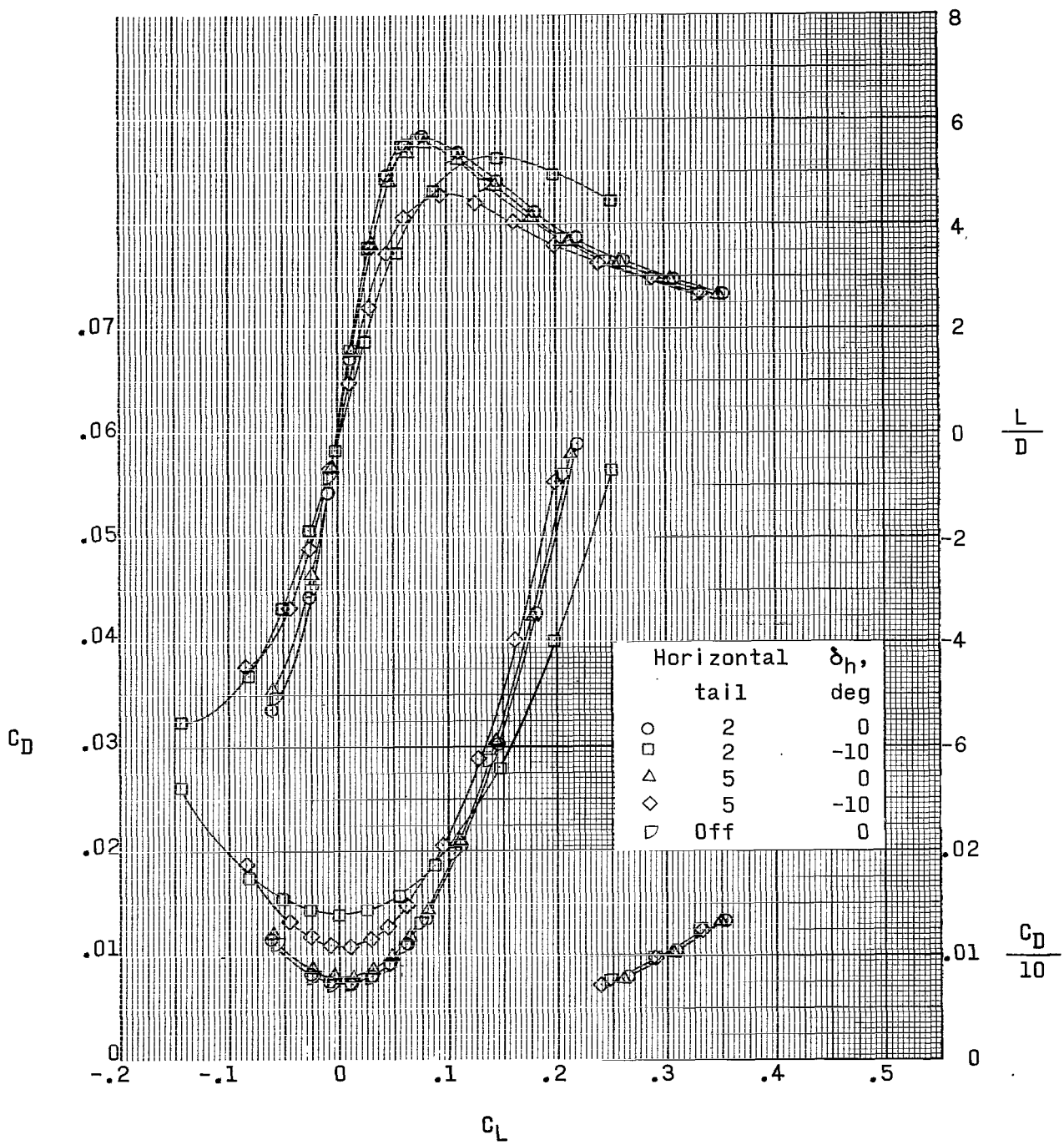

(e) Concluded.

Figure 12.- Concluded.

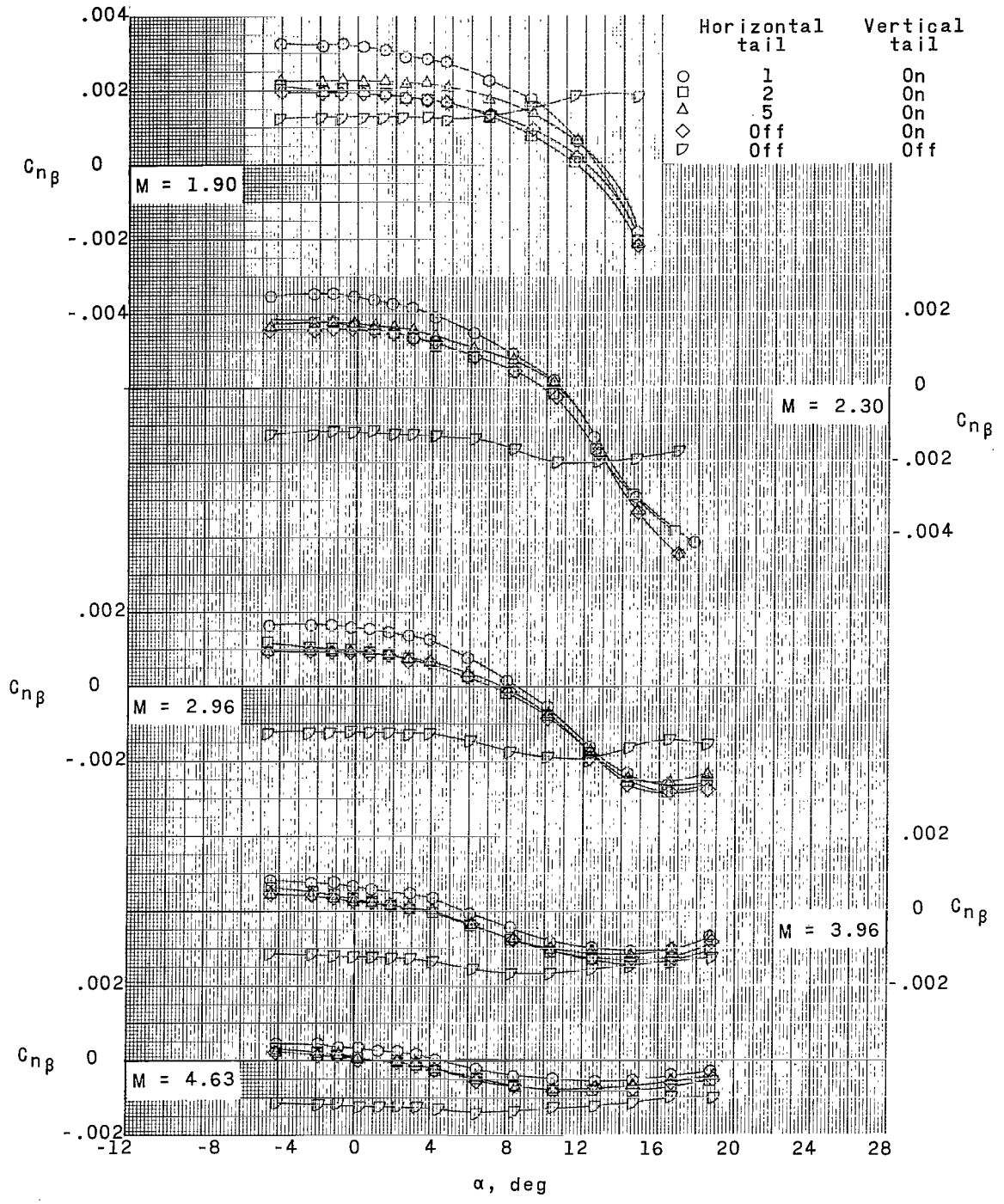

(a) Directional stability.

Figure 13.- Effect of horizontal-tail height on sideslip parameters. High wing; 0° dihedral.

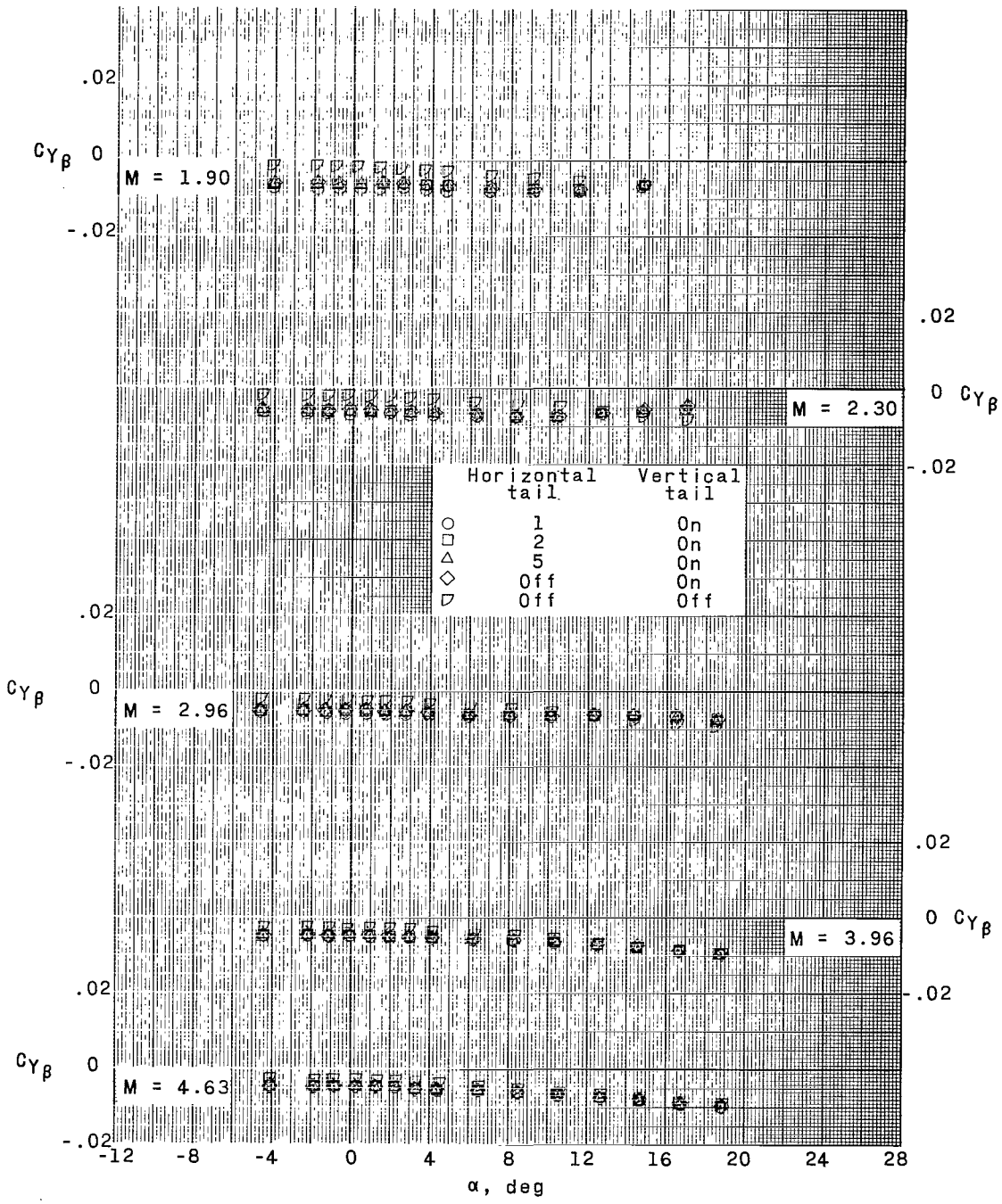

(b) Sideslip parameter.

Figure 13.- Continued.

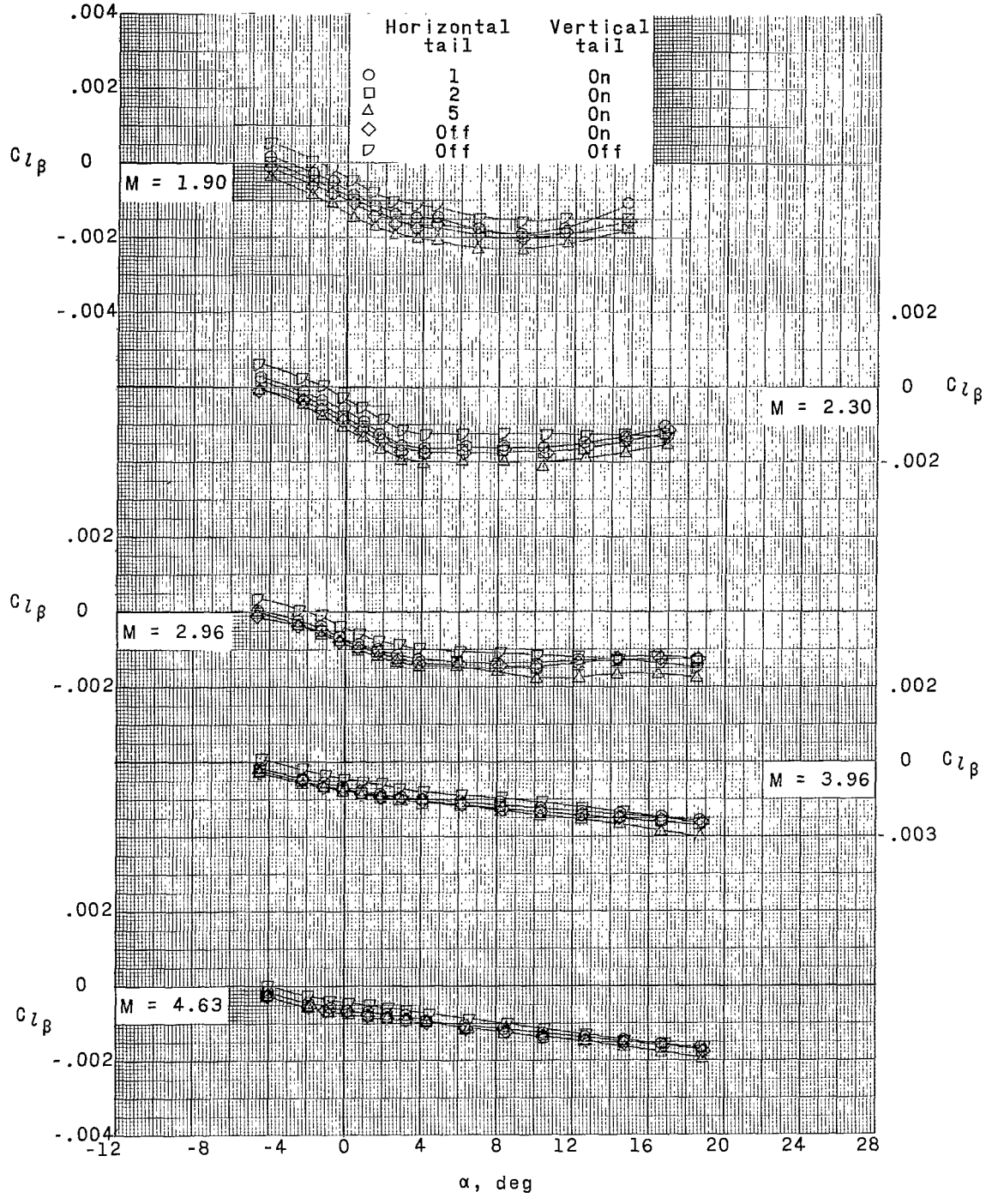

(c) Lateral stability.

Figure 13.- Concluded.

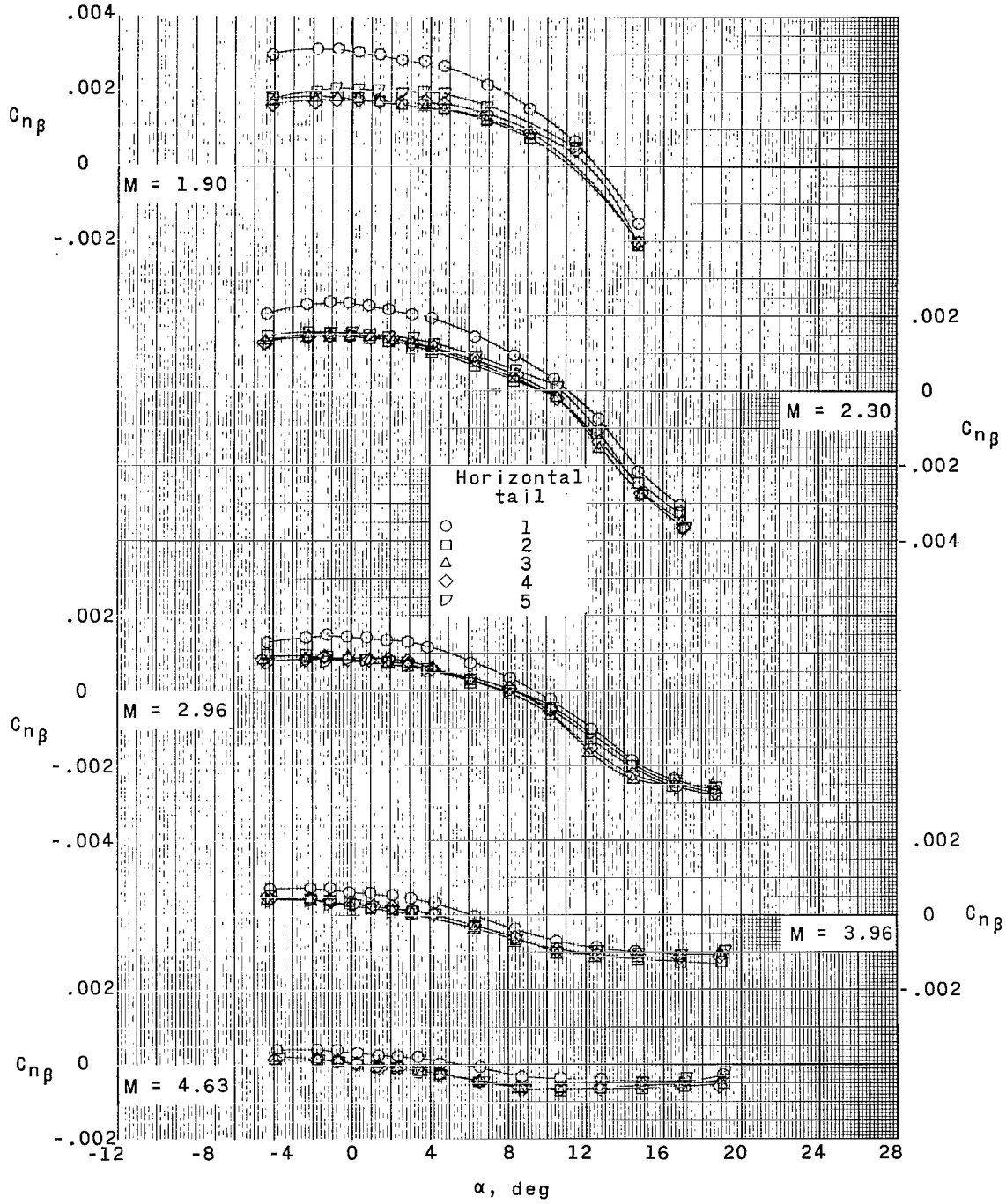

(a) Directional stability.

Figure 14.- Effect of horizontal-tail height on sideslip parameters. High wing; 5° dihedral.

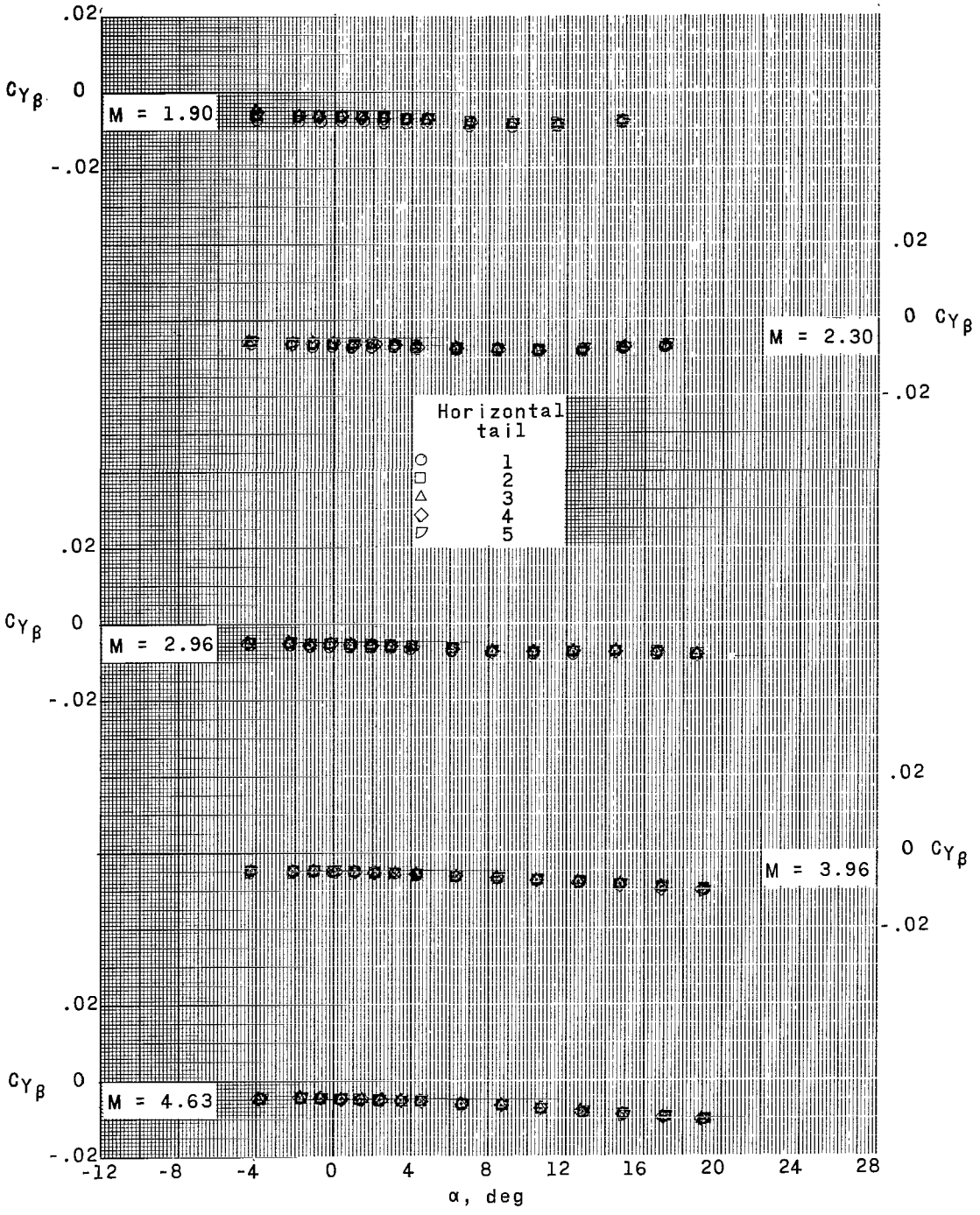

(b) Sideslip parameter.

Figure 14.- Continued.

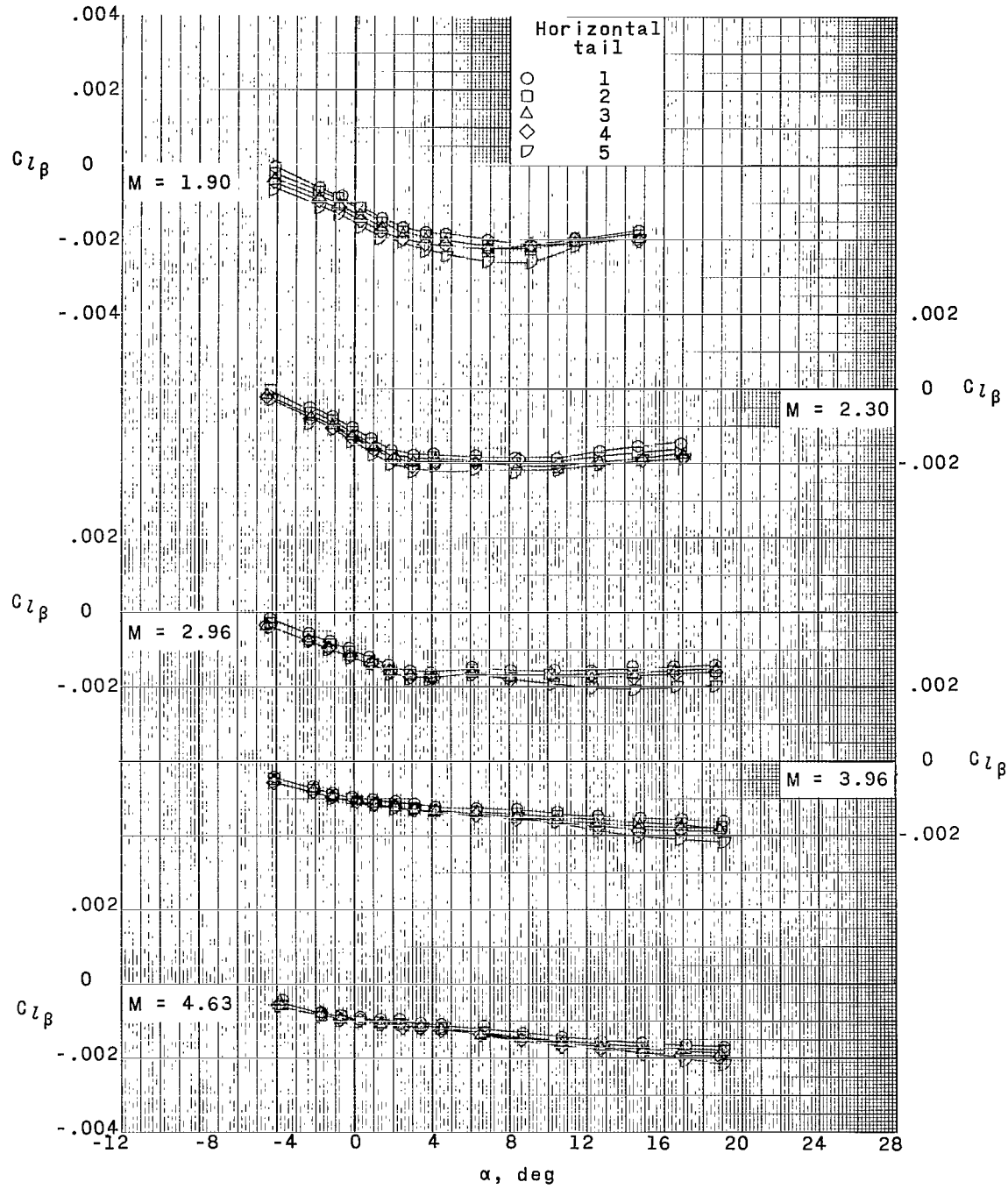

(c) Lateral stability.

Figure 14.- Concluded.

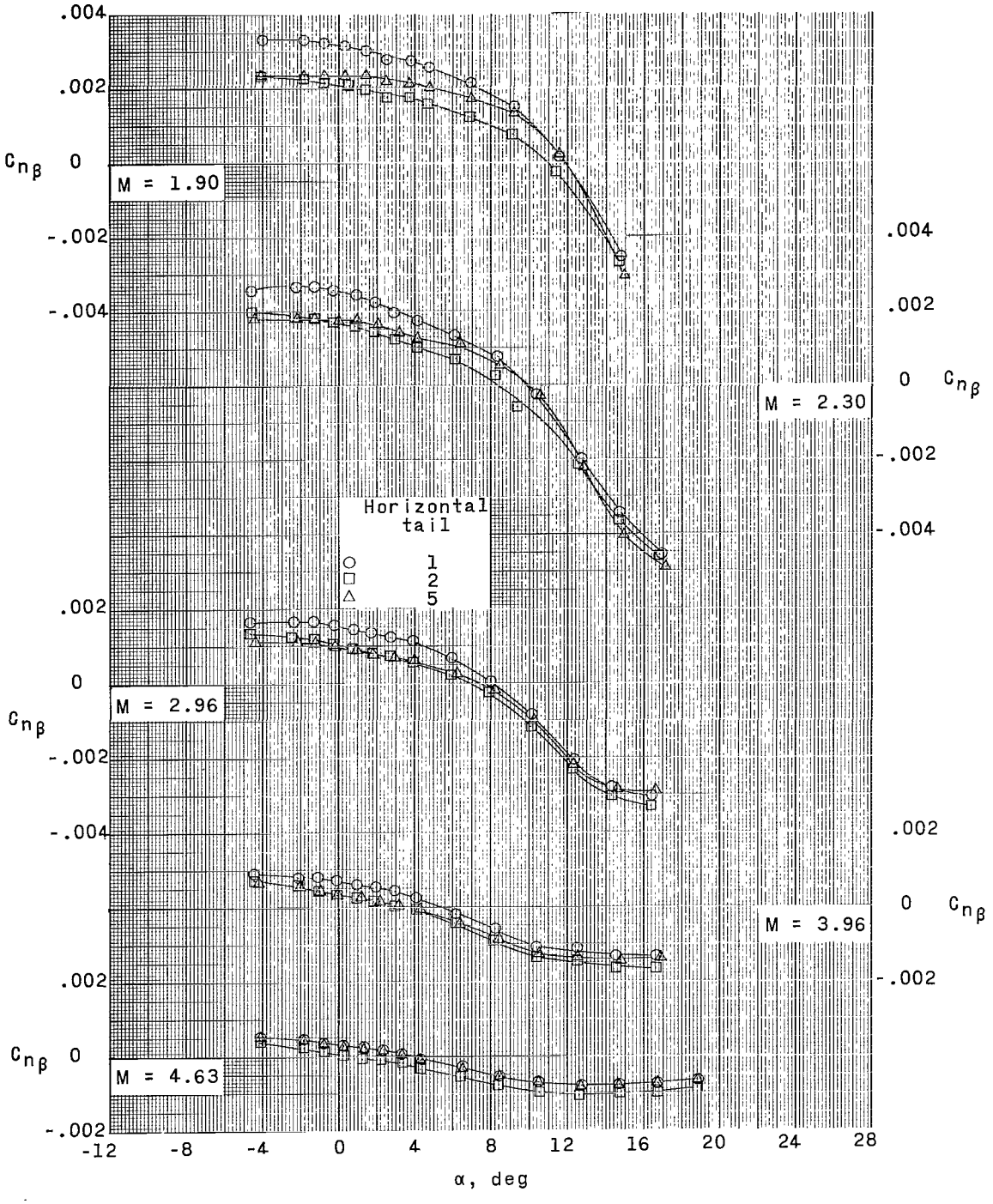

(a) Directional stability.

Figure 15.- Effect of horizontal-tail height on sideslip parameters. High wing; -5° dihedral.

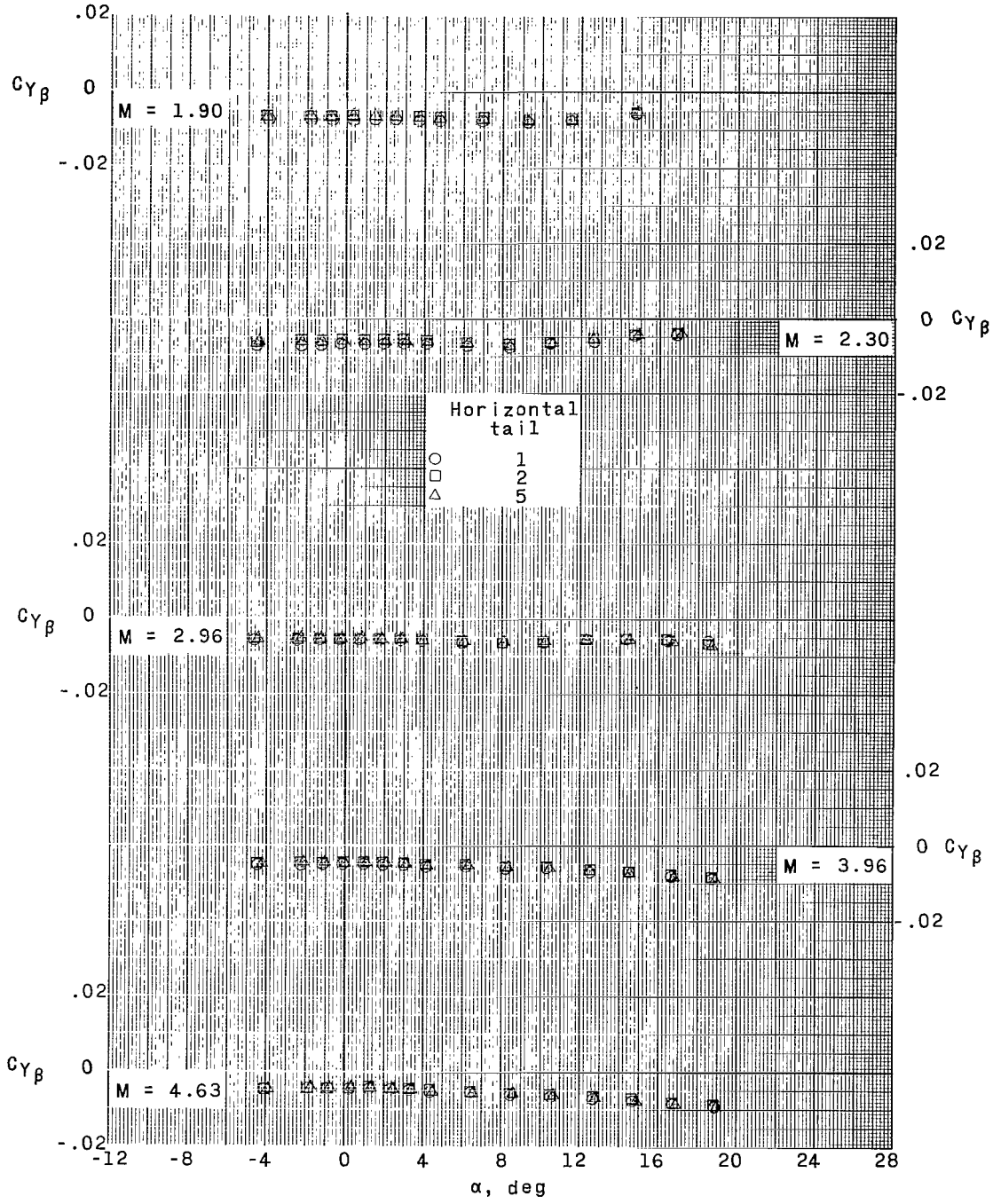

(b) Sideslip parameter.

Figure 15.- Continued.

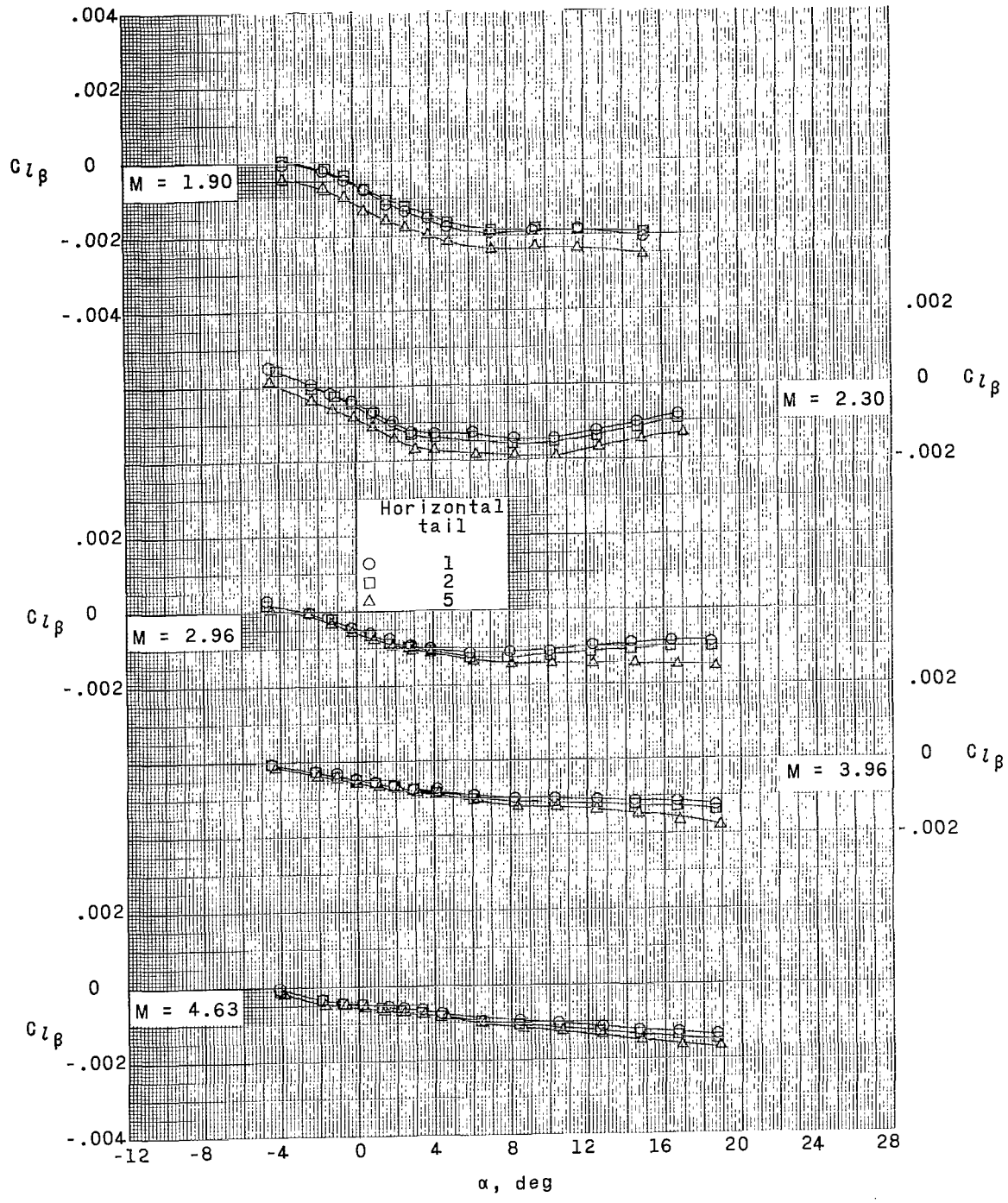

(c) Lateral stability.

Figure 15.- Concluded.

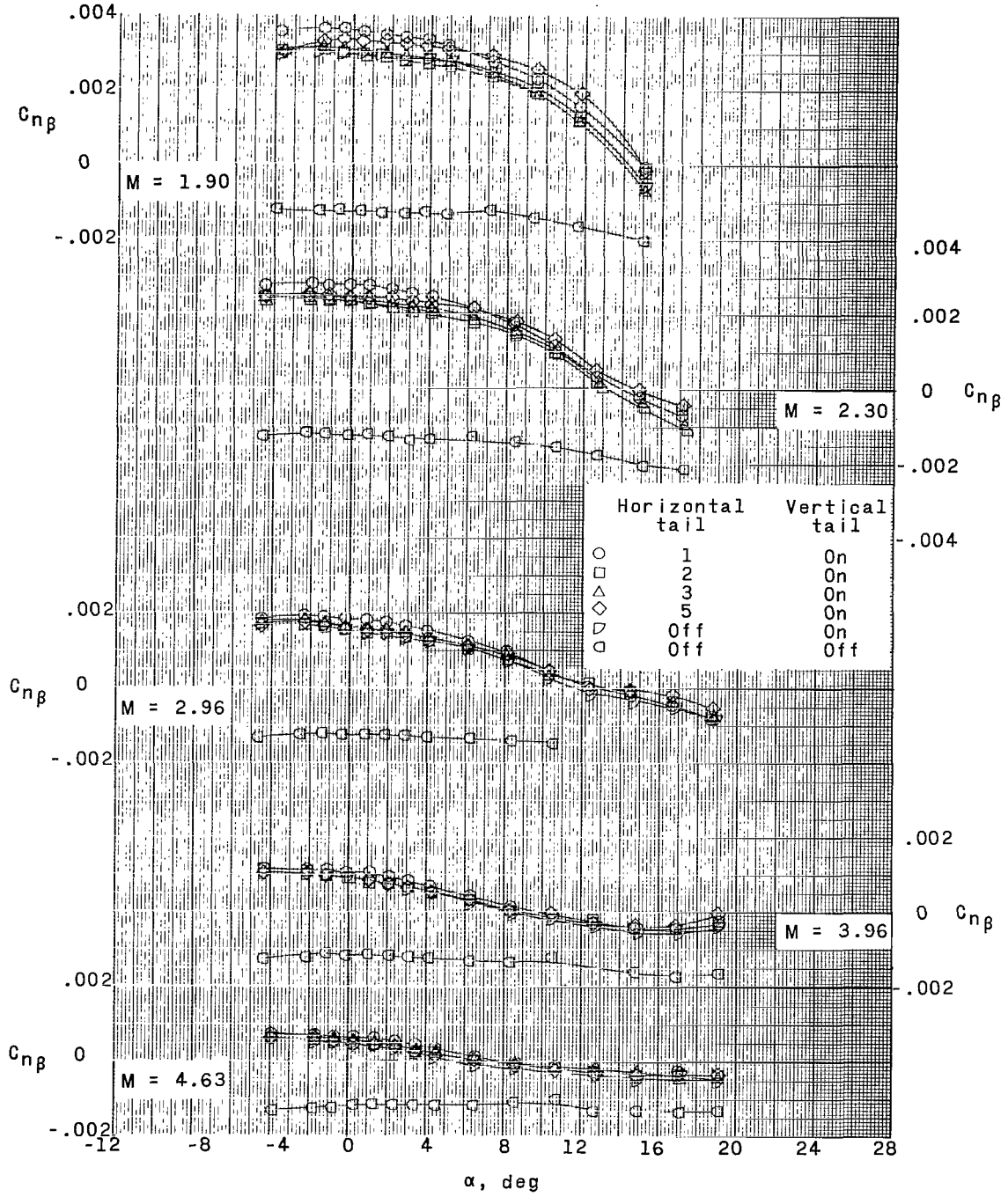

(a) Directional stability.

Figure 16.- Effect of horizontal-tail height on sideslip parameters. Low wing; 0^0 dihedral.

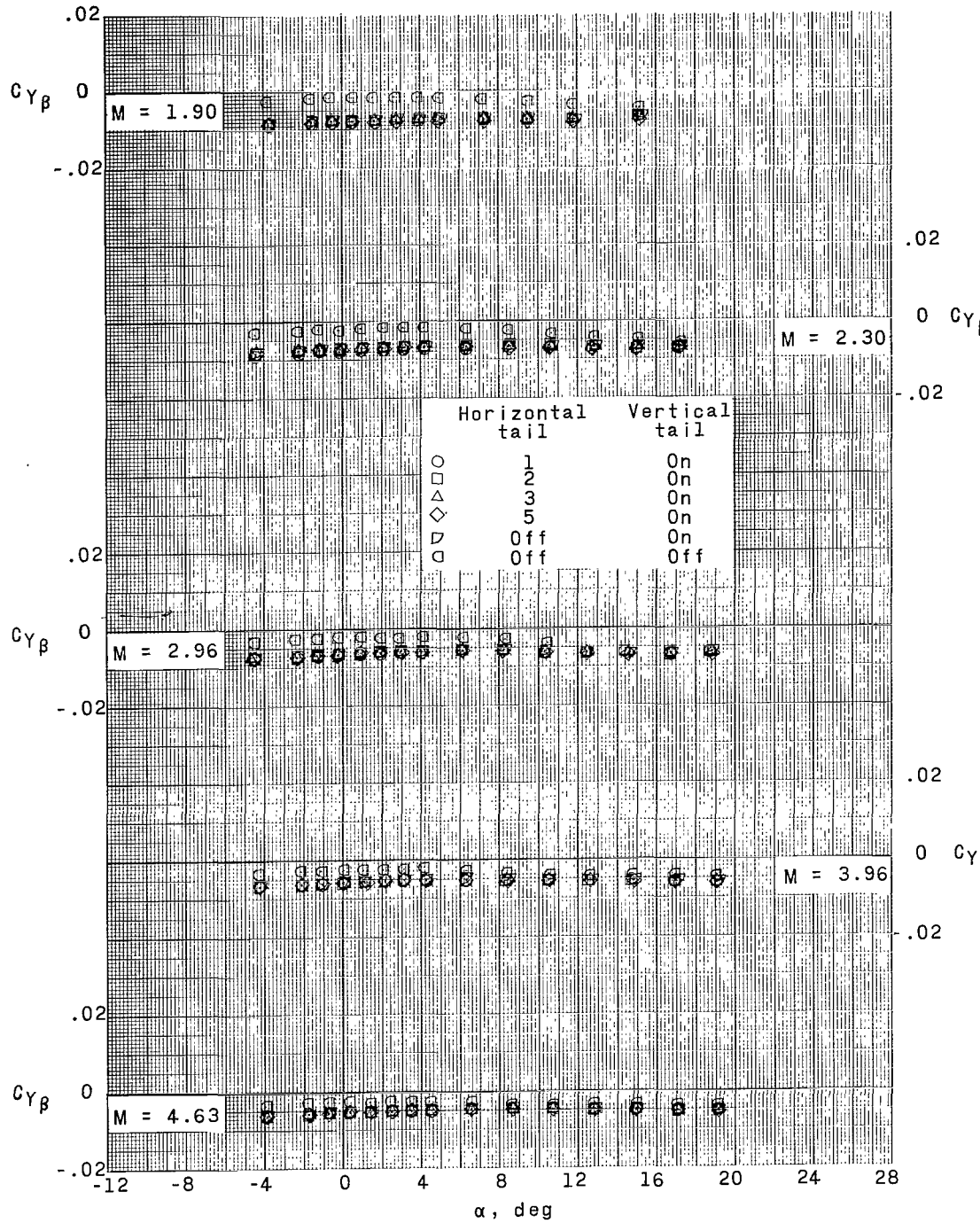

(b) Sideslip parameter.

Figure 16.- Continued.

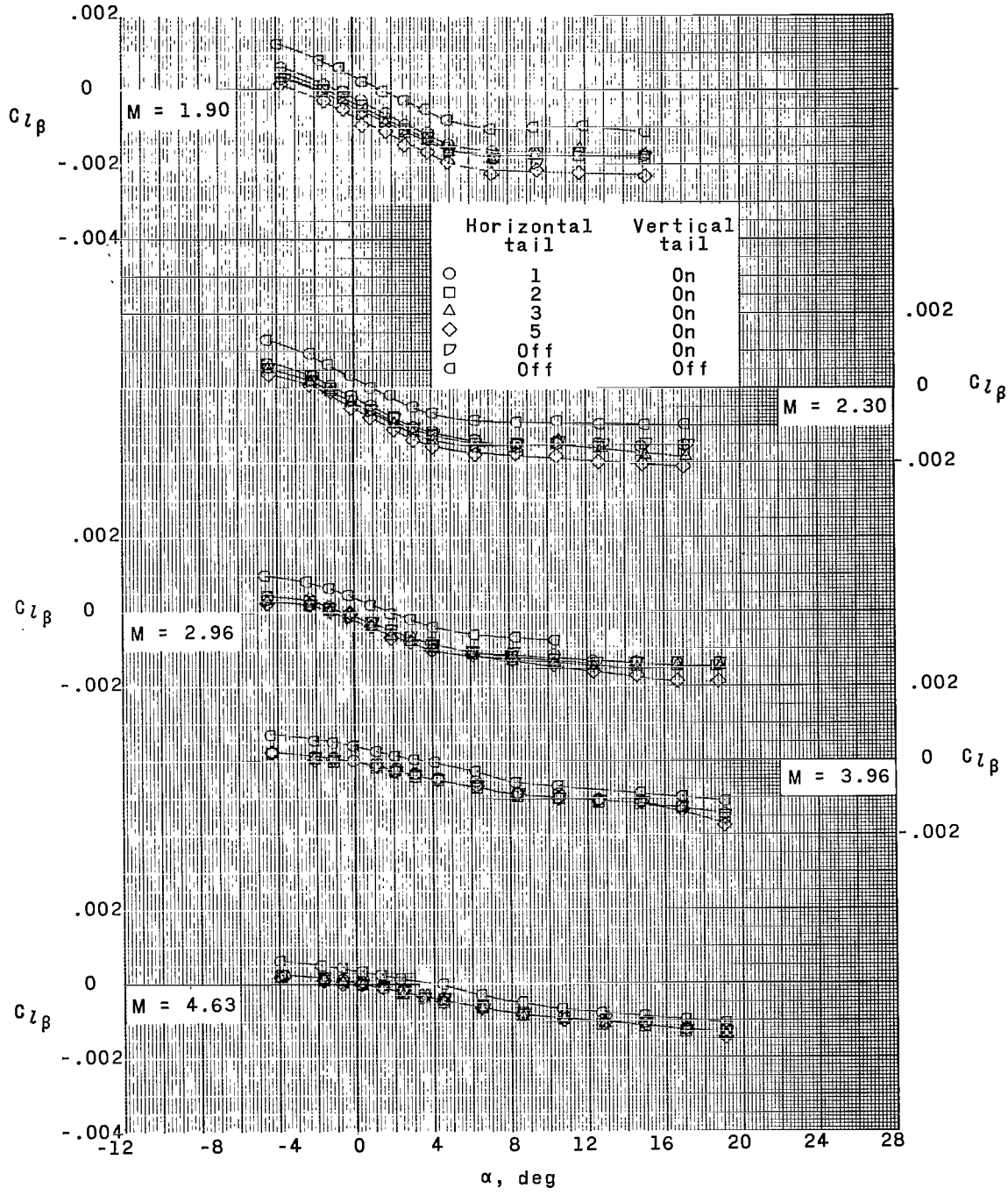

(c) Lateral stability.

Figure 16.- Concluded.

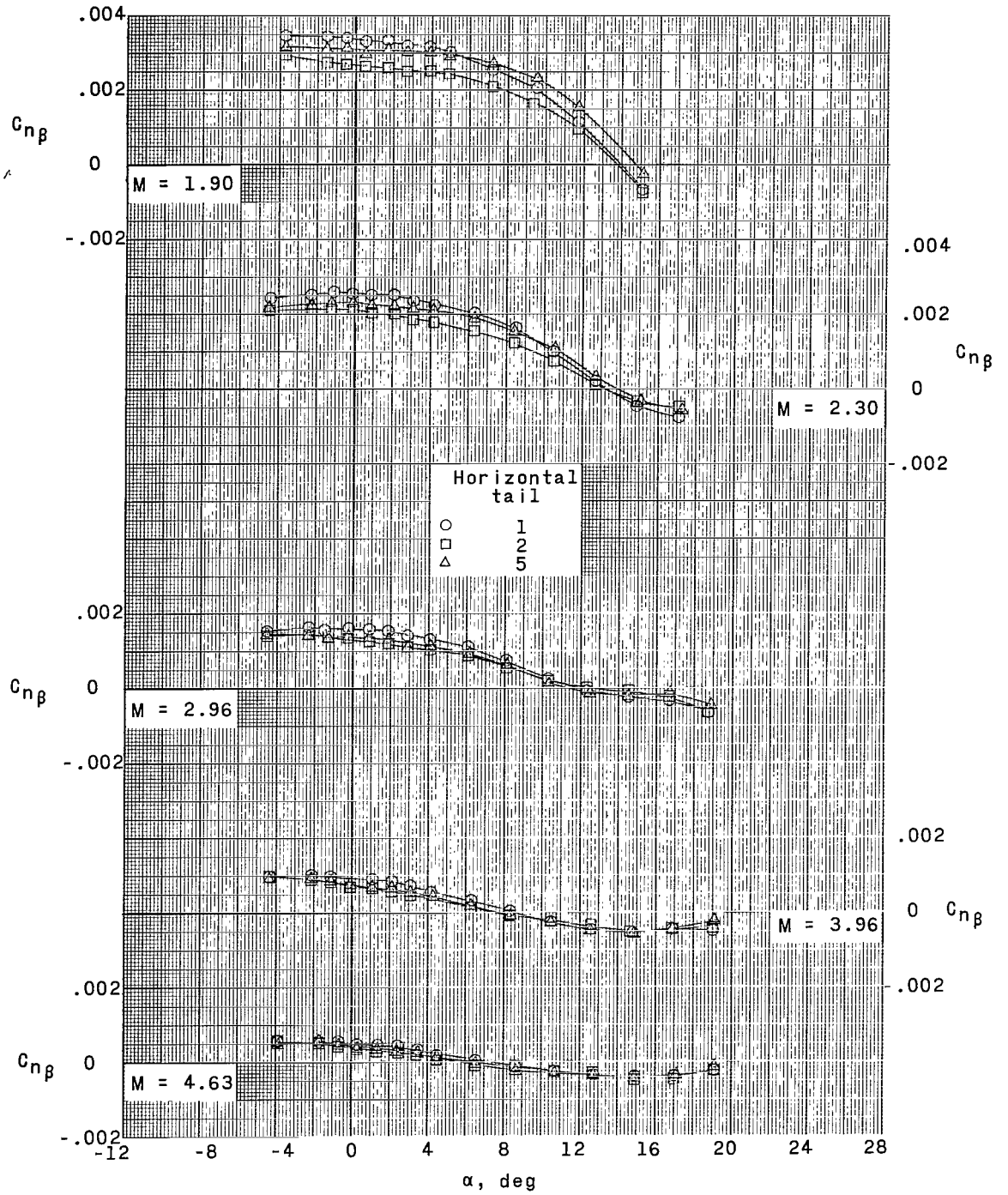

(a) Directional stability.

Figure 17.- Effect of horizontal-tail height on sideslip parameters. Low wing; 5° dihedral.

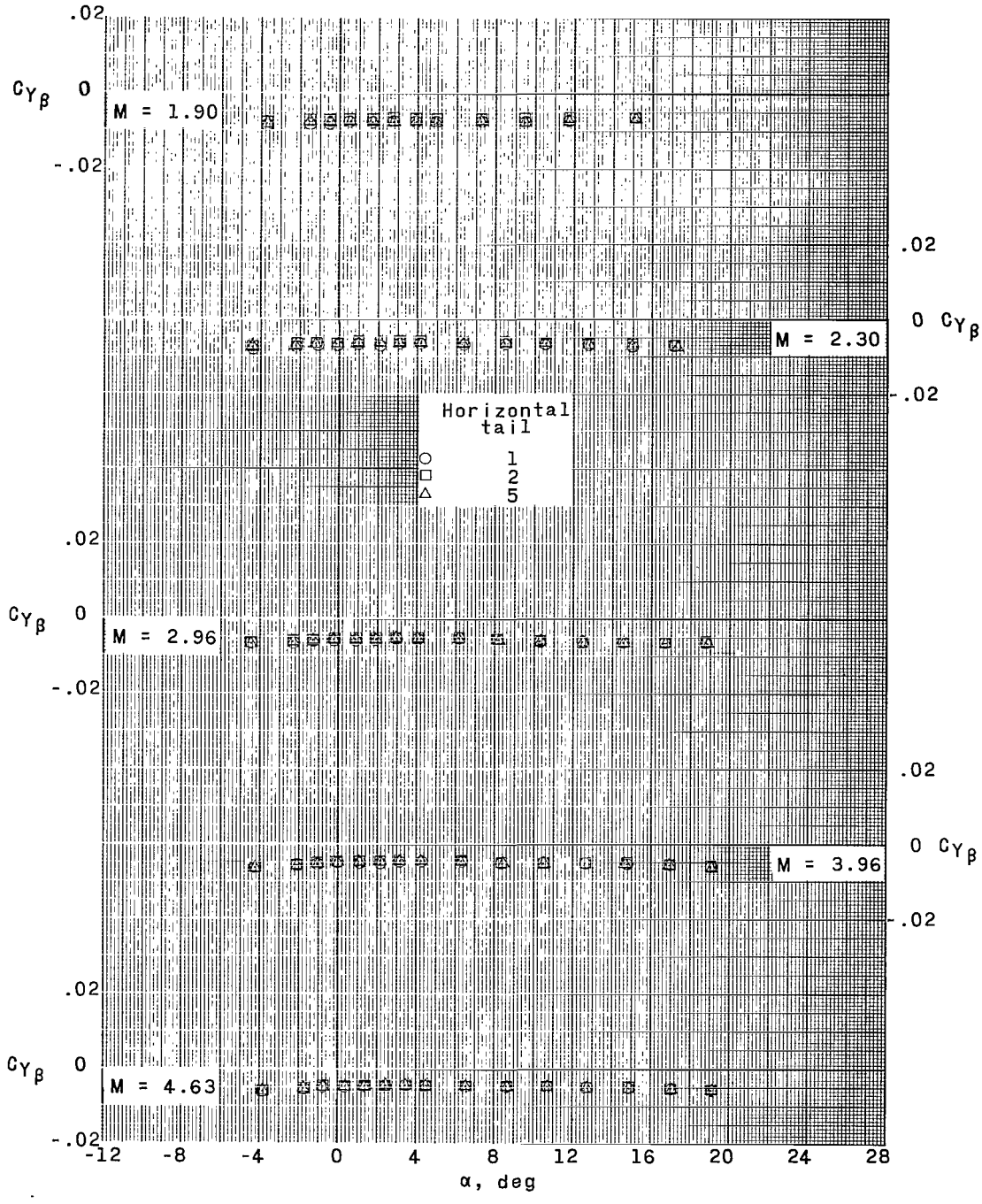

(b) Sideslip parameter.

Figure 17.- Continued.

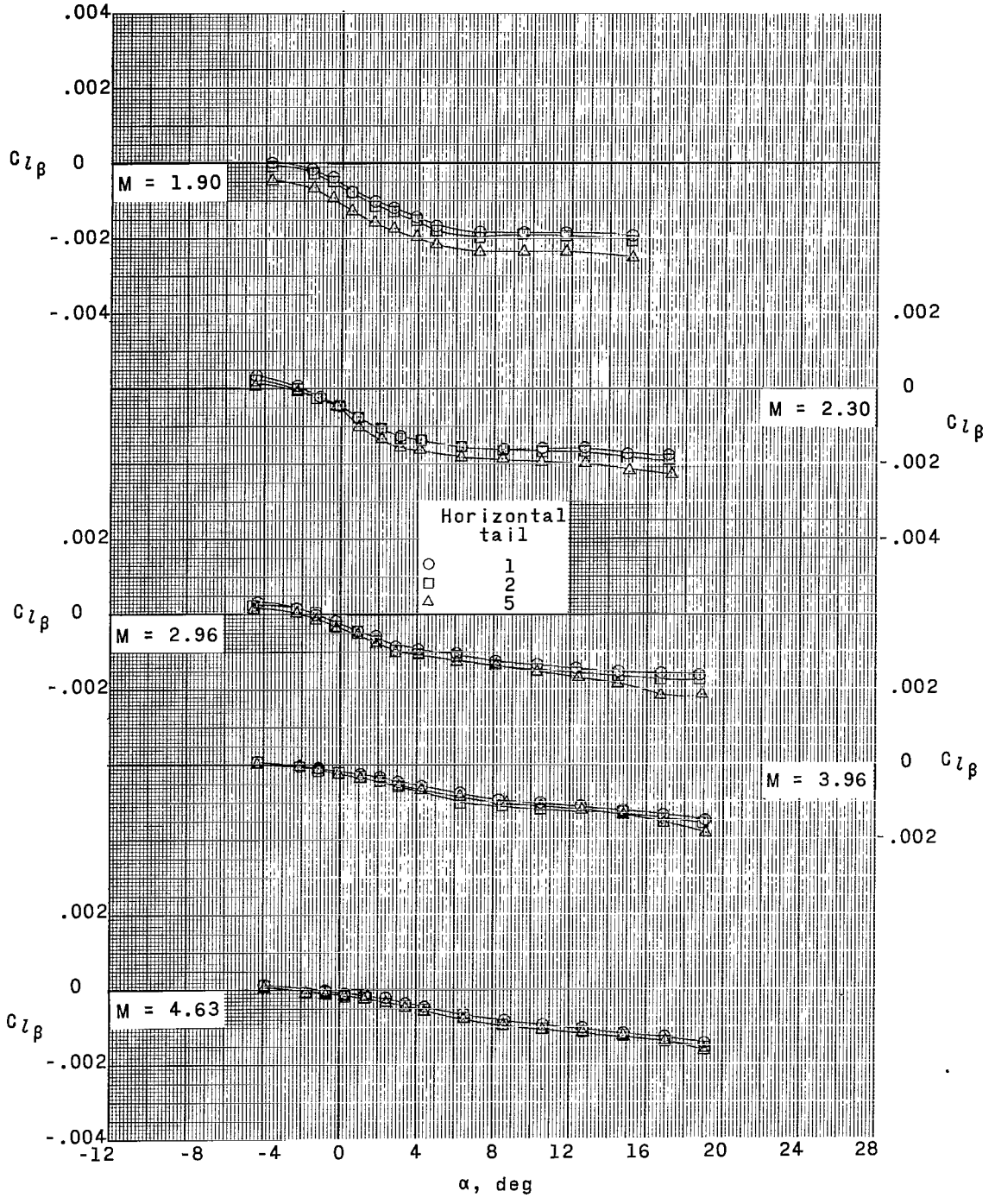

(c) Lateral stability.

Figure 17.- Concluded.

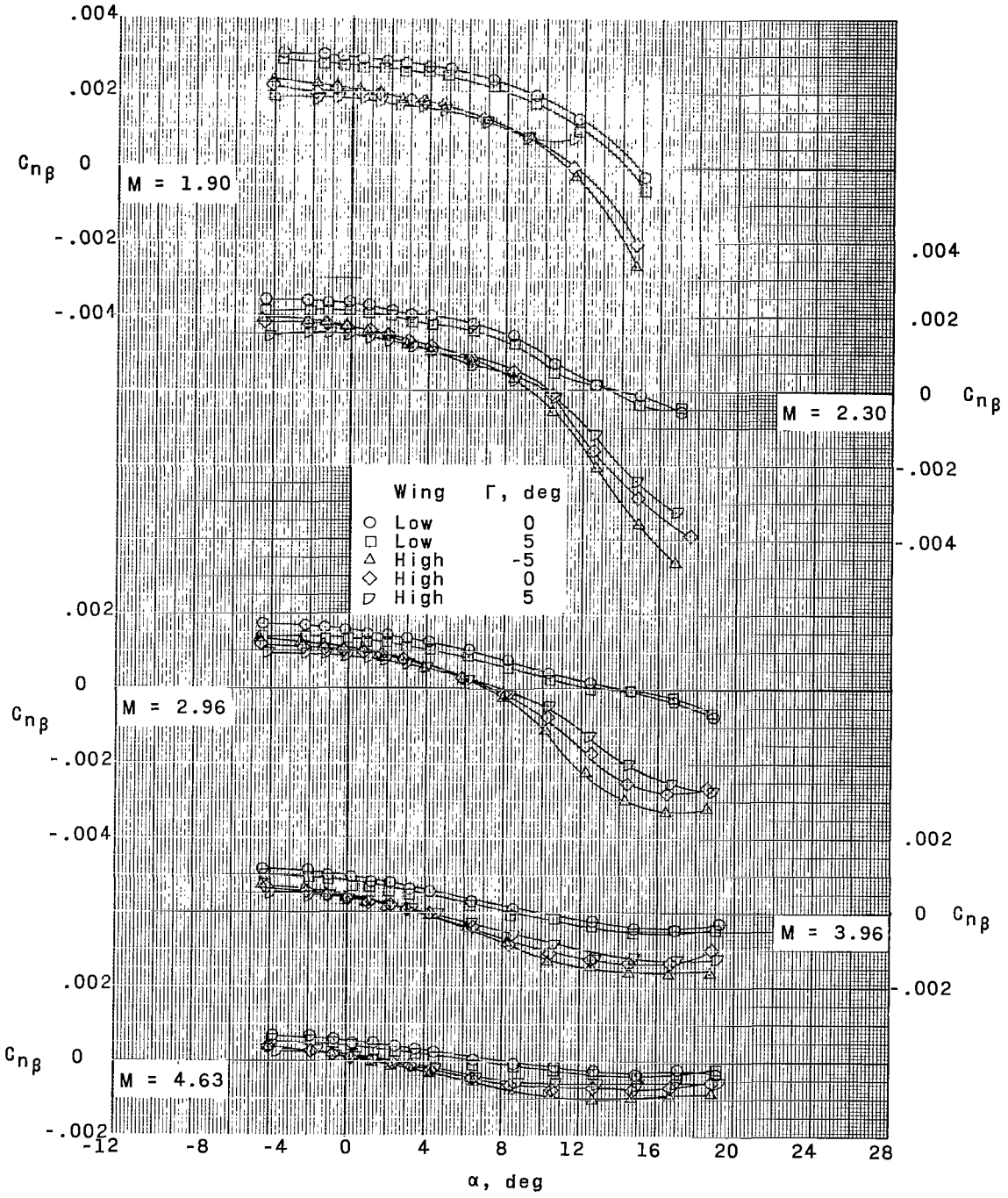

(a) Directional stability.

Figure 18.- Effect of wing height and dihedral on sideslip parameters. Horizontal-tail position 2.

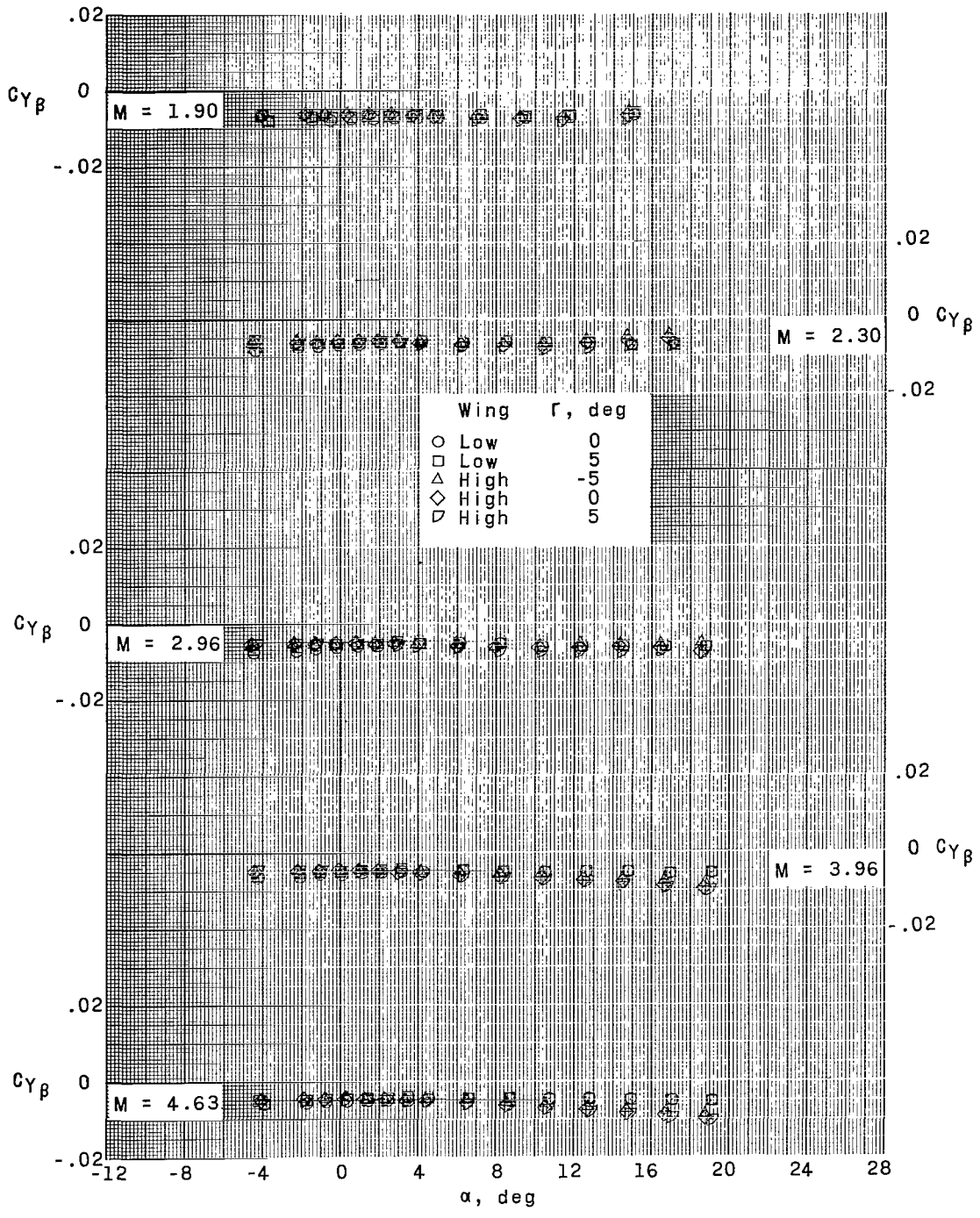

(b) Sideslip parameter.

Figure 18.- Continued.

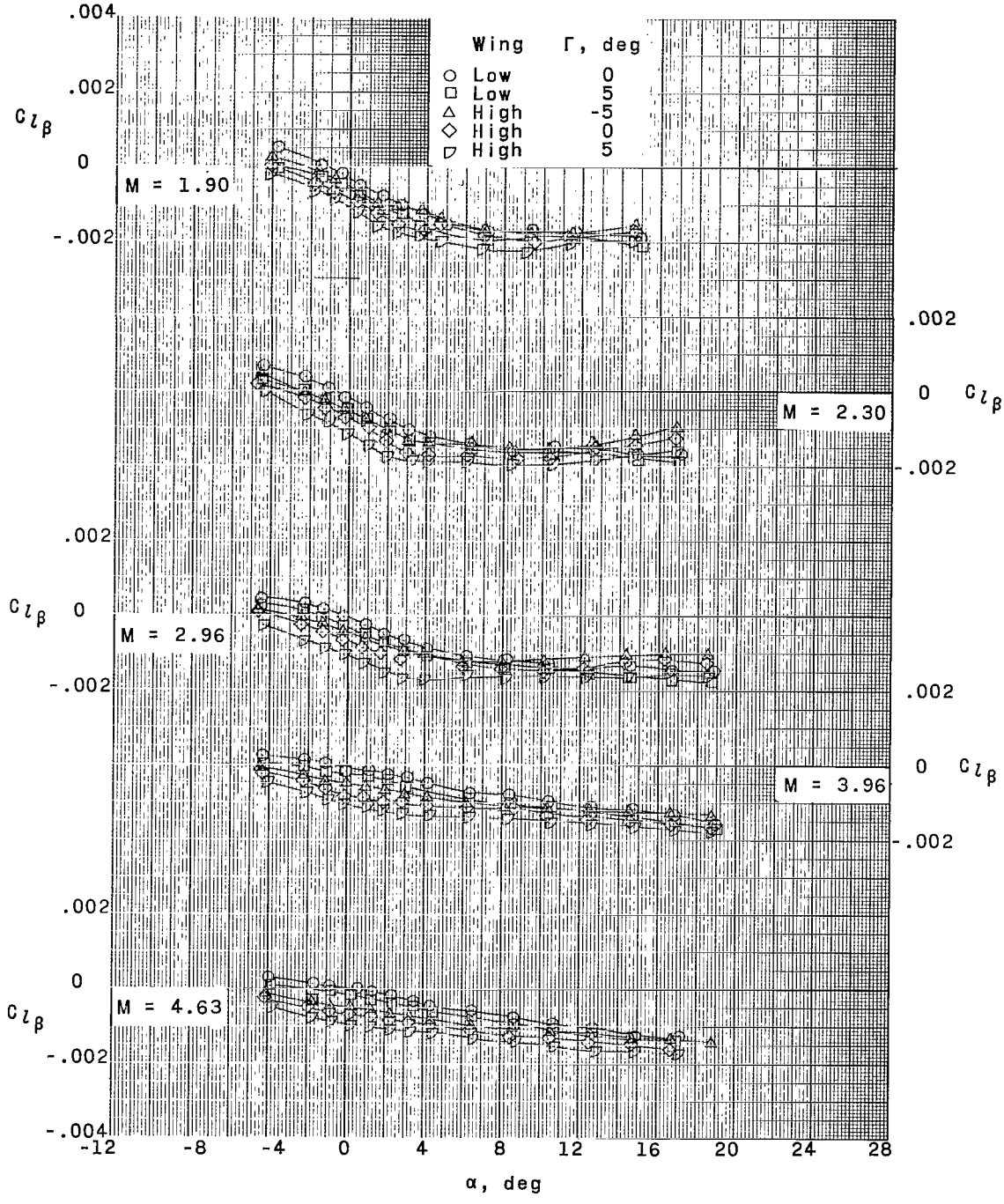

(c) Lateral stability.

Figure 18.- Concluded.

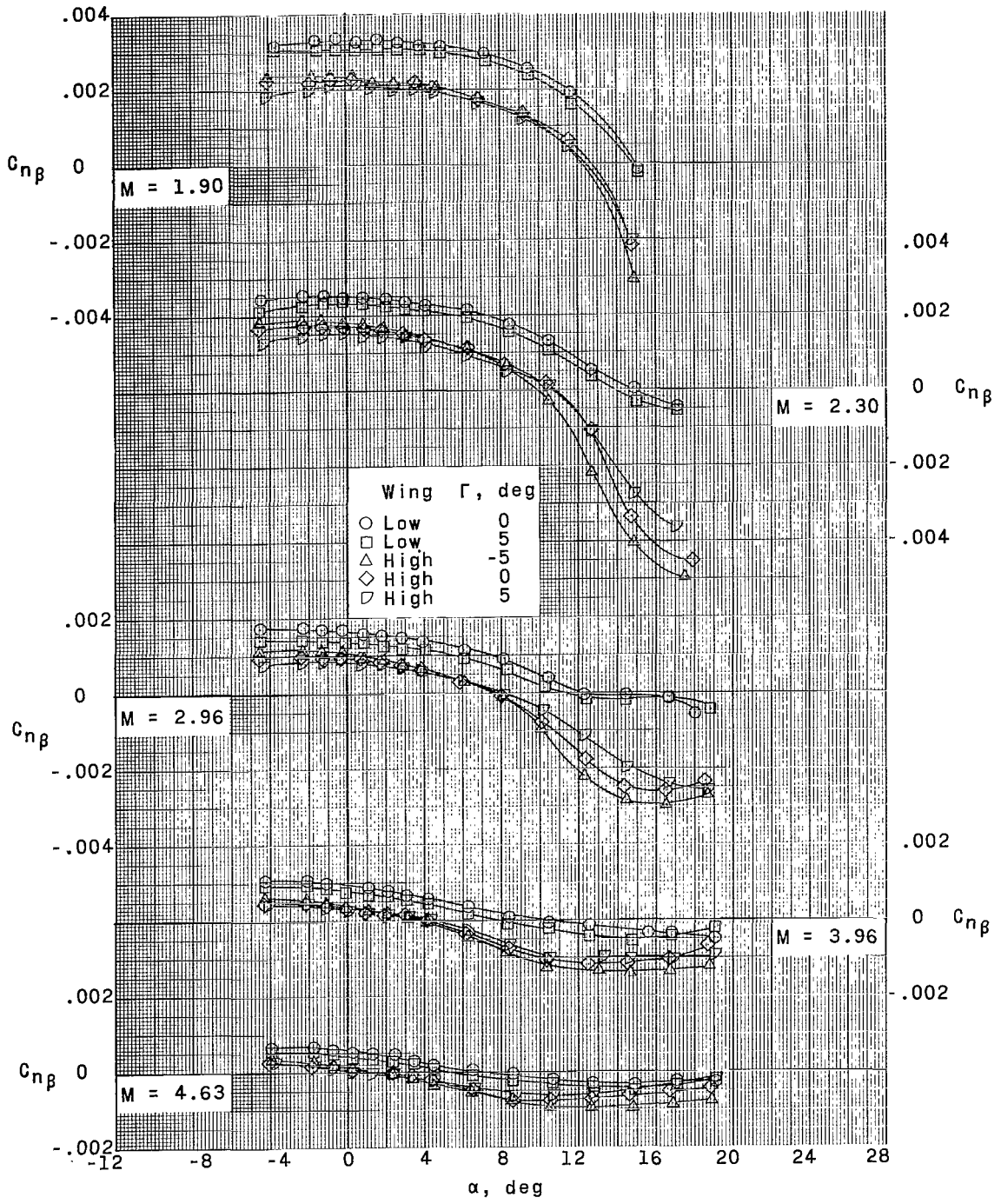

(a) Directional stability.

Figure 19.- Effect of wing height and dihedral on sideslip parameters. Horizontal-tail position 5.

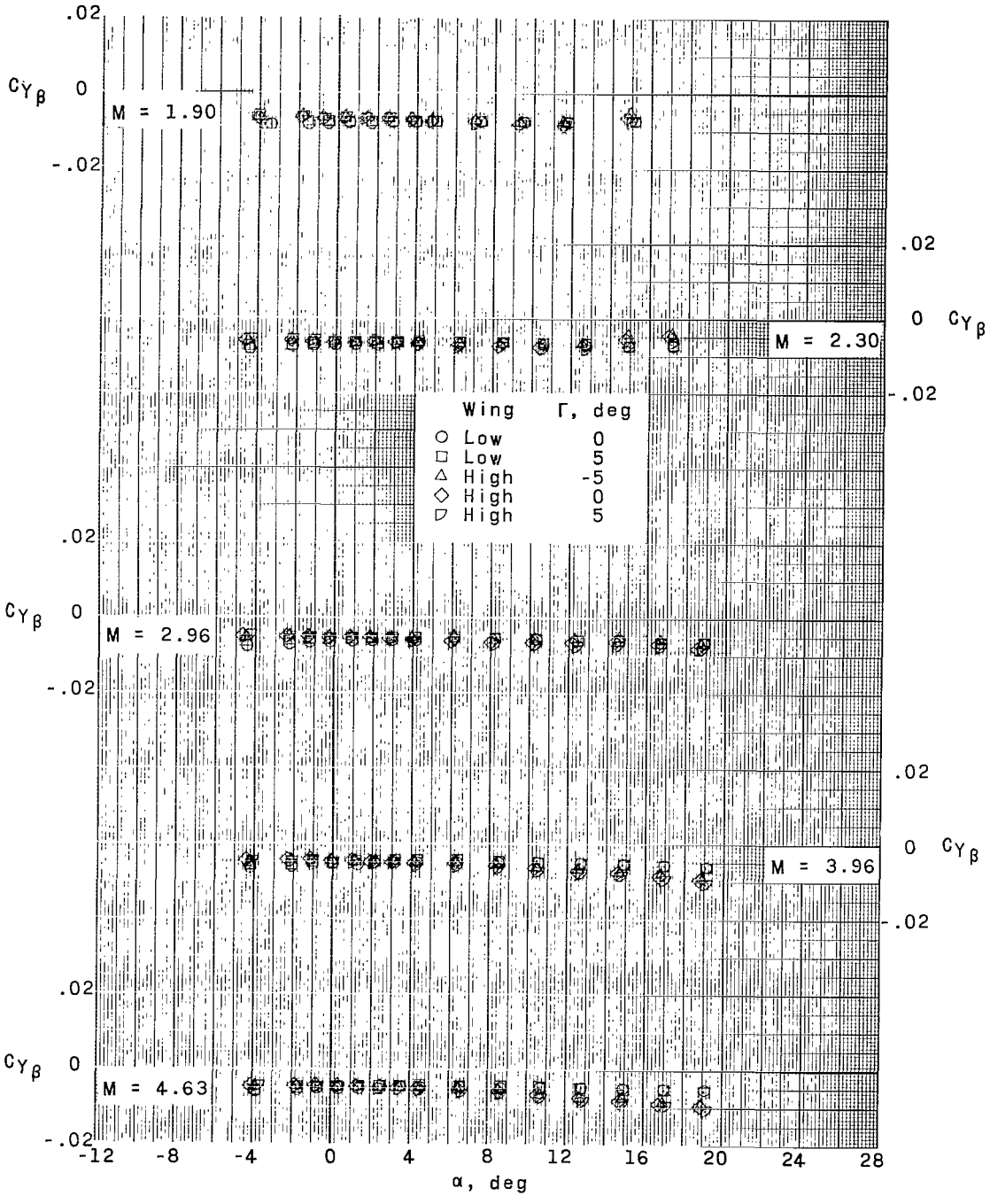

(b) Sideslip parameter.

Figure 19.- Continued.

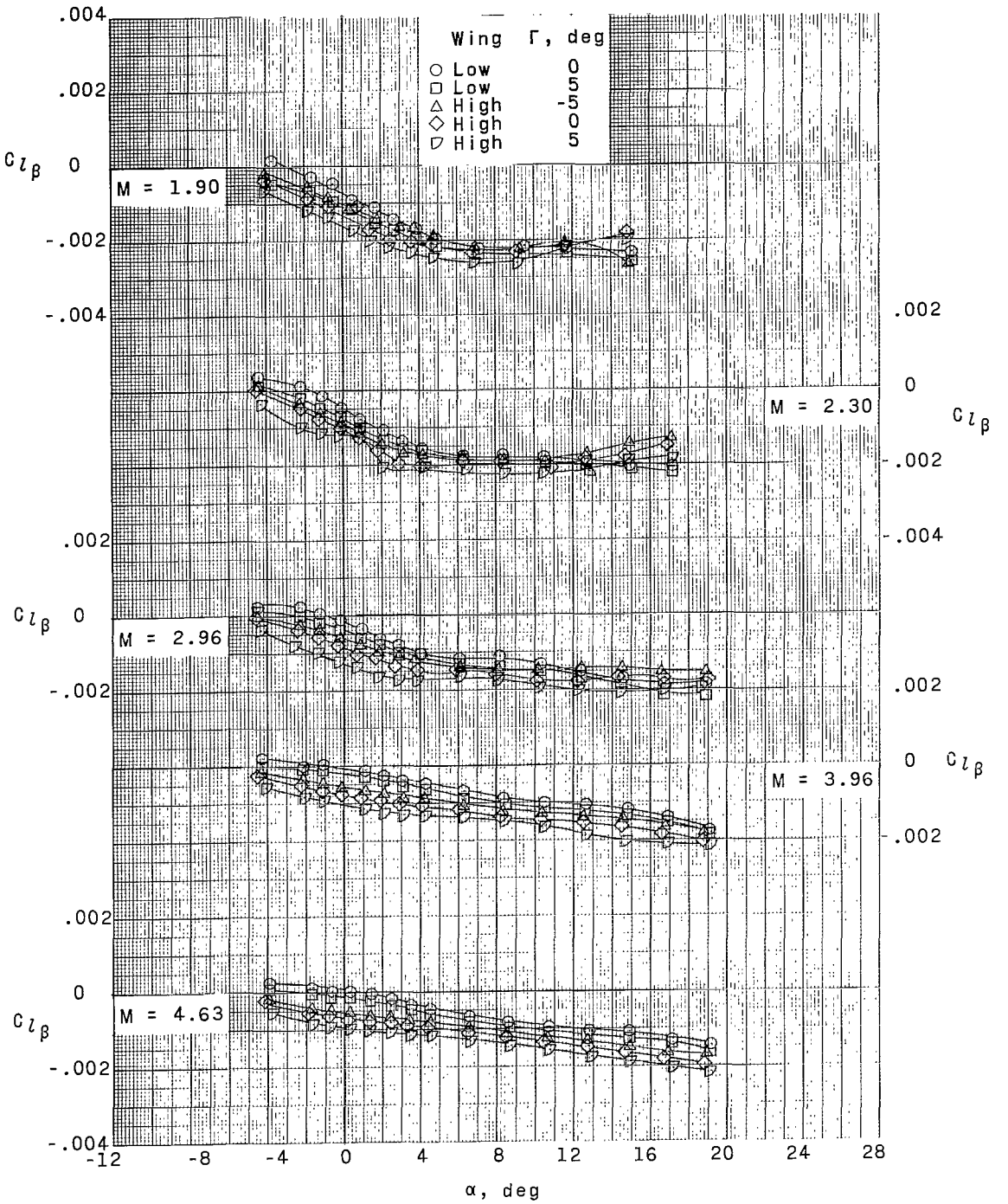

(c) Lateral stability.

Figure 19.- Concluded.

"The aeronautical and space activities of the United States shall be conducted so as to contribute . . . to the expansion of human knowledge of phenomena in the atmosphere and space. The Administration shall provide for the widest practicable and appropriate dissemination of information concerning its activities and the results thereof."

—NATIONAL AERONAUTICS AND SPACE ACT OF 1958

NASA SCIENTIFIC AND TECHNICAL PUBLICATIONS

TECHNICAL REPORTS: Scientific and technical information considered important, complete, and a lasting contribution to existing knowledge.

TECHNICAL NOTES: Information less broad in scope but nevertheless of importance as a contribution to existing knowledge.

TECHNICAL MEMORANDUMS: Information receiving limited distribution because of preliminary data, security classification, or other reasons.

CONTRACTOR REPORTS: Scientific and technical information generated under a NASA contract or grant and considered an important contribution to existing knowledge.

TECHNICAL TRANSLATIONS: Information published in a foreign language considered to merit NASA distribution in English.

SPECIAL PUBLICATIONS: Information derived from or of value to NASA activities. Publications include conference proceedings, monographs, data compilations, handbooks, sourcebooks, and special bibliographies.

TECHNOLOGY UTILIZATION PUBLICATIONS: Information on technology used by NASA that may be of particular interest in commercial and other non-aerospace applications. Publications include Tech Briefs, Technology Utilization Reports and Notes, and Technology Surveys.

Details on the availability of these publications may be obtained from:

SCIENTIFIC AND TECHNICAL INFORMATION DIVISION

NATIONAL AERONAUTICS AND SPACE ADMINISTRATION

Washington, D.C. 20546